UNIVERSITÄTSKLINIKUM HAMBURG-EPPENDORF

Institut für Immunologie

Institutsdirektor: Prof. Dr. med. M. Altfeld

Characterisation of single domain antibodies against the ADP-ribosylating Clostridium difficile toxin CDT and establishment of a murine infection model with the pathogen

Dissertation

zur Erlangung des Grades eines Doktors der Medizin
an der Medizinischen Fakultät der Universität Hamburg.

vorgelegt von:

Lucas Schumacher
aus Marburg

Hamburg 2020

(wird von der Medizinischen Fakultät ausgefüllt)

Angenommen von der
Medizinischen Fakultät der Universität Hamburg am:

10.02.2021

Veröffentlicht mit Genehmigung der
Medizinischen Fakultät der Universität Hamburg.

Prüfungsausschuss, der/die Vorsitzende: **Prof. Dr. rer. nat. Aymelt Itzen**

Prüfungsausschuss, zweite/r Gutachter/in: **Prof. Dr. med. Holger Rohde**

Acknowledgements

Firstly, I would like to express my gratitude to Prof. Dr. Friedrich Koch-Nolte for introducing me to the field of VHHs. I am very thankful and honoured to have had the opportunity to continue the research on *Clostridium difficile* specific VHHs started by Mandy Unger. I was always offered extensive support when problems arose, and Prof. Nolte inspired me numerous times to pursue different ideas into the field. Without the cooperation of Prof. Dr. Klaus Aktories and Dr. Carsten Schwan of the Institute of Toxicology, Freiburg, our work on clostridial toxins would not have been feasible.

Nearly equally supportive was Prof. Dr. Hans-Willi Mittrücker and his team, supervising the work on my murine infection model. During the establishment of the project, I received a close and warm-hearted support. The work contributed by our Microbiology, around Prof. Dr. Holger Rhode was also essential for the project.

I am especially grateful for being able to work with my laboratory colleagues of the Institute of Immunology. Anna Marei Eichhoff was a terrific laboratory partner and I was fortunate that she worked on similar projects during the same time span. Further, the senior scientific members Stephan Menzel and Welbeck Danquah consistently provided me with invaluable insight on experimental setups; Fabienne Seyfried, Alien Kruse, Marion Nissen, and Gudrun Dubberke patiently gave helpful technical support.

The Graduiertenkolleg “Inflammation and Regeneration” gave me the financial and academic support during my scientific work, which was indispensable during this research project.

Finally, I would like to express my gratitude to my family and friends. Without such a comprehensive support network, I could not have found the drive to complete this project. My parents, brother, and sister were always proud of what I am pursuing, which proved to be a driving motivation throughout my research endeavours. A particular mention is also directed towards my close friend Constantin Volkmann, with whom I enjoyed fruitful and incisive interactions during my medical dissertation.

1. Introduction

The following work comprises the characterisation of llama derived single domain antibodies (VHHs) directed against the transport component of the *Clostridium difficile* transferase toxin (CDTb) and the establishment of a murine *C. difficile* infection model. Prior to this work these VHHs had been isolated from immunized llamas.

1.1 *Clostridium difficile* infection

C. difficile is a gram-positive anaerobic rod capable of spore formation. This gut bacterium is the cause of antibiotic associated diarrhoea and spreads amongst humans by fecal-oral transmission. Upon its discovery the bacillus was believed to be commensal (Hall et al. 1935). However, during the last decades, the germ has emerged worldwide as the leading cause of infectious health-care associated diarrhoea. In the United States alone the rate of hospital discharges with *C. difficile* infection (CDI) has doubled between 2000 and 2010 and the economic burden associated is in excess of 1 billion US$ (Zimlichman et al. 2013, Reveles et al. 2014). The mean incidence for European hospitals is ~ 15 per 10.000 admissions (Jones et al. 2013). Non-epidemic PCR ribotypes of *C. difficile* usually cause mild, self-limiting diarrhoea with an infection-related mortality of 5%. However, the infection is often associated with other severe illness, which leads to an all-cause mortality of 15-20% (Lofgren et al. 2014). Documented by endoscopy, the fulminant cases often show pseudomembraneous colitis with haemorrhage and deep ulceration. Neuronal damage in the intestine by the ongoing inflammation can cause dilatation and decreased motility of the colon which can trigger a potentially fatal entity of CDI, toxic megacolon (Sayedy et al. 2010).

The majority of infections are associated with hospitalisation, but cases of community-acquired CDI have increased over the last decade (Khanna et al. 2012). Spores of *C. difficile* are ubiquitous in the environment and can be isolated even from food (Hensgens et al. 2012). In general, individuals with an intact immune system and commensal microbiota will eliminate the infection and/or become asymptomatic carriers (Leffler et al. 2015). The largest risk factor associated for infection is the depletion of the commensal microbiota by an antibiotic treatment. While some antibiotics, like clindamycin, cephalosporins and fluoroquinolones, have been identified as bearing the greatest risk, paradoxically, even metronidazole and vancomycin used for the treatment of CDI can incite the infection (Bingley et al. 1987, Slimings et al. 2014). Other risk factors, especially for recurrent infections, include age above 65 years, previous or ongoing hospitalisation, an underlying disease like renal failure and possibly antacid medications (D'Agostino et al. 2014). To study the

infection in animals, antibiotics are given prior to a challenge of *C. difficile* spores, in order to eradicate the microbiota. Different animal species have been used including hamsters, guinea pigs, and mice (Fekety et al. 1979, Knoop 1979, Chen et al. 2008). Mice are made susceptible to infection by administering five different antibiotics to the drinking water for three days and an injection of clindamycin one day ahead of infection (Fig. 1.1).

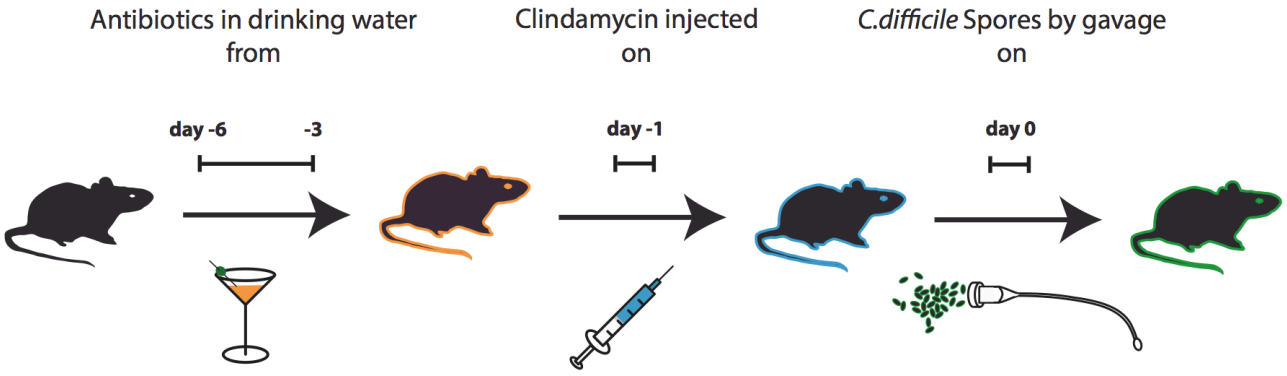

Figure 1.1: *C. difficile* infection (CDI) in mice. *C. difficile* infection (CDI) commonly develops in patients undergone antibiotic treatment, provoked by the depletion of the commensal microbiota in the gut. To reproduce these conditions in a murine infection model, an antibiotic regime is administered, following a infection of mice with *C.difficile*. The day of infection is referred to as day 0. For three days, from day -6 to -3, mice receive an antibiotic cocktail in the drinking water (kanamycin 0.4 mg/ml; gentamicin 0.035 mg/ml; colistin 850 U/ml, metronidazole 0.215 mg/ml and vancomycin 0.045 mg/ml). From day -3 onwards, normal drinking water. One day prior to infection, a single dose of 200 µg clindamycin is given by intraperitoneal injection.

When *C. difficile* has colonised the large intestine, the severity of the disease depends on the bacterial toxins produced. The main virulence factors are two rho-glycosylating toxins, toxin A and toxin B (Lyras et al. 2009, Kuehne et al. 2010). These two large clostridial cytotoxins inactivate small regulatory GTPases of the Rho family by glucosylation, which leads to a disruption of the cytoskeleton and other intracellular signaling pathways (Jank et al. 2008). Since the early 2000s, cases of more severe infections have received considerable attention involving the hyper-virulent *C. difficile* strain ribotype 027 (NAP1) (McDonald et al. 2005). The mortality rates associated are three times higher compared to other non epidemic strains (Loo et al. 2005, Warny et al. 2005). Besides higher fluoroquinolone resistance and enhanced toxin production, ribotype 027 is characterised by an additional toxin, *C. difficile* transferase (CDT) (Gerding et al. 2014). CDT is composed of two components and provokes a disintegration of the cell cytoskeleton by ADP-ribosylation of G-actin (Gulke et al. 2001).

1.2 Binary toxin CDT

The binary toxin CDT is produced by 5-30% of *C. difficile* strains (Gerding et al. 2014). CDT belongs to the family of actin ADP-ribosylating toxins. Members of this toxin family consist of two separate components. The two subunits CDTa and CDTb share close amino acid sequence homology to the iota toxin Ia and Ib of *C. perfringens* (Barth et al. 2004). The enzymatic component CDTa (48 kDa) consists of two homologous domains: The enzymatic activity is catalysed by the C-terminal ADP-ribosyltransferase domain, whereas the N-terminus possesses an enzymatically inactive 'pseudo'-ART domain that binds CDTb (Fig. 1.2 A) (Gulke et al. 2001). The transport component CDTb (98,9 kDa) is produced as a precursor protein that is activated by endogenous proteases releasing a 20 kDa peptide at the N-terminus (Fig. 1.2 B) (Barth et al. 2004). Lipoprotein-stimulated receptor (LSR) is the receptor of CDT which is physiologically involved in lipoprotein clearance (Papatheodorou et al. 2011).

Few studies have been done of CDT binding and its uptake. However conclusions can be drawn from the related iota toxin of *C. perfringens* which share the same receptor. Upon binding to LSR, CDTb oligomerizes into heptamers and lipid rafts accumulate on the cell surface, subsequently

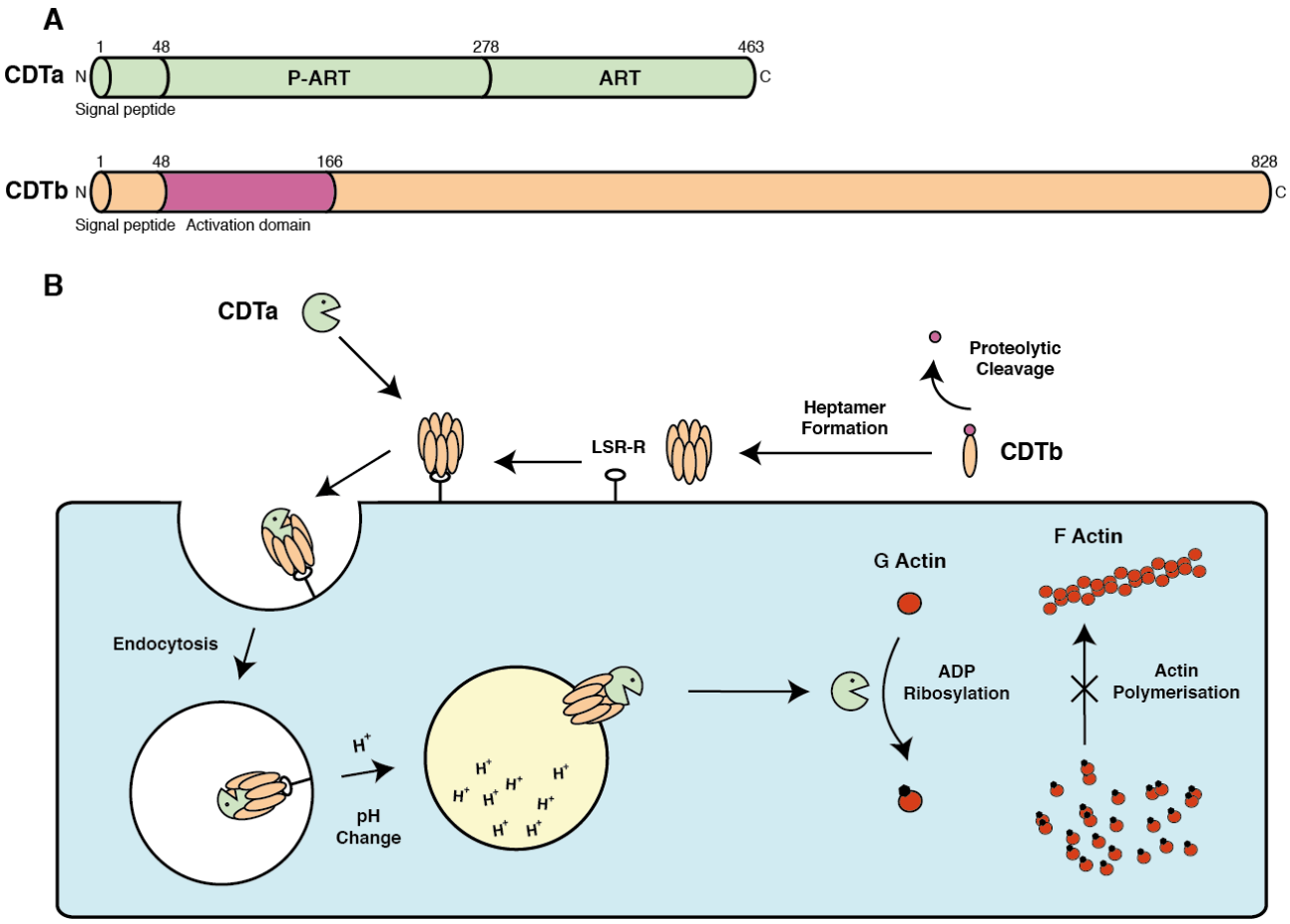

Figure 1.2: The binary AB toxin CDT. *C.difficile* transferase (CDT) belongs to the group of binary AB toxins and its toxicity is elicited by ADP-ribosylating G-actin. **(A)** CDT consist of two components: the the binding component CDTb and the biological active component CDTa, which possesses on its C-terminal end an ADP-Ribosyltransferase (ART) and a Pseudo-ADP-Ribosyltransferase (P-ART) region. **(B)** The receptor binding domain CDTb needs to be activated by proteolytic cleavage on the N-terminal end, before CDTb forms heptamers and binds to the LSR-receptor on the cell surface. Binding of CDTa causes the receptor-toxin complex to be internalised by the cell. A conformational change of CDTb is induced at low pH in endosomes, provoking an insertion of the CDTb heptamer into the membrane and pore formation. Subsequently CDTa enters the cells cytosol, where it ADP-ribosylates G-actin at arginine-177. In doing so, G-actin can no longer form F-actin leading to a depolymerisation of actin. Illustration inspired by Shen J Innate Immun. 2012; 4(2):149-58.

leading to binding of the enzymatic component CDTa (Papatheodorou et al. 2016). The complete toxin receptor complex is internalised to reach endosomal compartments. The low pH in endosomes most likely triggers the insertion of CDTb into the vesicle membrane by a conformational change (Papatheodorou et al. 2016). CDTa is translocated into the cytosol and ADP-ribosylates monomeric G-actin at Arg177. The ADP-ribosylated actin acts as a capping protein at the fast-polymerizing ends of actin filaments, thereby inhibiting the binding of unmodified G-actin, which eventually leads to depolymerisation of the actin cytoskeleton (Wegner et al. 1988). Furthermore, CDT induces the formation of microtubule based protrusions, that appear to enhance the adherence of *C. difficile* (Schwan et al. 2014). Recently, it was reported that CDT additionally suppresses protective host eosinophil responses via a Toll-like Receptor 2 (TLR2) dependent pathway (Cowardin et al. 2016). However, the precise mechanism of how CDT induces microtubule based protrusions or depletes eosinophils is not yet understood.

1.3 Llama derived single domain antibodies

Conventional antibodies found in mammals are composed of two light chains of 25 kDa, each of which is connected to a heavy chain of 50 kDa (Fig. 1.3). At the so called hinge-region, the two heavy chains are linked together by disulfide bonds. Antigen binding is determined by the two variable immunoglobulin domains V_L and V_H. The amino acid sequence of this region varies considerably between antibodies. Besides conventional antibodies, Camelids have evolved IgG isotypes composed only of heavy chains, so called heavy chain antibodies (hcAbs), lacking the light chain and the first constant domain of the heavy chain, C_H1 (Wesolowski et al. 2009). Extant members of *Camelidae* include two groups: *Camelini* of the Old World endemic to north Africa and Arabia (including camel and dromedary) and *Lamini* of the New World, endemic to South America

(including llamas, alpacas, vicuñas, and guanacos) (Stanley et al. 1994). In New World species, the proportion of hcAbs vs. conventional IgG antibodies in serum can reach 50-80%, whereas for the South American species it adds up to 10-25% (Blanc et al. 2009). Due to the unique structure of hcAbs, the antigen binding site is formed solely by a single variable domain. To differentiate

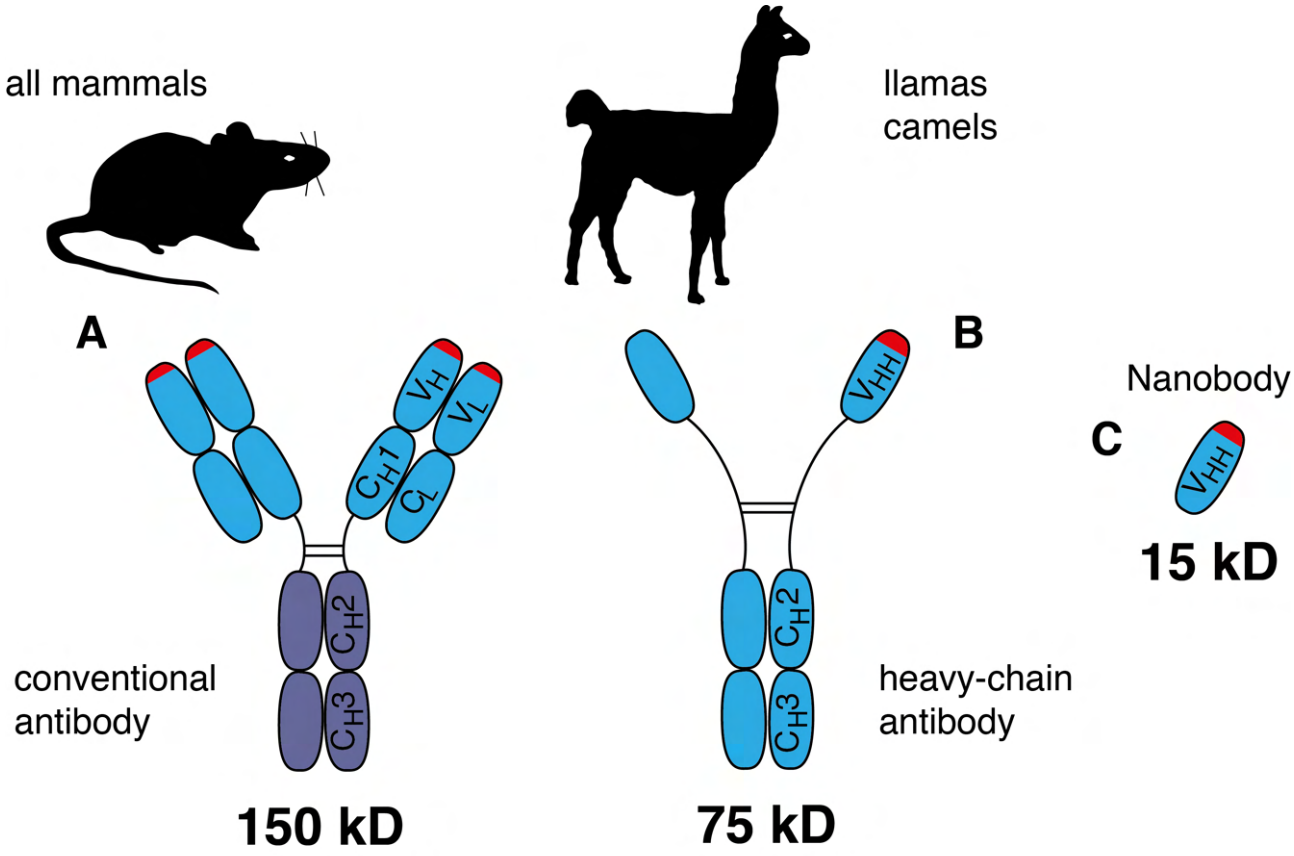

Figure 1.3: Single domain antibodies derived from heavy chain only antibodies. (A) The common IgG antibodies found in mammals are composed of two heavy and two light chains. The light chain is formed by two immunoglobulin domains (V_L,C_L) and the heavy chain by four immunoglobulin domains, one variable domain V_H and three constant domains C_H1 – C_H3. The variable region of the light chain V_L and the heavy chain V_H differ in their three hypervariable regions that determine the antigen specificity, whereas the constant domains are identical in structure and sequence among one IgG class. Via a flexible proline-rich hinge region between the C_H1 and and C_H2 domains, heavy chains are linked together by disulfide bonds. Each light chain associates also by a disulfide bond with one heavy chain between the CL and CH1 domains. A V_L-C_L and V_H-C_H1 fragment is referred to as the Fab fragment (fragment of antigen binding) and two C_H2-C_H3 fragments as the Fc fragment (fragment crystallisable). **(B)** A class of antibodies is found in llamas and camels consisting of two heavy chains only (hcAbs). These hcAbs lack the light chain and C_H1 domain, linking the the variable domain (V_HH) right to the remaining constant domains C_H2 – C_H3. The V_HH is solely responsible for antigen binding. **(C)** By isolating the RNA of peripheral blood lymphocytes from immunised llamas, V_HHs can be recombinantly produced as single domain antibodies. For their size (15 kDa) V_HHs are also denoted as nanobodies, differing markedly in size from a common IgG1 (150 kDa) or a hcAb (75 kDa).

between the variable domain of a conventional antibody's heavy chain (V_H), the domain is designated V_HH (variable heavy domain of heavy chain antibodies).

This single immunoglobulin domain can be cloned and produced recombinantly at a small size (~15 kDa), hence also called single domain antibodies or *nanobodies* due to dimensions in the nanometer range (2 nm × 3 nm) (Muyldermans 2013). The structure of conventional antibodies is stabilised by a hydrophobic patch in the framework region of the two variable domains supporting their pairing. This hydrophobic patch is replaced by hydrophilic amino acids in autonomous V_HHs, accounting for a high solubility. Furthermore, nanobodies show a high thermal and chemical stability (Muyldermans 2001). Their small size facilitates tissue penetration and leads to fast systemic clearance via renal filtration. Due to the modular nature of nanobodies, they are easy to convert into multivalent or multispecific formats that can be used to increase avidity, serum half life and neutralisation capability (Tijink et al. 2008).

The specificity of antibodies is determined by three highly variable loops within the variable domains. These complementarity determining regions (CDR1 - CDR3), are connected by four, more conserved, framework regions (FR1 - FR4). The framework regions form two ß-sheets connected by a canonical disulfide bond between FR1 and FR3. The paratope of conventional antibodies is usually flat and depends on six loops (V_L and V_H). In contrast, the CDR3 region of llama hcAbs often forms long, finger-like extensions up to 25 amino acids in length (Wesolowski et al. 2009). Thereby, VHHs can reach into crevices like the active site of an enzyme, which are normally not accessible to conventional antibodies (Desmyter et al. 1996, De Genst et al. 2006).

2. Material & Methods

2.1 Material

2.1.1 Lab Equipment

Equipment	*Firm/ Manufacturer*
Scale/ Balance Analytical Plus	Ohaus, Parsippany, USA
Autoclav Model 2540 EK	Tuttnauer Europe, Breda, Holland
Autoclav Varioklav	H+P Labortechnik GmbH, Oberschleissheim, Germany
Inkubator Biotherm 37	Julabo, Seelbach, Germany
Inkubator MCO-20AIC	Sanyo Electric Co., Tokio, Japan
Neubauer improved (chamber)	LO Laboroptik, Lancing, United Kingdom
ELISA-*reader* Victor	Perkin-Elmer, Waltham, USA
3D Laser Microscope VK 9700	Keyence, Mechelen, Belgium
Fluorescence microscope Axiovert 200M	Zeiss, Jena, Germany
Heating Block Thermomixer compact	Eppendorf, Hamburg, Germany
Refrigerated Centrifuge 5417R	Eppendorf, Hamburg, Germany
DNA gel electrphoresis 40-0708	Peqlab Biotechnologie GmbH, Erlangen, Germany
Single-Channel Pipettes Model Research	Eppendorf, Hamburg, Germany
pH-Meter InLab Routine pro	Mettler, Toledo, USA
Photometer Nanodrop 2000c	Peqlab Biotechnologie GmbH, Erlangen, Germany
Photometer Ultraspec 2000	Pharmacia Biotech, Freiburg, Germany
8 MP, 3264 x 2448 pixels, I9100 camera	Samsung, Seoul, South Korea
Sterile Workbench Typ BSB4	Gelaire, Sydney, Autralia
Analogue tube roller Mixer SRT6	Stuart, Staffordshire, UK
Inubator shaker Ecotron/ Unitron	inforsHT, Bottmingen, Switzerland
SDS-PAGE Novex MiniCell	Invitrogen, Karlsruhe, Germany
Low Voltage Gel electrophoresis	Bio-Rad, München, Germany

Spannungsgerät SDS-PAGE PowerPac 200	Bio-Rad, München, Germany
Thermocycler T3 / T Gradient	Biometra, Göttingen, Germany
Table Top Centrifuge 5424	Eppendorf, Hamburg, Germany
UV-Transilluminator Typ TI1	Biometra, Göttingen, Germany
Lab water bath Modell 1007	GFL, Burgwedel, Germany
Centrifuge Rotana 460 R	Hettich, Tuttlingen, Germnay
Centrifuge Rotors SA300/SLA300	Sorvall, Waltham, USA
Anaerobe Jar	Merck, Billerica, USA

2.1.2 Consumables

Equipment	*Firm/ Manufacturer*
Pipette tips various sizes	Eppendorf, Hamburg, Germany
Cell culture flask T-25, T-75, T-225	Nunc/ThermoFischer Scietific, Waltham, USA
Erlenmeyer flask various sizes	PP Corning Inc, Corning, USA
Syringes and needles, various sizes	BD Biosciences, Franklin Lakes, USA
Gloves, Safeskin	Kimberly-Clark, Dallas, USA
Hyperfilm ECL	Amersham-Pharmacia,
Microcentrifuge tubes various sizes	Eppendorf, Hamburg, Germany
Microplates various sizes	Greiner, Frickenhausen, Germany
Parafilm	Pechniney plastic packaging, Chicago, USA
Steriflip, Stericup	Merck, Billerica, USA
Falcon tubes 15 ml, 50 ml	Greiner, Frickenhausen, Germany
Serological pipettes various sizes	BD Biosciences, Franklin Lakes, USA
SDS-PAGE gels 10% and 12% NuPAGE	Invitrogen, Karlsruhe, Germany
CLO-Plates	bioMerieux, Marcy-l'Etoile, France
Armature grease	Fermit GmbH, Vettelschoß, Germany
Anaero Gen paper sachet	Oxoid /ThermoFischer Scietific, Waltham, USA
Dry anaerobic Indicator strips	BD Biosciences, Franklin Lakes, USA
Petridish	Merck, Billerica, USA
Whirl-Packs	Nasco, Fort Atkinson, USA

Disposable inoculation loop	Merck, Billerica, USA
µ-Plate Microtiter 96 well (glass bottom)	ibidi GmbH, Martinsried,Germany
96-Well microtiter plate	NUNC MaxiSorp, Rochester, USA
Corning Costar cell culture plates 6 well	Sigma-Aldrich, St. Louis, USA

2.1.3 Chemicals

Chemical	*Firm/ Manufacturer*
AEBSF	Merck, Billerica, USA
Aqua ad iniectabilia	Braun, Melsungen, Germany
Bacto agar	BD Biosciences, Franklin Lakes, USA
Bacto soyotone	BD Biosciences, Franklin Lakes, USA
Bacto tryptone	BD Biosciences, Franklin Lakes, USA
Bacto yeast extract	BD Biosciences, Franklin Lakes, USA
β-mercaptoethanol	gibco/life technologies, Carlsbad, USA
Carbenicillin	Serva, Heidelberg, Germany
Kanamycin	Sigma-Aldrich, St. Louis, USA
Gentamycin, Solution for infusion	ratiopharm, Ulm, Germany
Colitin, Solution for infusion	Forest, New York, USA
Metronidazol, Solution for infusion	Braun, Melsungen, Germany
Vancomycin	Hikma, London, United Kingdom
Clindamycin, Solution for infusion	Stragen, Köln, Germany
DMEM medium	gibco/life technologies, Carlsbad, USA
F17 media	Invitrogen, Karlsruhe, Germany
DNA Typing Grade Agarose	gibco/life technologies, Carlsbad, USA
dNTPs	Invitrogen, Karlsruhe, Germany
EDTA	Merck, Billerica, USA
Fetal calf serum, FCS	PAA/GE Healthcare, Chalfont St Giles, United Kingdom
Imidazole	Merck, Billerica, USA
IPTG	Roche, Basel, Switzerland
jetPEI	Polyplus-Transfection SA, Illkirch, France

LB Agar	BD Biosciences, Franklin Lakes, USA
LB Broth	BD Biosciences, Franklin Lakes, USA
2xYT	BD Biosciences, Franklin Lakes, USA
Taurocholate	Sigma-Aldrich, St. Louis, USA
L-Cystein	Sigma-Aldrich, St. Louis, USA
Brain Heart Infusion	Oxoid /ThermoFischer Scietific, Waltham, USA
Glycerol	Sigma-Aldrich, St. Louis, USA
Methanol	Merck, Billerica, USA
PFA (Paraformaldehyde)	Sigma-Aldrich, St. Louis, USA
Sulfuric acid	Sigma-Aldrich, St. Louis, USA
NuPAGE antioxidant	Invitrogen, Karlsruhe, Germany
NuPAGE sample reducing agent, 10x	Invitrogen, Karlsruhe, Germany
NuPAGE SDS-PAGE sample buffer, 4x	Invitrogen, Karlsruhe, Germany
Sodium chloride	Merck, Billerica, USA
Sodium phosphate	Merck, Billerica, USA
di-sodium phosphate	Merck, Billerica, USA
PBS	gibco/life technologies, Carlsbad, USA
Sucrose	Merck, Billerica, USA
TAE, DNA typing grade, 50x	Invitrogen, Karlsruhe, Germany
TMB substrate (3,3′,5,5′-tetramethylbenzidine)	Pierce/ThermoFischer Scietific, Waltham, USA
Tris-HCl	Sigma-Aldrich, St. Louis, USA
Tween-20	Sigma-Aldrich, St. Louis, USA
SOC-medium	Sigma-Aldrich, St. Louis, USA
Trypsin, 10x	Invitrogen, Karlsruhe, Germany
L-Glutamine, 200 mM	gibco/life technologies, Carlsbad, USA
Sodium pyruvate, 100 mM	gibco/life technologies, Carlsbad, USA
MEM, non essential amino acids, 10 mM	gibco/life technologies, Carlsbad, USA
NuPAGE transfer buffer, 20x	Invitrogen, Karlsruhe, Germany
roti®-Safe	Karl Roth GmbH, Karlsruhe, Germany
Triton X-100	Sigma-Aldrich, St. Louis, USA

2.1.4 Affinity Chromatography matrices

Matrix	*Firm/ Manufacturer*
Ni-NTA agarose	Qiagen, Venlo, Holland

2.1.5 Kits

Matrix	*Firm/ Manufacturer*
Qiaprep® Spin Miniprep kit	Qiagen, Venlo, Holland
Qiaprep® Spin Gel purification kit	Qiagen, Venlo, Holland
C. DIFF QUIK CHEK COMPLETE®	TECHLAB/Alere, Waltham, USA

2.1.6 Media, buffers and solutions

Bacterial culture media

Media	*Composition*
2xYT media	31 g/l in de-ionized water
LB broth	25 g/l in de-ionized water
LB Agar	25 g/l in de-ionized water, 15 g/l Agar
Brain Heart Infusion (BHIS)	BHIS medium per manufacture's instructions, 5 g of yeast extract to one liter of deionised water.After autoclavation, to the warm agar, 10 ml of filter-sterilized 10% (w/v) l-Cysteine and 10 ml of filter-sterilized 10% (w/v) taurocholat.
Brain Heart Infusion Agar	BHIS medium per manufacture's instructions, 8 g Agar, and 5 g of yeast extract to one liter of deionised water.After autoclavation, to the warm agar, 10 ml of filter-sterilized 10% (w/v) l- Cysteine and 10 ml of filter-sterilized 10% (w/v) taurocholat.
CLO-Plates	(BioMérieux) peptone 21g/l, sheep blood 50ml/l, cycloserine 0,1g/l, cefoxitine 0,008g/l, amphotericine B 0,002g/l

SOC (*super optimal broth*) Medium	2% Trypton (w/v), 0.5% Yeast extract (w/v), 8,6 mM NaCl, 2,5 mM KCl, 20 mM $MgSO_4$, 20 mM Glucose
All agar and media were autoclaved for 90 minutes	
Carbenicillin, stock 100 mg/ml	used at 100 µg/ml

Eukaryotic cell culture media

Media	*Composition*
Complete DMEM, 5% FCS	500 ml DMEM, 5 ml Glutamine, 5 ml Sodium pyruvate, 5 ml Hepes,5 ml MEM, non essential amino acids 25 ml FCS
F17 *feeding medium,*	Gibco® F17, 4 mM L-Glutamin, 0,1% Pluronic, 20% Trypton
F17-Complete Medium	Gibco® F17, 4 mM L-Glutamin, 0,1% Pluronic, 1% FCS, 0,5% G418
F17-Transfection Medium,	Gibco® F17, 4 mM L-Glutamin, 0,1% Pluronic

Bacterial cell lysis buffer

Buffer	*Composition*
TS lysis buffer	20% Sucrose w/v, 30 mM Tris-HCl, pH 8 1 mM AEBSF, ± 100 µg/ml Lysozyme in de-ionized water

SDS-PAGE buffers

Buffer	*Composition*
MES gel running buffer	1x MES buffer (Invitrogen) in de-ionized water

Sample preparation buffer	1x NuPAGE SDS sample buffer,1x NuPAGE sample reducing buffer
Blot buffer	1x NuPAGE transfer buffer, 10% Methanol, 0.1% Antioxidant in de-ionized water

DNA agarose gel electrophoresis buffers

Buffer	*Composition*
TAE gel running buffer	1x TAE buffer (Invitrogen) in de-ionized buffer
Sample preparation buffer	1x DNA loading dye (Fermentes)

TAE gel running buffer was autoclaved for 90 minutes

Affinity chromatography buffers

Buffer	*Composition*
Washing buffer (Ni-NTA)	2.65 mM Na_2HPO_4, 46.35 mM, NaH_2PO_4, 0.3 M NaCl, 3 mM Imidazole, pH 8 in de-ionized water
Elution buffer (Ni-NTA)	2.65 mM Na_2HPO_4, 46.35 mM, NaH_2PO_4, 0.3 M NaCl, 250 mM Imidazole, pH 8 in de-ionized water

All buffer were autoclaved for 90 minutes

2.1.7 Enzymes and Proteins

Protein/Enzyme	*Firm/ Manufacturer*

Antarctic Phosphatase	New England Biolabs GmbH, Frankfurt am Main, Germany
Bovine serum albumin, BSA	Merck, Billerica, USA
KOD-DNA-Polymerase	Merck, Billerica, USA
Lysozym (10 mg/ml)	Roche, Basel, Switzerland
Restriction enzymes NcoI, NotI und PciI, XbaI	New England Biolabs GmbH, Frankfurt am Main, Germany
T4 Ligase	Invitrogen, Karlsruhe, Germany
Recombinant CDTa und CDTb	kindly provided by Prof. Dr. Klaus Aktories, Freiburg, Germany

2.1.8 DNA and protein standards

Standard	*Firm/ Manufacturer*
GeneRule, 1kB (DNA)	Fermentas/Nunc/ThermoFischer Scietific, Waltham, USA
M Marker (protein)	Nolte lab (100 µg/ml BSA,75 µg/ml IgG, 10 µg/ml Lysozyme in 1x PBS)

2.1.9 Bacterial Strains

Bacteria	*Firm/ Manufacturer*
E.coli HB2151, Genotype: K12 D (*lac-pro*), *ara*, *nalr*, *thi/F'* [proAB, *lac*I_q, *lacZ*DM15]	Amersham Pharmacia Biotech, Uppsala, Sweden
E.coli XL-2 blue, Genotype: *end*A1 *sup*E44 *thi*-1 *hsd*R17 *rec*A1 *gyr*A96 *rel*A1 *lac* [F' proAB, lacI_q, lacZΔM15, Tn10(Tetr) Amy Camr]	Stratagene Europe, Amsterdam, Holland
C.difficile ATCC 43255, VPI 10463	American Type Culture Collection (ATCC), Manassas, USA

C.difficile 027/R27	kindly provided by the Institute for Medical Microbiology & Hygiene University of Saarland, Homburg/Saar, Germany

2.1.10 Cell lines

Cell lines	*Firm/ Manufacturer*
HEK293-6E human embryonic kidney cells, *Homo sapiens*	kindly provided by Dr. Yves Durocher, NRC Canada
HT29 (ATCC- HTB-38) colorectal adenocarcinoma , *Homo sapiens*	kindly provided by Prof. Dr. Holger Kalthoff, Universität Kiel

2.1.11 Mouse strains

Mouse strain	*Firm/ Manufacturer*
C57BI/6J	UKE mouse facility, Hamburg, Germany
C57BI/6J	Charles River, Wilmington, USA

2.1.12 Vectors

Vector	*Firm/ Manufacturer*
pHEN2	kindly provided by Dr. Fernando Goldbaum, Instituto Leloir, Buenos Aires, Argentina
pCSE2.5	kindy provided by Dr. Thomas Schirrmann, TU Braunschweig, Germany

2.1.13 Antibodies

Antibody	*Firm/ Manufacturer*
c-Myc-specific monoclonal mouse IgG1 (9E10) HRP	BD Biosciences, Heidelberg, Germany

2.1.14 Fluorescent dyes

Dye	*Firm/ Manufacturer*
Hoechst 33342	Molecular Probes, Eugene, USA
Rhodamin-Phalloidin	Molecular Probes, Eugene, USA

2.1.15 Oligonucleotides

Oligonucleotides used in this work were synthesised by "Metabion Gesellschaft für angewandte Biotechnologie GmbH (Planegg-Martinsried, Germany)":

CMV_F (pCSE2.5, *forward*) 5' -CGC AAA TGG GCG GTA GGC GTG -3'
Fdseq1 (pHEN2, *reverse*) 5'-GAA TTT TCT GTA TGA GG -3'
LMB3 (pHEN2, *forward*) 5'-CAG GAA ACA GCT ATG AC -3'
1067_68 (pCSE2.5, *forward*) 5'-TCG GAC ATG TCC GAT GTG CAG CTG CA -3'

2.2 Methods

2.2.1 Molecular biological methods

Transformation of chemically competent bacteria

Competent *E. coli* (XL2 from stock stored at -80°C) were thawed on ice and incubated for 30 min with ~ 0.1 µg plasmid DNA . Heat-shock was performed at 42°C for 30 seconds, followed by a further 2 min incubation on ice. 900 µl of SOC-medium (42°C) was added with a subsequent 60 min incubation at 37°C in a heat block at 450 rpm. The desired volume of bacteria was plated overnight on LB/Carbenicillin or 2YT/Carbenicillin agar at 37°C.

Preparation of plasmid DNA and quantification

For bacterial plasmid DNA, 5 ml of 2YT/Carbenicillin medium were inoculated with a single colony of transformed *E.coli* and cultivated overnight at 37°C and 230 rpm. The bacterial plasmid DNA was obtained using Qiaprep® Spin Miniprep kit following the manufactures protocol. The concentration was determined spectrophotometrically at 260 nm absorbance (conversion factor A_{260} = 1 = 50 µg/ml) using photometer Nanodrop 2000c.

Restriction digestion of DNA

DNA restriction digestion was performed with the according restriction enzymes following the manufacturer's recommendations. Typically, incubation was performed in a PCR thermocycler for 1-5 hrs in 20 µl volume at 37°C.

Polymerase chain reaction (PCR)

PCR reaction is a method used for the amplification of DNA fragments by means of the DNA polymerase enzyme. After restrictive digestion, DNA hydrogen bonds are broken at a high temperature (95°C), yielding DNA single strands. In the following annealing step at 58°C, primers bind to specific DNA sequences and permit the DNA polymerase to be recruited to the DNA. In the final elongation step (70°C), the DNA is duplicated via the polymerase enzyme by incorporating dNTPs.

In this work PCR reaction was used for amplification of VHH coding inserts from the phagemid vector pHEN2 in order to clone the inserts into the eukaryotic pCSE2.5 vector.

20 µl volume was used for PCR Reaction:

2 µl 10x Puffer für KOD-Polymerase

1,2 µl $MgSO_4$ (1,5 mM)

2 µl dNTPs (10 mM)

1 µl *forward primer* (10 mM)

1 µl *reverse primer* (10 mM)

0,5 µl KOD-DNA-Polymerase (1 U/µl)

x µl DNA (ca. 1 ng)

x µl ddH_2O

The reaction steps were carried out in the Thermocycler T3 using the following settings:

Temperature	*Time*	*Repeats*
95 °C	2 min	1 x
95 °C	20 s	30 x
58 °C	10 s	
70 °C	30 s	
70 °C	7 min	1 x
4 °C	Pause	

Ligation of DNA fragments

T4 Ligase was used in a volume of 10 µl in order to ligate vector and insert following manufactures instructions. For this purpose, insert was added to the vector at a ratio of 3:1, usually utilizing 50 ng of vector. Reactions were conducted at 16 °C overnight.

Agarose gel electrophoresis and extraction of DNA

For ligation DNA fragments (vector, insert) were size-fractionated by agarose gel electrophoresis. Agarose gel was prepared with 0,7 % agarose in 100 ml TAE buffer, heated in a microwave and, after having added 5 µl Roti®-Safe GelStain, poured into a gel tray. Samples were prepared with loading dye and put onto the hardened gel. Gels ran at 70-90 V. Using an UV-illuminator, DNA was visualised to identify the desired fragments. QIAquick gel extraction kit was used to extract DNA fragments following the manufacturer's protocol. DNA was eluted in 15-50 µl water, depending on the DNA visualised during UV illumination and hence its estimated concentration.

DNA sequencing

For sequencing, the services of SeqLab were used. 700 ng of DNA and 20 pmol of the according primer in total volume of 7 µl (de-ionised water) were submitted.

2.2.2 Protein biochemical methods

Preparation of bacterial periplasma lysates

The pHEN2 vector possesses a c-myc- and His6x-tag. Transformed *E.coli* HB2151 were used for protein production. HB2151 strain was cultured on LB agar plates containing carbenicillin to identify successfully transformed *E.Coli*. Transformed HB2151 *E.Coli* could overcome carbenicillin as the pHEN2 vector mediates resistance. Overnight 2 ml 2YT was inoculated by a single colony and incubated at 37°C, 240 rpm. 50 µl of this pre-culture was used to inoculate key cultures, 5 ml 2YT infusion containing carbenicillin. Cultures were incubated at 37°C at 240 rpm on the same day under the same conditions. Cultures were induced with IPTG when an optical density of OD_{600} 0.5 was reached and cultivated for another three hours. IPTG (Isopropyl-ß-D-1-thiogalactopyranosid) is a lactose analogram and induces protein production by means of the lac operon encoded on the pHEN2 vector. The pelB-leader sequence, also present in the pHEN2 vector, provokes the recombinant proteins to be delivered to the periplasmatic space. Following cultivation, cells were harvested by centrifugation at 4600 rpm for 15 min. The supernatant was discarded and bacteria pellets were resuspended in 5 ml TS lysis buffer, followed by an incubation on ice for 20 min in order to release periplasmatic proteins by an osmotic shock. Remaining cell debris were separated

from proteins by centrifugation at 15000 rpm for 30 min at 4°C. Proteins in supernatant were purified by affinity chromatography.

Protein purification by immobilised metal affinity chromatography

Periplasmatic lysates from bacteria were loaded on 1 ml Ni-NTA matrix columns. Flow-through was dispensed and proteins bound onto matrix due to His6x tag (part of the recombinant protein on the pHEN2 vector). Columns were washed once with 20 ml washing buffer. Proteins were dispensed from matrix with 1 ml elution buffer.

Sodium dodecyl sulfate polyacrylamide gel electrophoresis

SDS-PAGE can be used to size fractionate proteins by means of an electric field. Protein analysis by SDS-PAGE was performed by the NuPAGE® Novex® system under reducing conditions. First, proteins were mixed with sample buffer containing the anionic detergent SDS and heated to 70 °C. This denatures proteins and gives them a net negative charge. Further, samples were size-fractionated on 12% precast bis-tris gels in MES running buffer. The electrophoresis was carried out at 200 V, 110 mA for 40 min.

Coomassie blue staining

The Novex® colloidal blue staining kit was used for staining. The Coomassie blue staining makes protein bands on SDS-PAGE gels visible. This was carried out following the manufacturer's protocol. The dye, Coomassie brilliant blue, is a non-polar anion and stains proteins non-specific. Staining was performed overnight. Additional staining was removed by washing the gel in de-ionized water for 4 hrs. Gels were soaked in Novex® Gel-Dry drying solution and fixed and sandwiched between two transparent cellophane films to dry. For documentation the gels were scanned.

2.2.3 Cell biological methods

Cell culture of eukaryotic cells

Adherent cell line HT29 and suspension cell line HEK293-6E were cultured in filter-capped T-25 flasks (Nunc) in a steam-saturated incubator maintained at 37°C and 5% CO. Routinely, suspension cells were grown in F17-Complete Medium 1 % FCS, whereas adherent cells were retained in DMEM-Medium 5% FCS. Every two to three days cells were sub-cultivated (splitting) 1:5 to 1:20 into new T-25 flasks. During this process cells were washed once with PBS and detached from the flask with 1 ml of trypsin (trypsin for adherent cells only). Trypsin was inactivated with DMEM medium, at least three times of the volume, and cells were sub-cultivated into fresh media according to chosen ratio.

Determination of cell number using Neubauer chamber

Cell number per volume was determined in suspension using a Neubauer chamber. Adherent cells were treated with trypsin beforehand.

Transfection of eukaryotic cells and protein production

For expression of recombinant proteins in eukaryotic cells, *human embryonic kidney* HEK293-6E were used, which are optimised for recombinant antibody production (Zhang, Durocher et al. 2009). Transfections were conducted with the use of the jetPEI-System and 5 ml F17 transfection medium following the manufacturer's protocol. JetPEI transfection-reagent is a polyethylenimin that combines DNA particles into positively charged particles. These positive particles interact with anionic proteoglycans on the cell surface, causing endocytosis and thus making transfection more efficient. One day post transfection, cells were given an additional 125 µl of F17 feeding medium. On day six, medium was collected by centrifugation at 4000 rpm for 10 minutes to separate proteins from cells and stored for long term at 4°C. Protein production was routinely controlled by SDS-PAGE. In this work eukaryotic cells were transfected with the eukaryotic plasmid pCSE2.5 in a monovalent format carrying either a C-terminal c-myc-His6x or avi tag and in a bivalent format by fusion to the hinge, CH2, and CH3 domains of mouse IgC2c.

Cytotoxicity Assays

HT29 cells were subcultured (25.000 cells/well) onto 96 well microtiter plate with a glass bottom two days prior to experiment until they formed a half confluent monolayer. Furthermore a constant amount of CDT *C.difficile* toxin was incubated with selected VHHs in 200 µl of DMEM medium for 30 minutes at 37 °C. Subsequently, DMEM medium was removed from cells and VHH/CDT DMEM mixture was added and diluted if desired. The cell morphology was observed and documented by differential interference contrast microscopy using a Zeiss Axiovert 200M. The same microscope was used for fluorescence microscopy. For this reason the same cells received a follow up fixation for 10 minutes with 4% PFA in PBS. Cells were washed three times and stained for 15 minutes with Rhodamin-Phalloidin (1:3.500) and Hoechst 33342 (1:3000) in PBS. Till documentation cells were washed once more and stored in PBS. Rhodamin-Phalloidin is a high affinity F-actin fluorescent dye, whereas Hoechst 33342 colours the nucleus.

Differential interference contrast and fluorescence microscopy

Microscopical observation and documentation was carried out with a Zeiss Axiovert 200M, which was equipped with differential interference contrast and an Apotome. The microscope fitted two Plan-Apochromat 20x/0,8 and Plan-Apochromat 64x/1,4 lenses. A mercury-vapour lamp HBO103 acted as light source and Axiovision (Zeiss, Jena, Germany) software was used for processing microscopic recordings.

2.2.4 Immunological methods

Enzyme-linked Immunosorbent Assay

The antigen (in this work CDTb) was coated at 4°C in 100 µl 0,1 M $NaHCO_3$, pH 8,8 onto a 96-well microtiter plate overnight. Free binding sites were blocked with 1% BSA in PBS for 1 hr. Wells were washed with 200 µl PBS. VHHs from periplasmalysates (10 µl) or HEK-cell productions were incubated onto wells with bound toxins for 1 h at RT in 100 µl PBS/ 1% BSA. Afterwards wells were washed three times with PBS/0,05% Tween-20. Bound VHHs (recombinantly produced with a

c-myc-tag) were detected with an anti-c-myc peroxidase conjugated mouse antibody (1:3000 in PBS/1% BSA).

For epitope mapping, a competitive ELISA essay was conducted. Antigens were pre-incubated with 1 µg of VHH-mFc fusion proteins in 100 µl PBS/1% BSA for 30 minutes at RT. A preassembled binary complex was used for detection. For this, c-myc-tagged VHHs were pre-incubated for 1 h at RT in 100 µl PBS/1% BSA with peroxidase-conjugated c-myc-tag-specific mouse monoclonal antibody 9E11 (700 ng in PBS/1% BSA). 20 µl of the bivalent VHH antibody constructs (containing ~ 20 ng VHH) were added to the wells and incubation was continued for 30 minutes at RT. After three washes with PBS/0,05% Tween-20, 100 µl of substrate TMB were given onto the wells. Substrate incubation depended on the individual experiment and its background to signal ratio observed by the colour change. The reaction was stopped by adding 100 µl of sulfuric acid (1M). The optical density was measured at 450 nm using an ELISA-reader.

2.2.5 Radioactive methods

ADP ribosylation assay

In the presence of ^{32}P-NAD the ADP-ribosyltransferase CDTa radioactively labels its target protein actin by transferring ^{32}P-ADPR onto Arg177. This modification can be prevented, for example, by a specific inhibitor, e.g. a CDTa-blocking VHH. Radioactive ADP-ribosylation can also be prevented by prior ADP-ribosylation with unlabeled substrate. HT29 cells express the LSR-receptor and are sensitive to CDT. HT29 cells were cultured on 6 well culture plates. Each well was kept at a volume of 1 ml DMEM medium for 48 hours in a steam-saturated incubator maintained at 37°C and 5% CO. Cells were then treated with or without 2 nM CDT and 20 nM VHH in a volume of 1 ml DMEM. When rounding of CDT-treated cells became apparent, cells were washed with 2 ml PBS, harvested by trypsinization, and lysed in 40 µl PBS containing 0.5% Triton X-100 for 30 min on ice. To separate cytosolic HT-29 proteins from remaining cell debris, cell lysate was centrifuged for 5 min at 3000 rpm, the supernatant was transferred and centrifuged again for 5 min at 13000 rpm. The supernatant was used for radioactive ADP-ribosylation assays. Actin molecules that were so far not ADP-ribosylated due to inhibition of CDT by VHHs, would now be radioactively ADP-ribosylated. The ^{32}P-NAD was prepared as a mixture of 1 µM radioactive NAD with an activity of approximately 1 µCi/ reaction mixture. The reaction was carried out in a volume of 40 µl with 200

ng of CDT at 37°C for 15 min. Using 20 µl of 3x sample buffer, the anionic detergent of the SDS-PAGE NuPAGE® Novex® system, and heated for 10 minutes at 70 °C the reaction was terminated. 30 µl of the reaction mixture was analysed by SDS-PAGE to separate proteins. SDS-PAGE gel was dried and put into a film cassette containing radiographic film for 10 min at -80°C. The radiographic film was proceeded and fixed in automatic tabletop processor Curix 60. All steps handling radiographic film were carried out in the dark. After processing the film was scanned for documentation.

2.2.6 Methods used for mouse infection

Clostridium difficile culture of spores and vegetative forms

In this work the two strains VPI 10463/ATCC 43255 and ribotype 027 of *C. difficile* were used. For isolation of spores, *C. difficile* was cultured on BHIS agar containing L-cysteine and taurocholate overnight at 37°C in an anaerobic jar. Using Anaero Gen paper sachet following the manufacturer's protocol, an anaerobic atmosphere was created. This was verified by placing anaerobic indicator strips in the anaerobe jar. A single colony was spread onto one BHIS agar plate and cultured for 5-7 days at 37°C in an anaerobic jar to induce spore formation. The spores and residual vegetative cells were recovered by flooding the agar plate with 5 ml of ice-cold, deionised, sterile water. The suspension was divided onto 2 ml micro centrifuge tubes, centrifuged for 1 min at 14,000 x g, room temperature. The pellet was resuspended in 1 ml deionised, ice-cold water in order to wash and release the spores from its mother cells. The centrifugation and washing steps were repeated five times. All remaining vegetative bacteria were killed at 60°C for 20 minutes. After the last centrifugation step, the pellet was resuspended in either 500 µl of deionised water and stored at room temperature or deionised water containing 20% (w/v) glycerol and stored at -80 °C. Titers of *C. difficile* stocks were determined by plating serial dilution on BHIS agar containing L-cysteine and taurocholate. Experiments described in this study were performed with a stock containing 5×10^6 CFU/ml, while the inoculum used for one mouse was 10^6 CFU/200µl.

Mice

Experiments were performed with C57BL/6J mice (female only, 7- 20 weeks old) purchased from Charles River Laboratories or from the Animal Facility, University Medical Center Hamburg-Eppendorf. All mice were housed under specific pathogen-free conditions in the central animal facility of the University Medical Center Hamburg- Eppendorf. All animal experiments were conducted according to the German animal protection law. All mice experiments were approved by the Behörde für Gesundheit und Verbraucherschutz of the City of Hamburg under the permit 118/09. For the time of an experiment mice were weighed on a daily basis.

Antibiotics used in mouse experiments

Experiments with an antibiotic treatment prior to infection (day 0) involved an antibiotic cocktail in the drinking water and clindamycin injection. The antibiotics kanamycin 0.4 mg/ml; gentamicin 0.035 mg/ml; colistin 850 U/ml, metronidazole 0.215 mg/ml and vancomycin 0.045 mg/ml were administered in the drinking water on days -6 to -3 prior to infection. From day -3 onwards, mice received normal drinking water. A single dose of 200 µg clindamycin was given on day -1 by intraperitoneal injection. For one experiment 600 µg of clindamycin was administered as two consecutive doses of 300 µg clindamycin.

Quantitative culture of *C. difficile* of the colon

The entire colon tissue with its intestinal content was removed from mice at the end of the experiment, chopped into pieces and taken up in 2 ml deionised, sterile water in Whirl-Packs. Tissue and intestinal content were reduced to smaller pieces in Whirl-Packs to perform dilution series. Dilution series were conducted on selective agar specific for *C. difficile,* CLO Agar Plates. CLO Agar Plates were placed in an anaerobic jar for 48 hrs at 37 °C. CFU were counted and titer for complete colon was estimated.

Microscopy

Mice were sacrificed on day 2 post infection to investigate histological evidence of infection. Cecum and colon tissues were removed from mice. Tissue was fixed in 5 ml PBS containing 4 % buffered PFA at 4°C. Subsequently tissue was transferred to 5 ml PBS. Histological embedding and staining was conducted by the Mouse-Pathology Facility, University Medical Center Hamburg-Eppendorf. Briefly, tissues were embedded in paraffin, stained using Hematoxylin-Eosin and cut into 4 µm thick slices. Microscopical observation and documentation was carried out with 3D Laser

Microscope VK 9700, Keyence, Mechelen, Belgium. The software VK-Analyzer provided by the manufacturer was used for processing microscopic recordings. Microscope and software were kindly provided by Prof. Samuel Huber, University Medical Center Hamburg-Eppendorf.

MALDI-TOF and Immunoassay.

The presence of *C. difficile* in cultures and in the stool of mice was confirmed on a regular bases by the department of Medical Microbiology, Virology and Hygiene, University Medical Centre Hamburg-Eppendorf by mass spectrometry MALDI-TOF (Matrix-assisted-laser-desorption-ionization time-of-flight) using the MS Microflex LT/SH instrument (Bruker Daltonik GmbH, Leipzig, Germany) and *C. difficile* Immunoassay C. DIFF QUIK CHEK COMPLETE (TECHLAB).

3. Results

The following chapter will subdivided into two parts. At first, the results regarding the CDTb specific single domain antibodies will be presented. The data regarding the *C. difficile* infection mice, thereafter.

3.1 Characterisation of llama-derived single domain antibodies

Prior to this work, the Nolte lab immunized a llama with recombinant CDT (enzymatic component CDTa and transport component CDTb) (Unger et al. 2015). Phage libraries were generated from cDNA of peripheral blood lymphocytes and toxin-specific VHHs were identified after several panning rounds on CDT. The following section focuses on VHHs specific for the transport component of CDT, CDTb.

3.1.2 Identification and overview of the characterised single domain antibodies

Table I gives an overview of four families of single domain antibodies (VHHs) obtained by panning on CDTb and selected for further analyses. Individual VHHs were grouped into families according to their amino acid sequence and length of the CDR3 region (Tabel I, see also sequence alignment in Supplementary Fig.6.1). Sequence comparisons revealed eleven VHH families specific for CDTb (Supp. Fig 6.1). Four of which were selected for further analyses. Many VHHs were found several

anti-CDTb

VHH Family	Number of Isolates	Variations	Differences	CDR3
L-3	**34**	**9**	**2-19**	**RGY**
L-15.1	**39**	**10**	**1-17**	**KVGANILTRSIGYKY**
L-15.3	**4**	**1**	**0**	**TNKVYTDGRLEEYDY**
L-19	**2**	**1**	**0**	**DGRSNLRANYDSADYGMAY**

Table I: The amino acid sequence characteristics of the single domain antibodies. VHHs were grouped into families according to their distinct amino acid sequence. The name indicates the presence of a *short* or *long* (S/L) hinge region, an additional disulfide-bridge between CDR2 and CDR3 (+/-) and the number of amino acids in their CDR3 region. The number of clones found during *panning* of the same family are denoted as isolates. The range of the amino acid differences among the family members is given, as well as the CDR3 sequence. The position of the variant amino acid is highlighted in grey.

times during the panning rounds of the phage libraries (Table I, No. of isolates). The VHH family L-15.1 contains ten different variants evidently derived from one clone with very similar but slightly different sequences, whereas for L-19 only one clone was found (Table I, variants). Variants within a family with several members are distinguished by an alphabetical numbering (e.g., a-e). The variants differed by 2-19 amino acids for the L-3 family and by 1-17 amino acids for the L-15.1 family (Table I, differences). Positions with distinct amino acids in the CDR3 region within a family are highlighted in gray (Table I, CDR3).

3.1.2 Production of VHHs in *E. coli* and analysis of the binding specificity

Initially, VHHs were compared for expression levels in *E. coli* and their binding capacity to CDTb. Therefore, HB2151 *E. coli* cells were transformed with the VHH-encoding pHEN2 plasmid and protein expression was induced using IPTG. Proteins were harvested after three hours by osmotic shock. 10 µl of the VHH containing periplasmic fractions were size fractionated by SDS-PAGE and proteins were stained using Coomassie blue. The results show two prominent bands in most samples with a molecular mass of 14-20 kDa (Fig. 3.1, arrows). The upper band corresponds to the expected weight of a VHH with a C-terminal c-myc and hexahistidine (6xHis) tag. The lower band could correspond to VHHs lacking the C-terminal tag. Indeed, using immobilized metal affinity chromatography (Ni-NTA), the upper band could be purified, the lower could not (not shown). The concentration of VHHs in the periplasmic fractions varied considerably among the *E. coli* cultures.

The crude periplasmic lysates were used for ELISA on immobilised CDTb using peroxidase-conjugated-c-myc-specific antibodies (Fig. 3.1). A stronger signal with CDTb compared to the control protein bovine serum albumin (BSA) was observed for nearly all VHHs, confirming their specificity for CDTb. Some VHHs, however, like L-3b and L-3d, showed only very weak signals, despite high production levels (Fig. 3.1). For L-15.1f, the low production level correlates with a weak signal. To overcome the problems of inconsistent production levels, promising VHHs were subcloned into the eukaryotic expression vector pCSE2.5 that was specifically designed for the production of secretory proteins in suspension cultures of HEK293-6E cells in serum free medium (Zhang et al. 2009, Schirrmann et al. 2010). Another reason for switching the production system from bacterial cells to eukaryotic cells was the potential of endotoxin contamination (lipopolysaccharide) by *E. coli* that could interfere in an eukaryotic cellular assays.

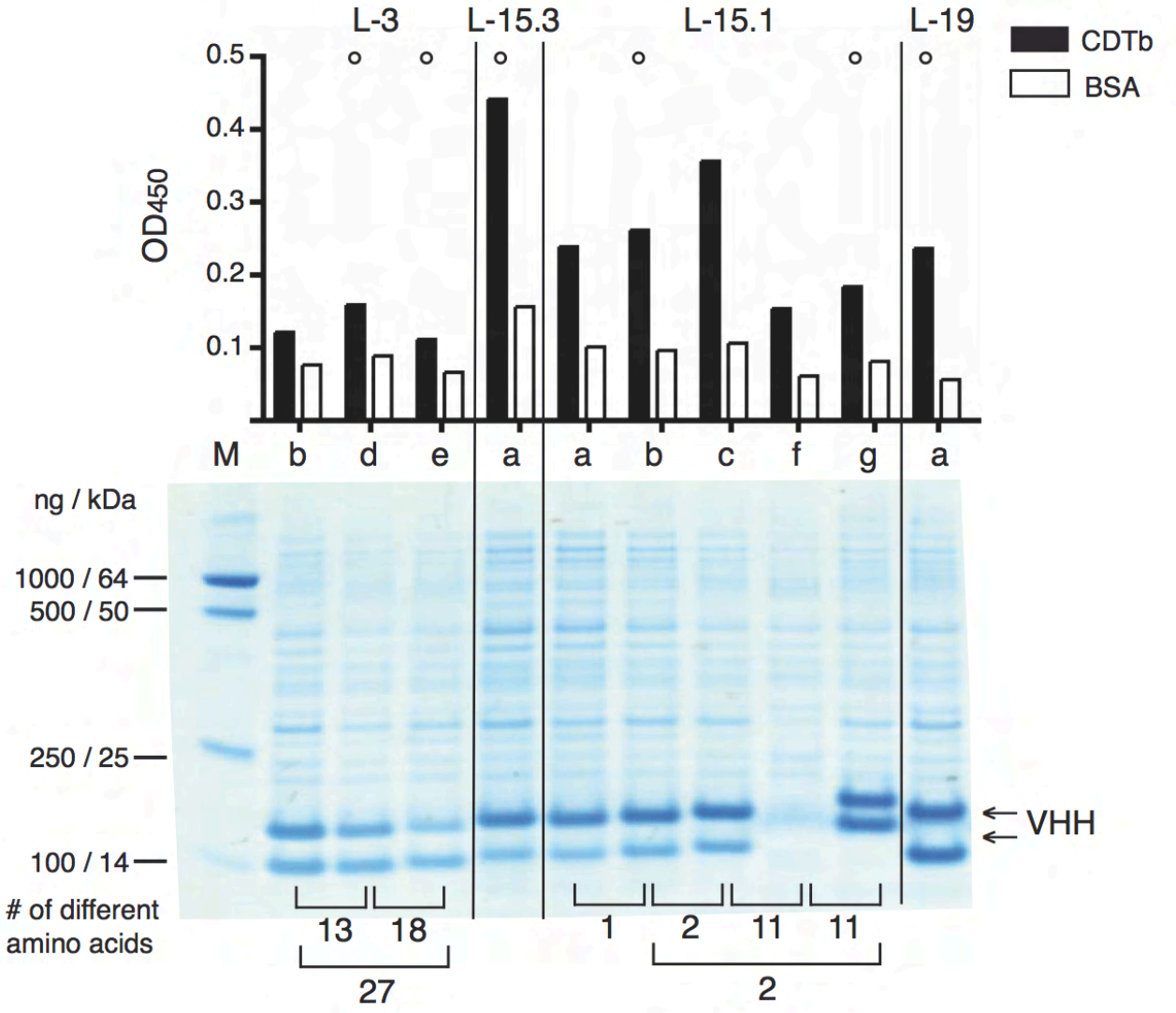

Figure 3.1. Comparison of VHHs expression in *E. coli* and evaluation of binding specificity for CDTb. Transformed *E. coli* HB2151 with pHEN2 plasmid of the VHHs families l-3, l-15.3, l-15.1 and l-19 were cultured in 5 ml 2YT infusion containing carbenicillin. When an OD_{600} of 0.5 was reached cultures were induced with IPTG and cultivated for an additional three hours. Cells were harvested and the outer cell wall was opened by TS lysis buffer to release periplasmatic proteins by osmotic shock. 10 µl of the periplasmatic fraction was size fractionated by SDS-PAGE and stained using Coomassie blue (bottom). To estimate the size (kDa) and amount (ng) of protein produced a marker (M) was also size fractionated with a known protein size and concentration. The bands apparent between 14-20 kDa correspond to the estimated size of VHHs. The number of different amino acids between two family members are indicated at the bottom. Using ELISA the specificity of VHHs for CDTb was estimated (top). 100 ng of CDTb (black column) or BSA (white column) was coated at 4°C onto a 96-Well microtiter plate overnight. After blocking free binding sites with 1% BSA in PBS, 10 µl of the periplasmatic fractions in 100 µl PBS/1% BSA was incubated for 1 hr onto wells coated with antigen or control protein. Subsequently, wells were washed three times with PBS/0,05% Tween-20 and VHHs detected with an anti-c-myc peroxidase conjugated mouse antibody (1:1000 in PBS/1% BSA). Wells were washed another three times and 100 µl of TMB was given onto wells. The colour change was stopped by 100 µl 1M sulfuric acid and measured at 450 nm using an ELISA-*reader*. White circles represent the VHHs chosen to be subcloned into the

3.1.3 Reformatting coding sequences into eukaryotic expression vector

Seven VHHs were chosen to be subcloned into the pCSE2.5 vector: L-3d and e, L-15.3, L-15.1b, c, g and L-19. VHH inserts were subcloned into three versions of the pCSE2.5 vector that differ by the C-terminal tag (Fig. 3.2). The monomeric VHH format with a c-myc/hexahistidine tag was kept in one version (not shown). Additionally, VHHs were linked to an avi-tag or to the hinge, CH2 and CH3 domain of a mouse IgG2c antibody (mFc), to yield a bivalent heavy chain antibody format.

VHH coding inserts were amplified by PCR from the pHEN2 vector. The restriction endonucleases NcoI and NotI were used to digest the templates. Within the coding regions of some VHHs an internal NcoI restriction site was present. If so, a PciI restriction site was generated using a forward primer followed by digestion with PciI and NotI. PciI and NcoI produce compatible ends for feasible ligations. The pCSE2.5 vectors were digested using NcoI and NotI to obtain the vector backbone, which was ligated to the VHHs inserts (Fig. 3.2).

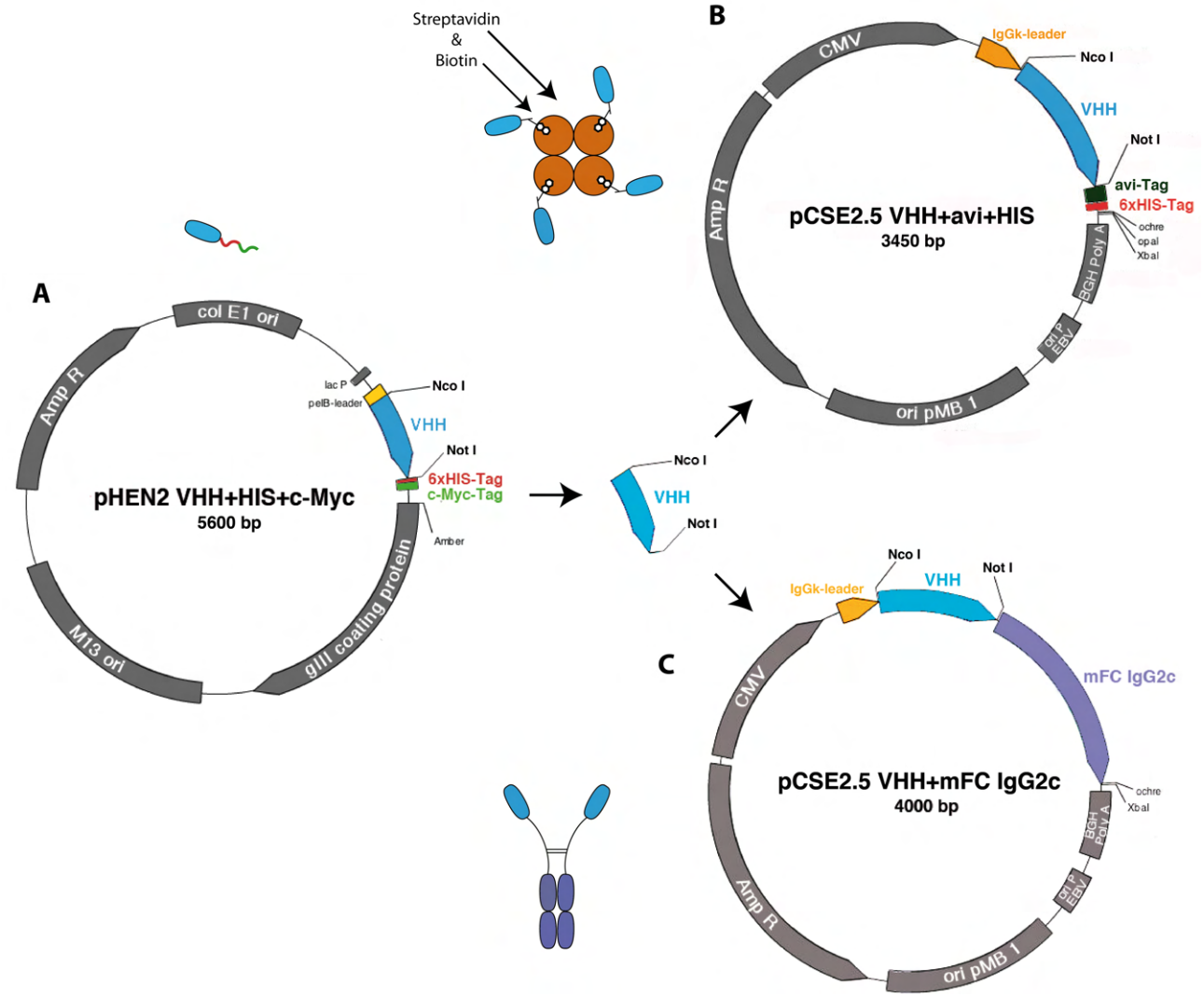

Figure 3.2: VHHs sequences were subcloned from pHEN2 into three different eukaryotic vectors: pCSE2.5 His-myc, pCSE2.5 avi and pCSE2.5 mIgG2c. (A) VHH inserts PCR amplified from pHEN2 were restriction digested with NcoI and NotI. Likewise vector pCSE2.5 was digested to create a new backbone with complementary ends. The VHHs inserts were ligated into three different pCSE2.5 vector backbones, which all differ by their C-terminal *tag*. For the pCSE2.5 c-myc-His6x format the original end was kept, featuring an His6x- and c-myc *tag* (not depicted). **(B)** Furthermore VHHs were given an avi-*tag*, which can be biotinylated to potentially bind VHHs to streptavidin. **(C)** For the final format VHHs were subcloned upstream of the hinge, CH2 and CH3 domains of mouse IgG2c to generate chimeric llama/ mouse IgG2c

3.1.4 Comparative analyses of binding affinities of reformatted VHHs

HEK-6E cells were transiently transfected with the different pCSE2.5 vectors and cultured for six days in serum-free medium. The supernatants were harvested and proteins in 10 µl aliquots of the supernatants were analyzed using SDS-PAGE and Coomassie staining. The results show prominent bands corresponding to the expected size of the recombinant proteins (Fig. 3.3 A). VHHs carrying the c-myc/6xHIS- or avi-tag correspond to bands at 15-20 kDa and VHH-Fc fusion proteins (Nb-mFc) to bands at 45 kDa. Bands in the background most likely derive from endogenous secretory proteins of the HEK cells and/or from lysed cells. Compared to the protein production in *E.coli* (Fig. 3.1), less background proteins are apparent and no double bands are observed (Fig. 3.3 A). The yield of recombinant VHHs can be estimated by comparing the bands to a loaded marker proteins of known concentrations. Hence, yield of the monovalent VHHs as well as the bivalent VHHs account for approximately ~1 µg nanobody per 10 µl HEK-6E cell supernatant.

To assess affinities for CDTb, an ELISA was performed using serial dilutions of monovalent VHHs. CDTb was immobilized over night on a microtiter plate and free binding sites were blocked with BSA. Wells were incubated with titrated c-Myc-tagged VHHs in HEK cell supernatants for one hour. Wells were washed and bound VHHs were detected by incubation for 30 min with a peroxidase conjugated c-myc-specific mouse monoclonal antibody. The optical density at 450 nm (OD_{450}) is plotted against the VHH concentration (nM) on a logarithmical scale (Fig. 3.3 B). With reducing VHH concentrations the OD_{450} signal declined in a sigmoidal manner. The dissociation constant (K_d) for each VHH can be deduced from the half-maximum signal observed, where the half-maximal binding occurs. Compared to the L-3 and L-15.1 VHH family, L-19 and L-15.3 showed higher OD_{450} signals and are therefore depicted separately (Fig. 3.3 B). While the maximal OD_{450} signal was higher for L-19 than for L-15.3, the signal for L-19 declined at lower concentrations compared to L-15.3. The K_d value for L-15.3 was estimated to be ~ 9 nM and for

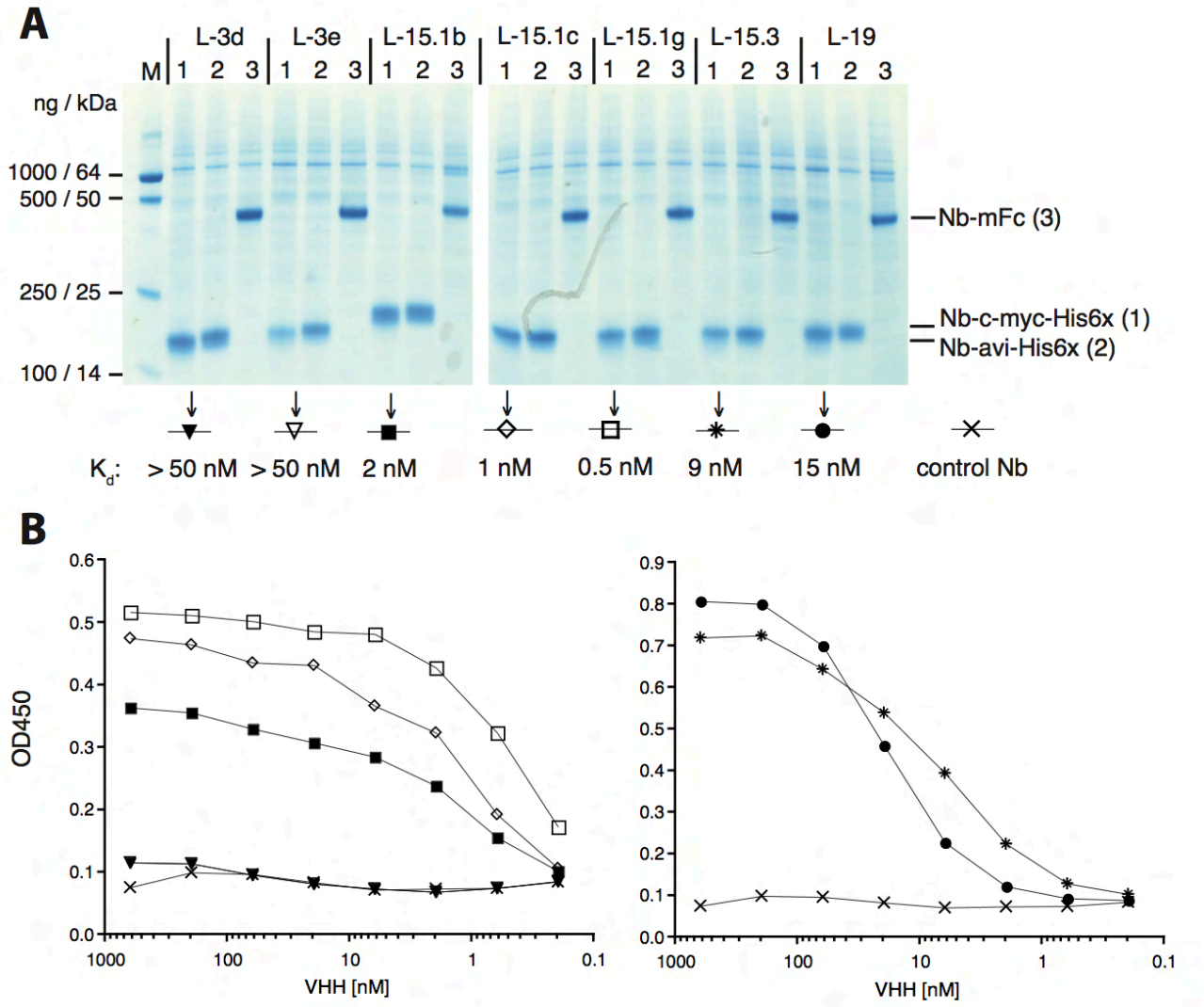

Figure 3.3: Expression of VHHs in eukaryotic cells and affinity comparison by ELISA. (A) HEK-6E-cells were transfected with different pCSE2.5 variants and cultured for six days in serum free media to produce VHH constructs. Supernatant and cells were separated by centrifugation and 10 µl of supernatant were analysed by SDS-PAGE and coomassie blue staining. The first bands (1) at ~15-20 kDa correspond to VHHs with c-myc-His6x *tag*, the second band (2) to VHHs with avi *tag* and the highest band (3) at ~45 kDa to VHH-mouse Fc fusion proteins. **(B)** The affinities of monovalent VHHs were analyzed by ELISA. 100 ng of CDTb per well was immobilised on a 96-well microtiter plate at 4°C overnight. Free binding sites were blocked with 5% BSA in PBS. Diluted VHHs starting at a concentration of 10 µg/ml were incubated for 1 hr, followed by three washing steps with PBS/0,05% Tween-20. Bound VHHs were detected with a c-myc-specific peroxidase conjugated mouse antibody (1:1000 in PBS/1% BSA). After three more washing steps the colour change was initiated with the substrate TMB and stopped with sulfuric acid. The optical density was measured at 450 nm in an ELISA-*reader*.

L-19 ~ 15 nM. The highest affinity, i.e. lowest K_d value of 0.5 nM was seen for L-15.1g. Other family members of this family, i.e. L-15.1b and L-15.1c, also showed high affinities of ~ 1-2 nM. The amino acid sequences among the three L-15.1 VHHs family members differ only by one or two amino acids, with VHH L-15.1g showing a single amino acid substition in the CDR3 (Supp. Fig.

7.1). Only very low signals were observed for L-3d or L-3e indicating that these nanobodies have only low affinities for CDTb (Fig. 3.1). Consistently, stronger signals were observed when these nanobodies were employed in bivalent format (see next section).

3.1.5 Mapping of differential epitopes

To evaluate whether VHHs bind the same or individual epitopes, a competitive binding ELISA was conducted (Fig. 3.4). A schematic representation of the experimental set-up is shown in Fig 3.4B. For detection, monovalent VHHs were converted to a bivalent format by pre-incubation with a peroxidase-conjugated c-myc-specific monoclonal antibody. For blocking, 1 µg of nanobody-Fc fusion proteins were incubated with the immobilised CDTb, before the addition of ~50 ng of the bivalent VHH-enyzme-antibody constructs. As a positive blocking control, the same VHH (VHH-

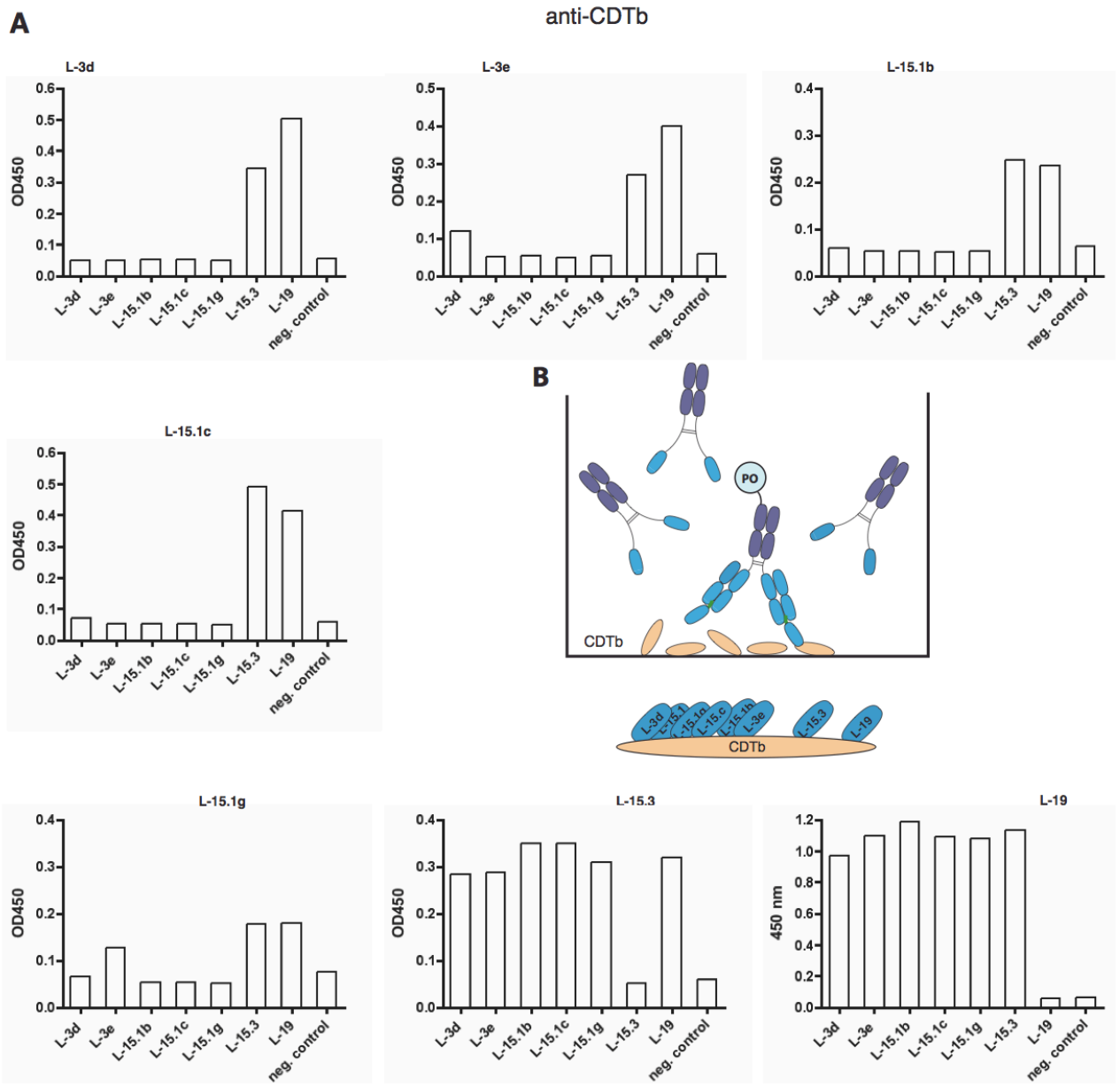

Figure 3.4: Relative epitope mapping on CDTb using bivalent VHH formats. VHHs were subjected to a competitive binding ELISA to analyse their relative epitope binding. **(B)** A schematic illustration is given for the experimental setup (top) and for the relative epitopes found (bottom). Immobilised CDTb on a 96-well micrometer plate was exposed to 1 µg of unlabelled VHH-mFc fusion proteins in 100 µl PBS/1% BSA for 30 minutes. In the meantime 100 ng of monovalent VHHs were pre-incubated for 1 h at RT in 100 µl PBS/1% BSA with c-myc peroxidase conjugated mouse antibodies (1:1000 in PBS/1% BSA) to create a bivalent VHH. These bivalent VHH antibody constructs were now given onto wells labeled by VHH-mFc fusion protein and co-incubated for 30 minutes. After three washing steps with PBS/0,05% Tween-20, 100 µl of substrate TMB was given onto wells for 60 min. Reaction was stopped by sulfuric acid. The optical density was measured at 450 nm using an ELISA-*reader*. As a negative control BSA was coated instead of CDTb. **(A)** Each VHH was used once for detecting a potential unoccupied binding site (stated above each diagram) and a signal could not be seen, when the same VHH antibody construct was used for pre-incubation. If a signal is observed the two VHHs are likely to bind CDTb independently.

mFc fusion protein) was used for pre-incubation as for detection (bivalent VHH/antibody construct). As a negative control BSA was coated instead of CDTb.

As expected, the results show no signal with the VHH construct used for detection (indicated on top of each diagram) when the same VHH (indicated on the bottom of the diagram) was used for pre-incubation, thereby blocking the respective epitope (Fig. 3.4 A). A negative signal by another VHH likely represents blocking of the epitope of the detection VHH, whereas a positive signal likely represents a distinct epitope bound by the pre-incubated VHH-mFc fusion proteins. The conclusion of the competitive binding ELISAs are depicted in Fig. 3.4 B bottom. The two families L-3 and L-15.1 seem to bind the same or overlapping epitopes, whereas the families L-15.3 and L-19 seem to bind independent epitopes.

3.1.6 Inhibiting cell cytotoxicity mediated by CDT in HT29 cells

A potential protective effect of the selected CDTb-specific VHHs on CDT-mediated cytotoxicity was examined in a cellular cytotoxicity assay with the human colon adenocarcinoma cell line HT29, since it expresses the CDTb receptor LSR (Papatheodorou et al. 2011). Initially, the half-maximal effective concentration (EC_{50}) for CDT was determined. Cells were cultured for two days until 50% confluency. HT29 cells were treated with titrated concentrations of (CDTa + CDTb) for 4 h before monitoring the morphology of the cells by differential interference microscopy (Fig. 3.5). The results show rounding and detachment of the cells at high toxin concentrations (250 ng/ml CDTa + 500 ng/ml CDTb). At the lowest toxin concentration (2 ng/ml CDTa + 4 ng/ml CDTb), the cell integrity was still intact. The EC_{50} was estimated to be ~ 12 ng/ml CDTa + 24 ng/ml CDTb.

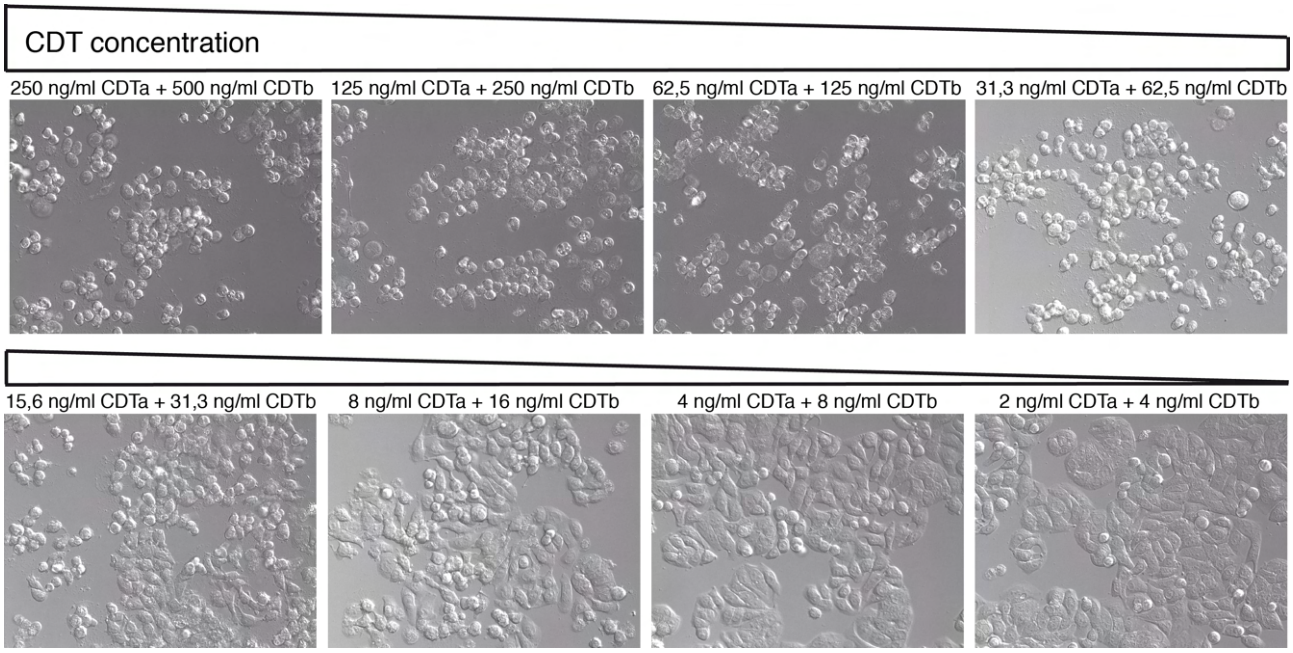

Figure 3.5: Determining effective cell cytotoxic concentration of CDT on HT-29 cells. Two days prior to experiment human colorectal adenocarcinoma cells (HT29) were subcultured (25.000 cells/well) onto microtiter 96 well plate with a glass bottom till a half confluent monolayer was formed. Starting from 500 ng/ml CDTb and 250 ng/ml CDTa a serial dilution was generated by a factor of two in DMEM Complete medium. Cells were incubated with different toxin concentrations for 4 hr at 37°C and then fixed with paraformaldehyde. The morphology of cells was evaluated and documented by differential interference microscopy using a Zeiss Axiovert 250. This experiment was conducted with the kind help of Anna Eichhoff, Insitute of Immunology, University Medical Center Hamburg-Eppendorf.

Next, an 8-fold excess of different VHHs (60 ng/ml) were pre-incubated with the two fold EC50 of CDT (24 ng/ml CDTa and 50 ng/ml CDTb) for 30 min before addition to HT29 cells at 50 % confluency. After incubation for 4 h cells were fixed and cell morphology was monitored by differential interference microscopy (Fig. 3.6). Cytoskeletal integrity was assessed by fluorescence microscopy using Rhodamin-Phalloidin and Hoechst (Fig. 3.7). Rhodamin-Phalloidin stains intact filamentous F-actin (red) but not monomeric G-actin, and Hoechst stains DNA. As a positive control, VHH L+8 was used, a CDTa-specific VHH previously described by our group, that inhibits the cytotoxic effects of CDT (Unger et al. 2015). The results show a complete disruption of the cytoskeleton after treatment of HT29 cells with CDTa + CDTb in the presence of an irrelevant control VHH and in the absence of any exogenously added VHH, visible as rounding of all cells and a lack of Rhodamin-Phalloidin staining compared to untreated cells (Fig. 3.6, Fig. 3.7, first row). As expected, cells incubated with CDTa + CDTb and the CDTa-specific VHH L+8 remain mostly attached and show a bright Rhodamin-Phalloidin staining. Similarly, cells treated with CDTa + CDTb in the presence of members of the CDTb-specific L-15.1 family appear intact, judged by

light microscopy and the presence of phalloidin staining. In contrast, no protective effects were detected for the VHH families L-3 and L-19.

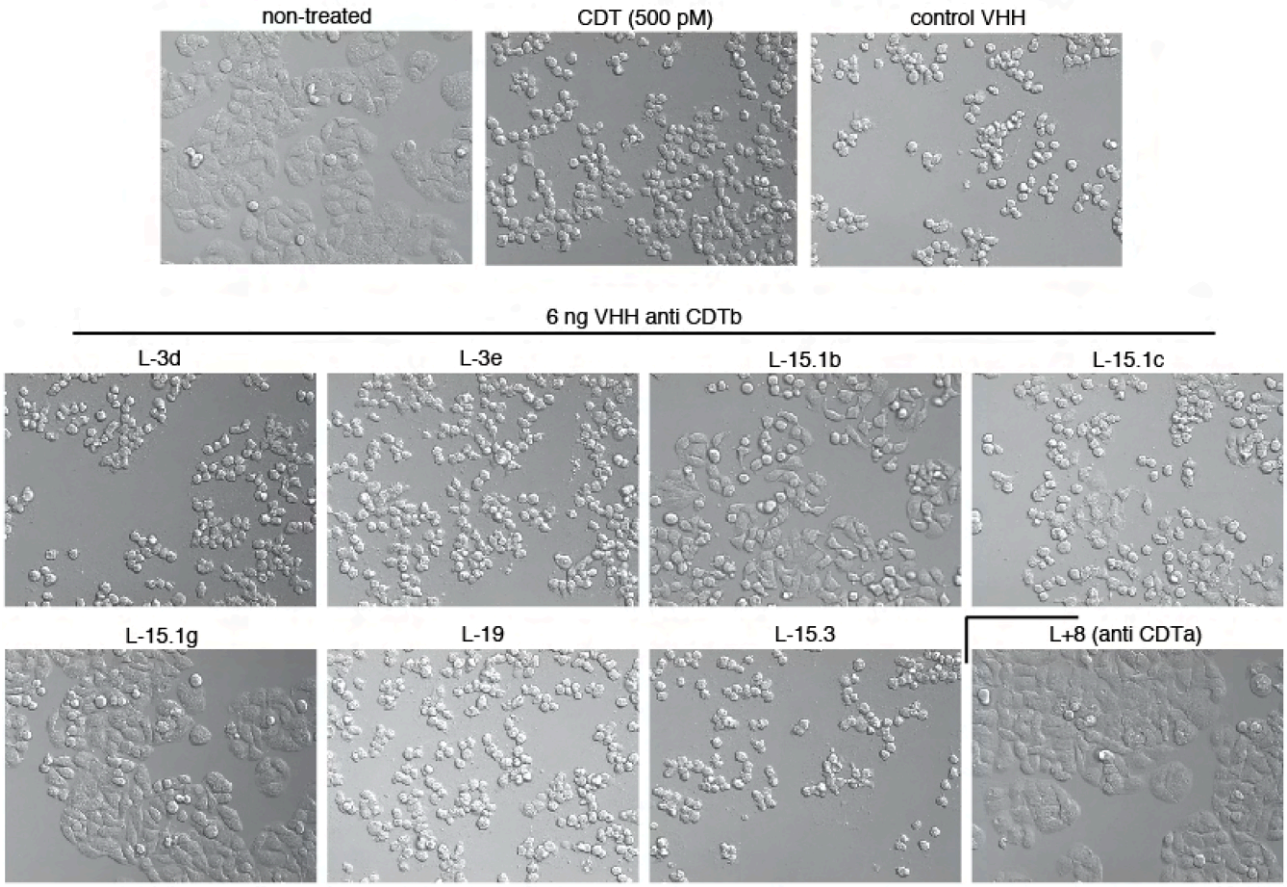

Figure 3.6: Visualising the effect of VHHs on HT29 cells treated with CDT using differential interference microscopy. HT29 cells were subcultured on a microtiter 96 well plate with a glass bottom two days prior to experiment until they formed a half confluent monolayer. For 30 min at 37°C in DMEM complete medium 24 ng/ml CDTa, 50 ng/ml CDTb (500 pM) and 60 ng/ml of different VHHs (4nM) were pre incubated, corresponding to an 8-fold excess of VHH vs. toxin. The mixture was given onto HT29 cells for 4 hr. Cell morphology was evaluated and documented by differential interference microscopy using a Zeiss Axiovert 250.

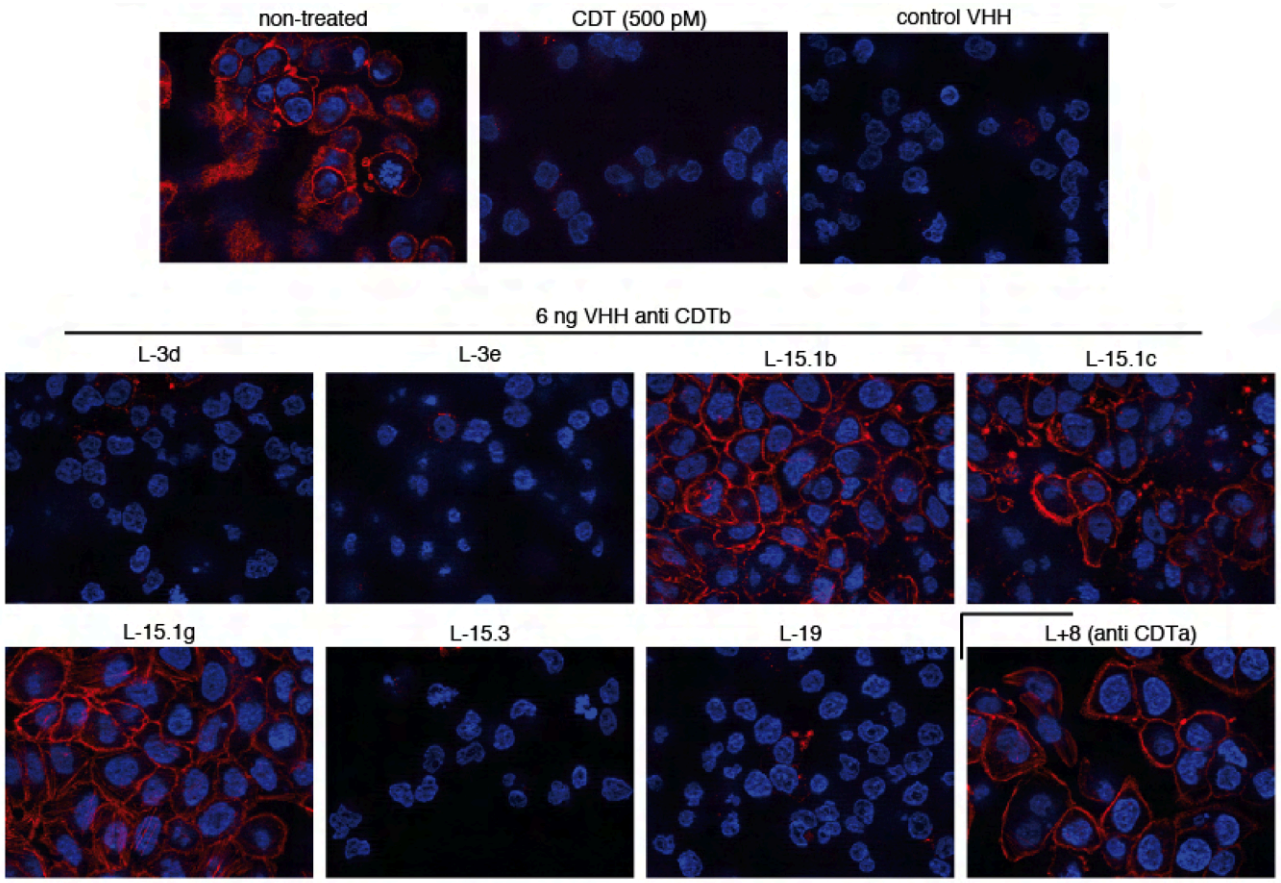

Figure 3.7: Visualising the effect of VHHs on HT29 cells treated with CDT using fluorescence microscopy. HT29 cells were cultured and treated with CDT and VHHs as described for Fig. 4.6. Additionally wells were washed with 200 µl PBS, fixed for 10 minutes with 4% PFA in PBS, then washed another three times and stained for 15 minutes with Rhodamin-Phalloidin (1:3500) and Hoechst 33342 (1:3000) in PBS. Cells were observed and documented using a Zeiss Axiovert 200M microscope.

As saturating levels of L-15.1 VHHs prevented the cytotoxic effect of CDTa + CDTb, a titration analysis was performed to assess the effective molar ratio of these single domain antibodies towards CDTb. The VHHs were diluted in six steps by a factor of two from 7.5 nM to 250 pM and preincubated with 500 pM CDTa + CDTb. Cells were treated with CDTa + CDTb for 4 h and cellular integrity was assessed by fluorescence microscopy and interference contrast microscopy. At the highest concentration of 7.5 nM VHH (CDT:VHH ratio about 1:16), vital cells and intact F-actin could be seen for all VHHs (Fig. 3.8 and Fig. 3.9). As the concentration was lowered, signs of disruption of the cells cytoskeleton became apparent, for L-15.1c already at a ratio of 1:8. For L-15.1b and L-15.1g, a protective effect was detectable at lower concentrations (CDT:VHH ratio 1:4, 1:2). Even at the equimolar concentration of CDT:VHH L-15.1g, signs of an intact cytoskeleton can be observed. Similarly, the l+8 single domain antibody directed against the enzymatic component of CDT, protected cells from the cytotoxic effects of CDTa + CDTb.

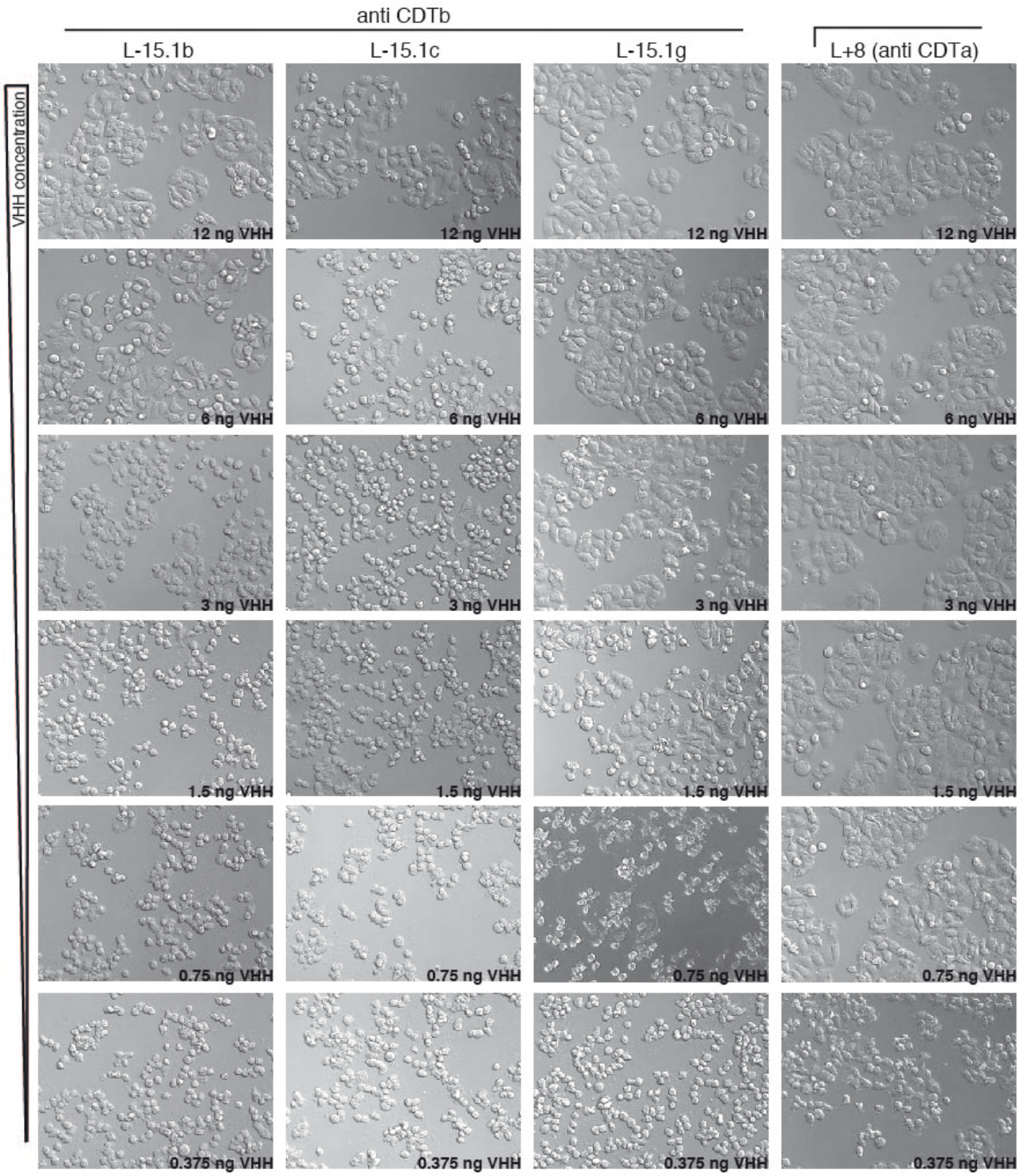

Figure 3.8: Titration of CDT neutralising VHHs on HT29 cells. HT29 cells were subcultured on a microtiter 96 well plate with a glass bottom two days prior to experiment until a half confluent monolayer formed. VHHs were diluted in six steps by a factor of two, starting from 7.5 nM till 250 pM. The dilution series were pre incubated with 500 pM CDTa+b for 30 min at 37°C in DMEM complete medium until given onto HT29 cells for 4 hr. The molar toxin vs. VHH ratio ranges from about 1:16 till 1:0.5. The morphology of cells was evaluated and documented by differential interference microscopy using a Zeiss Axiovert 200M microscope.

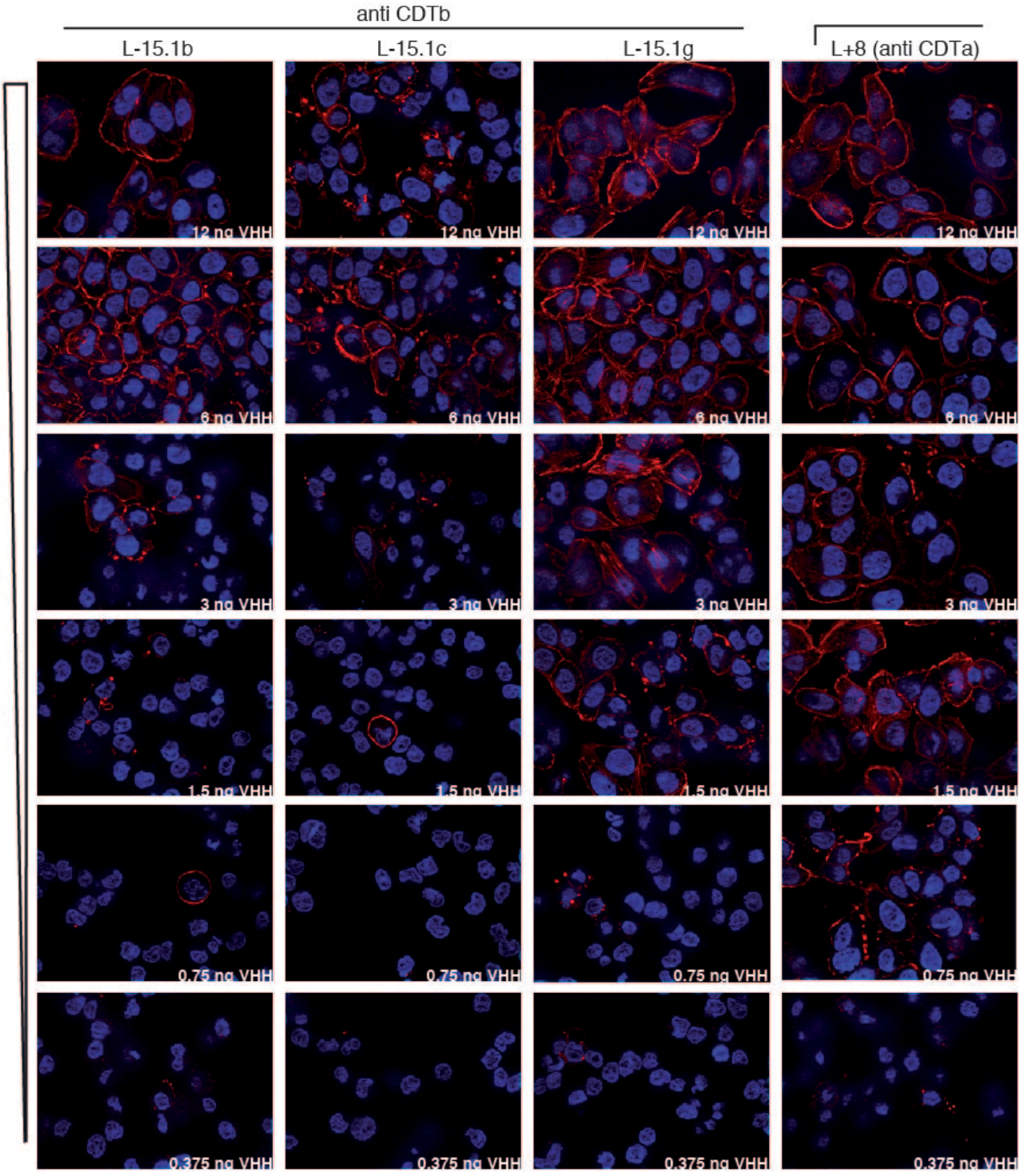

Figure 3.9: Fluorescence microscopy images of HT29 cells treated with CDT and dilution series of neutralising VHHs. HT29 cells were cultured and treated with CDT and VHHs as described for Fig. 4.8. Additionally cells were fixed for 10 minutes with 4% PFA in PBS, then washed three times and stained for 15 minutes with Rhodamin-Phalloidin (1:3500) and Hoechst 33342 (1:3000) in PBS. Cells were observed and documented using a Zeiss Axiovert 200M microscope.

3.1.7 Preventing CDT induced ADP-ribosylation of actin

To assess whether CDTb-specific VHHs could indirectly prevent CDTa-catalyzed ADP-ribosylation of actin, a radioactive ADP-ribosylation assay was performed (Fig. 3.10). The experimental set up is illustrated schematically in Fig 3.10A. HT-29 cells were incubated for 4h in the presence of 2 nM CDTa +CDTb and 20 nM VHH. In case of toxin entry into the cell, actin would be ADP-ribosylated with non-radioactive endogenous NAD^+ by the enzymatic activity of CDTa. However, actin should not be ADP-ribosylated if the CDTb-specific VHH blocked entry of CDTa into the cytosol. When rounding of cells was observed in cells treated with CDTa + CDTb (after ~3h of incubation), cells were washed, trypsinized, lysed, and cytosolic proteins were obtained by removal of cellular debris by high speed centrifugation. The lysate containing cytosolic proteins was now treated with radioactive ^{32}P-NAD^+ and CDTa. All un-modified actin would then be radioactively ADP-ribosylated. Proteins were size fractionated by SDS-PAGE and the dried gel was exposed to a radiographic film. No signal could be detected in samples not treated with ^{32}P-NAD^+ (lane 1). Control cell lysates incubated with CDTa and ^{32}P-NAD showed a prominent radiolabeled band at ~ 40 kD corresponding to ^{32}P-ADP-ribosylated actin (lane 2). In contrast, cells treated with CDTa + CDTb showed a strongly reduced incorporation of radiolabel into this band, indicating prior ADP-ribosylation of actin by translocated CDTa using cellular NAD as substrate (lane 3). In contrast,

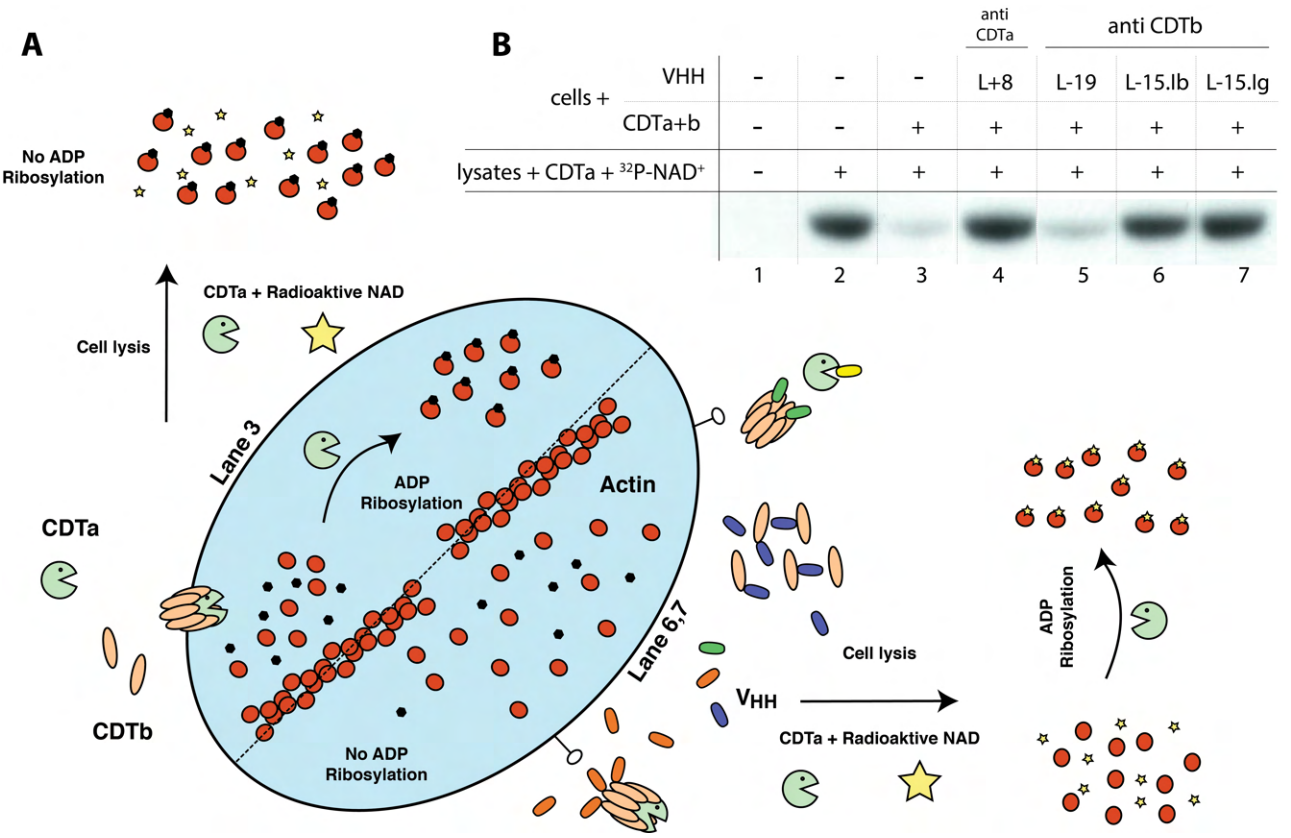

Figure 3.10: CDTb specific VHHs l-15.1b and l-15.1g block CDTa mediated ADP-ribosylation of actin in HT29 cells. (A) Schematic representation of the experimental set-up: If the CDTb specific VHHs intervene with the enzymatic activity of CDT, an inhibition of the intracellular ADP-ribosylation of actin by its enzymatic counterpart CDTa should be detectable. The CDT complex on its own can effectively bind cells and deliver the enzymatic component to the intracellular compartment, shown in the left of the cell towards the top. CDTa (pacman, green) entering into the cell via heptamerized cell-bound CDTb (orange). Actin is ADP-ribosylated at Arginin-177. Subsequently after cell lysis the position for transferring the radioactive ADP-ripose is already occupied and actin can not be labeled (corresponding to lane 3 (B)). However if cells are treated with CDT in the presence of single domain antibodies capable of inhibiting CDTb, intracellular actin should not be altered. Depicted in the bottom of the cell to the right, with the addition of VHHs (oval structures with multiple colours). After obtaining cytosolic proteins by cell lysis and removing other cell debris by centrifugation, monomeric actin should not be labeled in the presence of CDTa and radioactive NAD^+ (corresponding to lane 6,7 (B)). **(B)** Therefore HT-29 cells, cultured on two six well plates, were treated with 2 nM CDT and 20 nM VHH in a volume of 1 ml DMEM complete medium respectively. At this point actin was ADP-ribosylated by endogenous NAD^+, if CDTa entered the cells cytosol. By then no radioactive ^{32}P-NAD was used. When rounding of cells became apparent, cells were trypsinized and lysed in 40 µl PBS containing 0.5% Trition X-100 for 30 min on ice. Cytosolic proteins got separated from remaining cell debris by two centrifugation steps: 5 min at 3000 rpm and 5 min at 13000 rpm. Starting from here the supernatant was used for radioactive ADP-ribosylation. The ^{32}P-NAD^+ was prepared as a mixture of 1 µM radioactive NAD^+ with an activity of approximately 1 µCi/ reaction mixture. The reaction was carried out in a volume of 40 µl with 200 ng of CDTa at 37°C for 15 min. The reaction was terminated by 20 µl of 3x sample buffer at 70 °C for 10 minutes. The reaction mixture was size fractionated by SDS-PAGE. A radiographic film was exposed for 10 min to the dried SDS-PAGE gel and processed in automatic tabletop prozessor Curix 60. A schematic representation of the experiment is given.

lysates from cells incubated with CDTa + CDTb in the presence of L-15.1b or L-15.1g a prominent radiolabeled band was observed (lane 6+7). This is compatible with the interpretation that entry of CDTa was blocked by the CDTb-specific nanobody. Lysates from cells incubated with CDTa + CDTb in the presence of L-19 showed weak ^{32}P-ADP-ribosylation of actin (lane 5), comparable to that of control cells (lane 3). The decreased labeling of actin most likely reflects unabated ADP-ribosylation of actin by CDTa with endogenous cellular NAD incubation. Note that incubation of cells with CDTa + CDTb in the presence of CDTa-specific VHH L+8 also effectively prevented ADP-ribosylation with endogenous NAD+ as substrate. Evidently, washing of the cells prior to lysis removed excess VHH l+8, since maximal ^{32}P-ADP-ribosylation of actin was observed in cell lysates upon addition of exogenous CDTa and ^{32}P-NAD as substrate (lane 4).

3.2 A mouse model for *C. difficile* infection

In humans, *C. difficile* typically induces diarrhoea and colitis in patients after antibiotic treatment. Due to the loss of the microbiota in the gut after an antibiotic regime, *C. difficile* is able to colonise and cause infection. Previous studies reported an infection model in mice consisting of an pretreatment with antibiotics in drinking water (kanamycin, gentamicin, colistin, metronidazole and vancomycin) followed by a single i.p. injection of clindamycin prior to oral challenge with toxin-A and toxin-B expressing *C. difficile* in PBS (Chen et al. 2008). In mice the microbiota of the gut is influenced by several factors like familial transmission (Ubeda et al. 2012), housing (Ley et al. 2005) and food (Turnbaugh et al. 2009). The experiments described below were performed with the aim of establishing a mouse infection model with CDT-expressing strains of *C. difficile* in the animal facility of the University Medical Center Hamburg-Eppendorf.

3.2.1 Generation of *C. difficile* stocks.

Two different strain of *C. difficile* were successfully cultured and used in the experiments. Ribotype 027 (R27) was kindly provided by the Institute for Medical-Microbiology and Hygiene, Saarland University and VPI 10463 (ATCC 43255) was purchased from the American Type Culture Collection, Manassas, USA. The maintenance of *C. difficile* was carried out as previously described (Sorg et al. 2009) and detailed in the Materials & Methods section. *C. difficile* stocks were heated for 20 min at 60 °C to kill all vegetative bacteria (Sorg et al. 2009). Using dilution series, the titer of the *C. difficile* stock was found to be 5×10^6 CFU/ml for the strain VPI 10463 (ATCC 43255) and 3×10^8 CFU/ml for R27. The suspensions of both stocks remained at the same titer over time (controlled by dilution series). Hence, the stock was assumed to be spores only. The Department of Medical Microbiology (UKE) confirmed on a regular base *C. difficile* cultures by mass-spectrometry (MALDI-TOF) and *C. difficile* immunoassay (C. diff Quick Check Complete; Techlab).

3.2.2 Colonisation of C57Bl/6J mice by two strains of *C. difficile* (ATCC 43255, R27)

Differences in the pathogenicity of *C. difficile* strains correlate partially with difference in toxins produced by these strains (McDonald et al. 2005). Strain ATCC 43255 produces the rho

glucosylating toxin A and toxin B. Ribotype 027 additionally produces the binary ADP-ribosylating toxin CDT.

C57BL/6J mice, purchased from Charles River or obtained from the Animal Facility of the UKE were housed under specific pathogen-free conditions in the central animal facility (UKE). Four groups of mice (n=7) were pretreated with an antibiotic cocktail in the drinking water on day -6 to

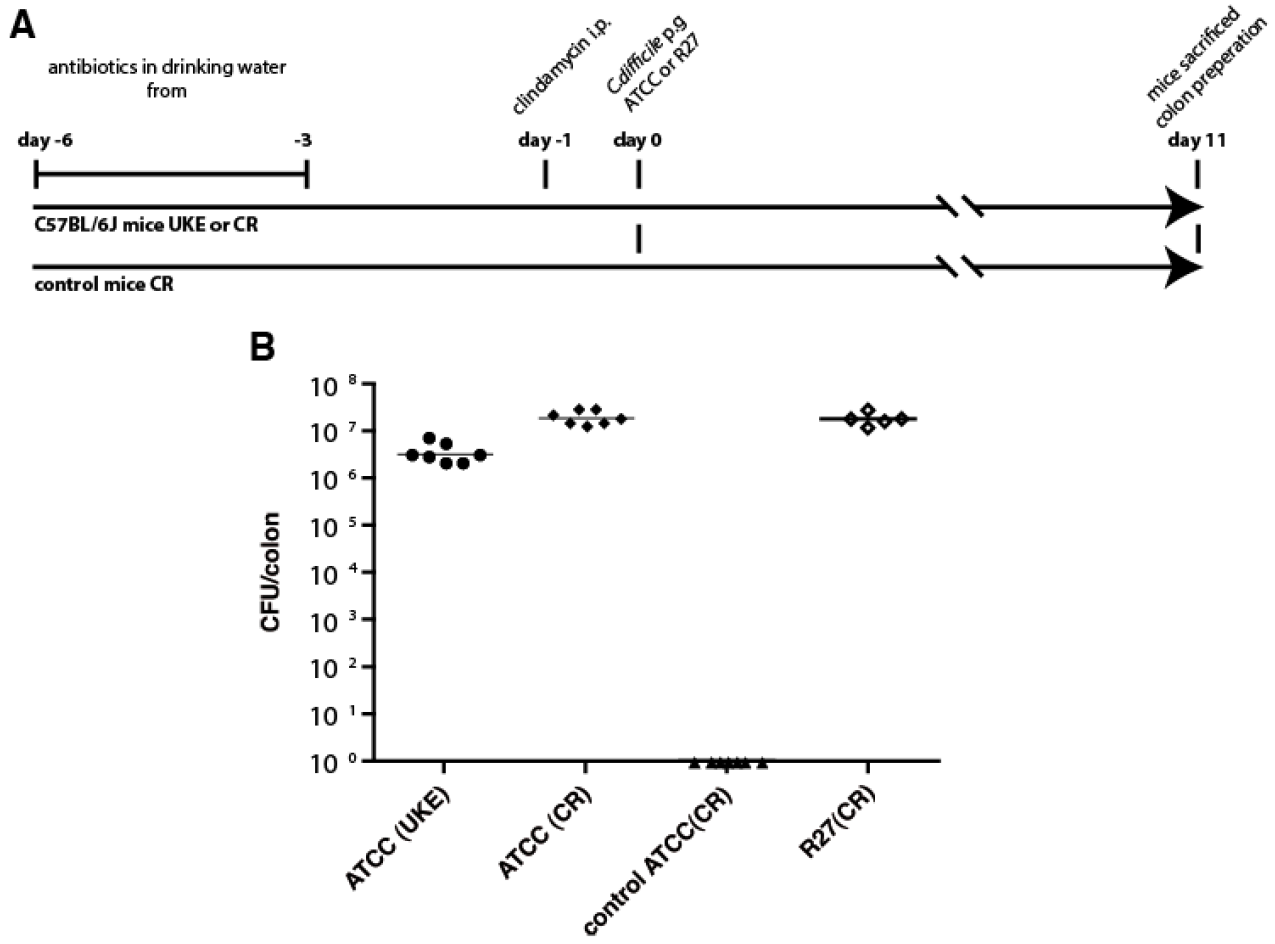

Fig. 3.11: Colonisation of C57BL/6J mice with *C.difficile* strains ATCC 43255 and R27. Prior to the experiment all mice were housed for three weeks in the central animal facility of the University Medical Center Hamburg-Eppendorf (UKE). C57BL/6J mice were obtained either from the animal facility of the UKE or purchased from Charles River (CR). **(A)** Mice (n = 7) were administered antibiotics in drinking water from day -6 to -3 (kanamycin 0.4 mg/ml, gentamicin 0.035 mg/ml, colistin 850 U/ml, metronidazole 0.215 mg/ml and vancomycin 0.045 mg/ml) and 200 µg clindamycin injected intraperitoneally on day -1. A control group did not receive any antibiotics. On day 0 mice were infected either with *C. difficile* strain R27 or ATCC 43255 (10^6 CFU) per os in 200 µl PBS. Mice were sacrificed on day 11 post infection and the entire colon with its contents was removed and homogenised for analysis. The number of colony-forming units (CFU) of *C. difficile* for the whole colon was evaluated by dilution series using CLO agar plates, (BioMérieux), cultured for 48 hrs in an anaerobe jar. **(B)** *C. difficile* colony forming units per colon on day 11 after infection.

-3 prior to infection (kanamycin, gentamicin, colistin, metronidazole and vancomycin). 200 µg of clindamycin was administered by intraperitoneal injection one day before infection. Either 10^6 CFU *C. difficile* ATCC 43255 or ribotype 027 were given on day 0 by oral gavage (Fig. 3.11 A). A control group did not receive any antibiotics, but was infected with *C. difficile* ATCC 43255.

To quantitatify colonization of the colon by *C. difficile*, the entire colon tissue of individual mice was homogenized in 2 ml deionised sterile water in Whirl-Packs. Colonies were quantified after plating of serial dilutions on CLO Agar Plates. All mice pretreated with an antibiotic regime, regardless of animal facility or *C. difficile* strain used, showed a detectable colonisation of the colon by *C. difficile* on day 11 after infection (Fig. 3.11 B). In contrast, no *C. difficile* colonies could be recovered from mice that had not been treated with antibiotics (Fig. 3.11 A, control ATCC(CR)). The estimated CFU in the colon ranged from 2.3- 8×10^6 for ATCC (UKE), 1.4- 3.2×10^7 for ATCC (CR) and 1.2- 2.8×10^7 for R27 (CR).

3.2.3 Signs of *C. difficile* Infection

To investigate the effects of the antibiotic regime on *C. difficile* infection in the mouse model, mice were given different doses of clindamycin (Fig. 3.12). Two groups of mice (n= 6) received antibiotics as described above in the drinking water from day -6 to -3. However, one group was treated with 200 µg and the other with 600 µg of clindamycin on day -1 before infection. Mice were administered 10^6 CFU *C. difficile* ribotype 027 spores by gavage on day 0. During the course of the experiment the weight of the mice was monitored every day from day -5 prior to until day 2 post infection and on four additional time points thereafter until day post infection (Fig. 4.12 A). A weight loss after the infection with *C. difficile* was apparent in mice treated with 200 µg of clindamycin, whereas the weight of mice treated with 600 µg clindamycin stayed constant. Noteworthily, weight in both groups decreased transiently during oral antibiotic treatment (measured on day -5 to -3), followed by a recovery on normal drinking water. The titer of *C. difficile* in the colon was analysed by serial dilution and selective agar on day 12 after infection (Fig. 3.12 B). From both groups of mice, regardless of the amount of clindamycin used, high levels of *C. difficile* (10^4 - 5 x 10^5 spores/colon) could be recovered.

During the course of the experiment, mice showed signs of disease, most notably diarrhoea and soiling of cages. Two days after infection with *C. difficile,* the nesting paper and cages of mice

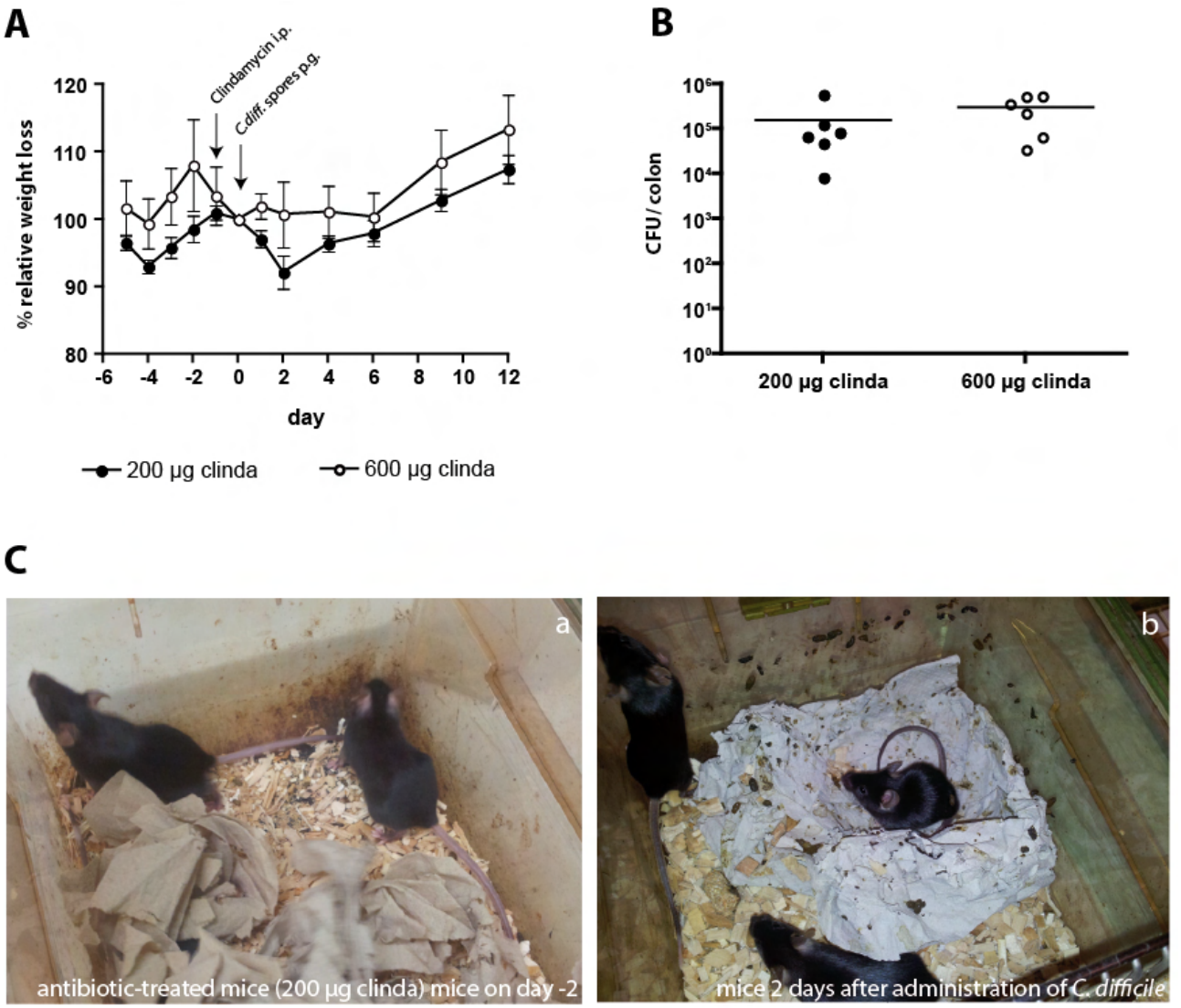

Fig. 3.12: Soiling of cages as an indicator of *C. difficile* induced diarrhoea. Groups of C57BL/6J mice (n = 6) purchased from Charles River Laboratories received antibiotics in drinking water from day -6 to -3 . 200 or 600 µg clindamycin was administered on day -1 by intraperitoneal injection. On day 0 mice were infected with an inoculum of 10^6 CFU *C. difficile* R27 in 200 µl PBS. **(A)** Weight of mice was determined daily form day -5 till day 6 and on day 9 and 12. Weight was related to the day of infection (day 0 =100%). **(B)** Mice were sacrificed on day 12 and the titer of *C. difficile* for the whole colon was evaluated by serial dilution. **(C)** Mice use paper provided in cages for nesting. (b) Healthy mice deposit solid excrements in the opposite corner of the cage and the paper used for nesting is clean. (a) Diarrhoea induced by infection with *C. difficile* is evident 2 days post infection by soiling of the cages and soiling of the nesting paper. Paper tissues were renewed daily. Photographs were obtained with an 8 MP, 3264 x 2448 pixels, Samsung I9100 camera.

showed a much higher level of soiling with soft stool compared to two day before the infection (Fig. 3.11 C).

3.2.4 *C. difficile*-induced diarrhoea is evident by soiling of cages and nesting paper

Signs of *C. difficile* infection became apparent in mice as diarrhoea, low consistency and high frequency of the stool. Quantifying of stool changes throughout an experiment was difficult.

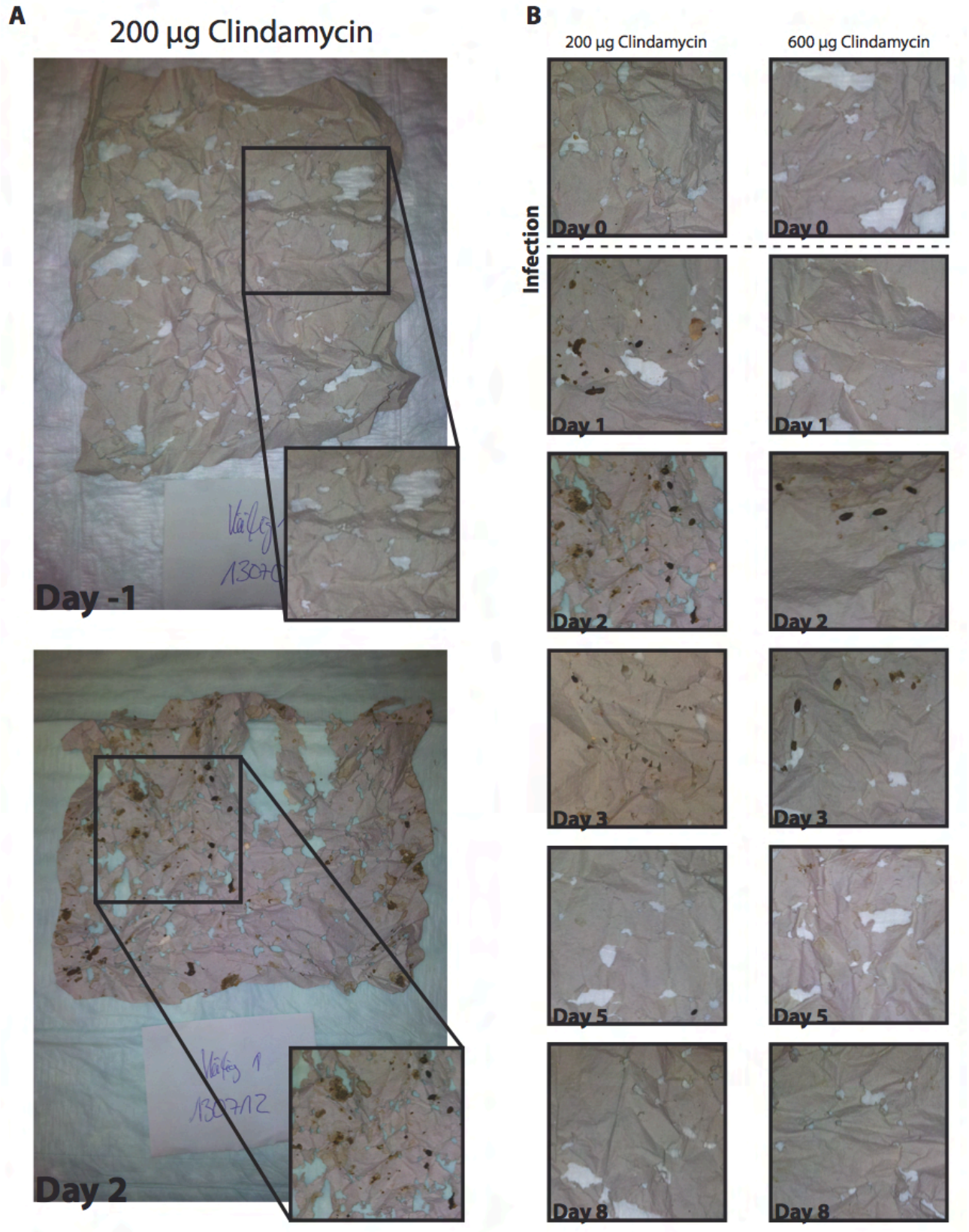

Figure 3.13: Time course of soiled bedding during infection with *C. difficile.* Nesting paper of the two groups of mice (n = 6) treated 200 or 600 µg clindamycin, were documented from day -1 till day 8 post infection. Mice were infected and treated as described for Fig. 4.11. Paper in cages was renewed daily and photographed with a Samsung I9100 camera. **(A)** Characteristic photos of entire nesting papers and representative details (inset) obtained before (day -1) and after infection (day 2). **(B)** Representative details of nesting papers photographed during the course of the experiment from day 0 to day 8.

Besides the stool itself, infected mice also behaved differently in their nesting pattern. Normally, mice nest with paper provided on one side of the cage and do not defecate on their nesting site. Infected mice soiled their nesting site, as evidenced on paper provided in the cages.

Thus, to monitor infection, paper in cages was fotographed and renewed daily. Two groups of mice (n=6) were treated with antibiotics in drinking water, different doses of clindamycin (200 and 600 µg) and infected with 10^6 CFU *C. difficile* ribotype 027 spores, as described before (Fig. 3.11). One day before the infection no apparent soiled bedding was seen, compared to two days after the infection with *C. difficile* (Fig. 3.13 A). A representative detail (inset) of the nesting paper was fotographed and the nesting papers were monitored for a period of eight days after infection (Fig. 3.13 B). On the day of the infection, the nesting paper of both groups showed no obvious soiling. The first soiled bedding started one day after the infection within the group of mice treated with 200 µg of clindamycin. On day 2, signs of infection were also seen in mice treated with 600 µg of clindamycin and continued until day 5 after infection. Both groups of mice returned to their normal nesting behaviour after seven days and no further soiling of nesting paper could be documented from day 8 onwards.

3.2.5 Weight loss observed during *C. difficile* infection

A second experiment was performed out to further investigate weight changes during the infection with *C. difficile* with two groups of mice (n=7). In this experiment mice were transferred daily into new cages with fresh floor covering, nesting paper and food. One group was infected with 10^6 CFU *C. difficile* R27 spores (Infection), the other with PBS only by gavage (Control). Both groups were pretreated with an antibiotic cocktail in the drinking water on day -6 to -3 prior to infection (kanamycin, gentamicin, colistin, metronidazole and vancomycin) and 200 µg clindamycin was administered by intraperitoneal injection one day before infection. Mice were weighed daily; from day -5 until day 4 and on six consecutive days until day 20 post infection.

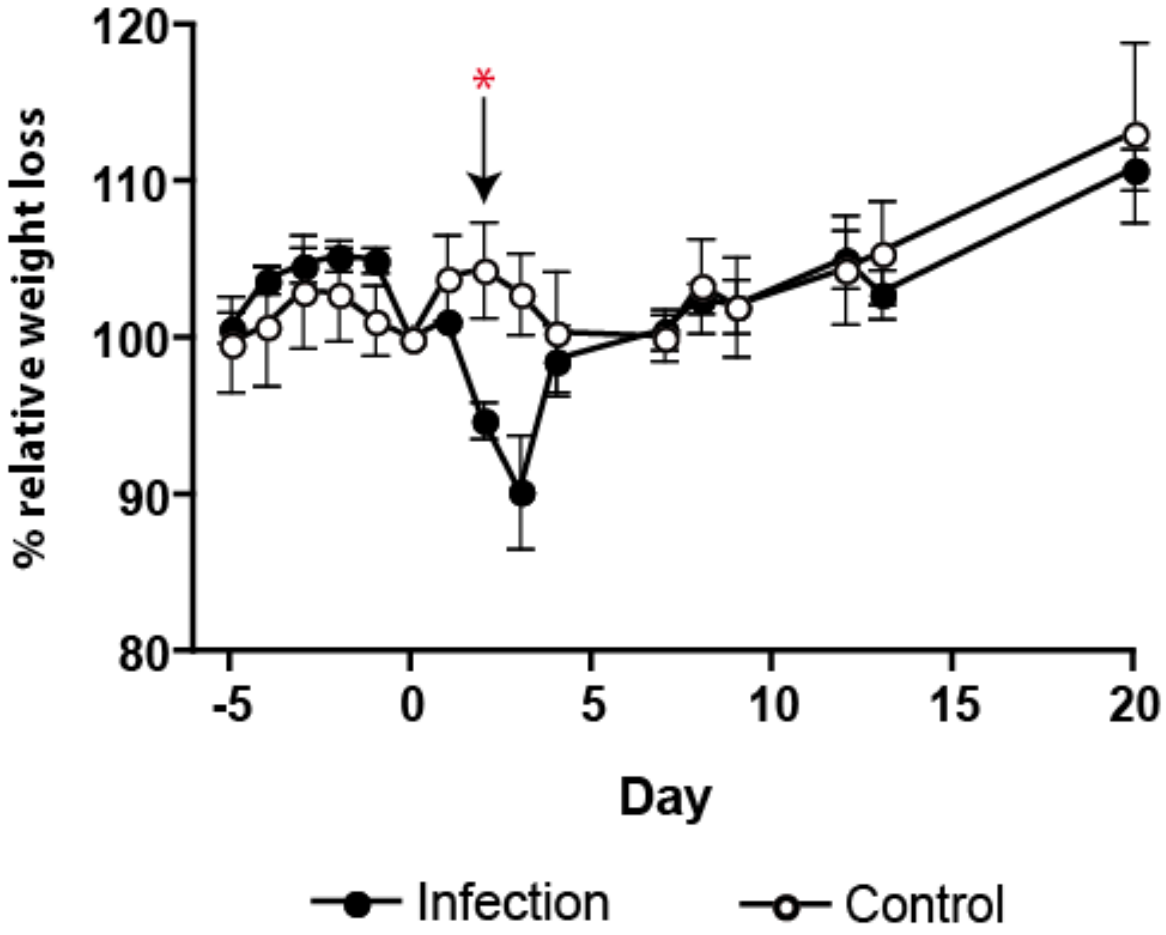

Figure 3.14: Infected mice show a weight slump in comparison to control group. All mice were housed for three weeks in the central animal facility of the University Medical Center Hamburg-Eppendorf before the course of the experiment. In this experiment mice were transferred daily into new cages with fresh floor covering, nesting paper and food. C57BL/6J mice (n= 7) purchased from Charles River Laboratories were treated with antibiotics as illustrated schematically in Fig. 4.10A. On day 0 mice were infected with an inoculum of 10^6 CFU *C. difficile* R27 in 200 µl PBS (Infection) or with 200 µl PBS only (Control). Weight of mice was determined daily form day -5 till day 4 and on several following days till mice were sacrificed 20 days after infection. Weight was related to the day of infection (day 0 =100%). Per group an additional 5 mice were sacrificed two days after infection for histological analysis, indicated by red starlet (see also Fig. 4.14, 4.15).

Mice infected with *C. difficile* showed a greater weight loss than mice treated with PBS only (Fig. 3.14). A strong loss of weight was seen in infected mice two days after infection. On day three a weight slump of more than 10% was observed in some mice. Subsequently, mice recovered their weight and even regained some by day seven, which equalled approximately to the same body weight as the control mice. Until day 20, both groups gained weight again in a similar and steady manner.

In parallel, another two groups of mice (n= 5) were treated in the same experimental way as described above. One group was given *C. difficile* by gavage and the other with PBS only. These mice were sacrificed two days after infection for histological analysis (indicated by red starlet Fig. 3.14).

3.2.6 Histological evidence of intestinal inflammation

C. difficile typically causes intestinal inflammation in mice (Buffie et al. 2012). The previous findings indicated a pathology induced by the second day after infection. As outlined above, two groups of mice were treated with antibiotics in the drinking water, clindamycin and with *C. difficile* spores R27 (Infection) or PBS only (control). Mice were sacrificed on day two after infection. The caecum and colon of the mice were removed, fixed overnight in 4 % paraformaldehyde, embedded in paraffin, cut into 4 µm thick slices and stained using Hematoxylin-Eosin.

Pathological features became apparent in the caecum and colon on the second day after infection with *C. difficile*, compared to mice in the same experimental scheme without infection (Fig. 3.15 and Fig 3.16). The observed characteristics included oedema in the submucosa (double

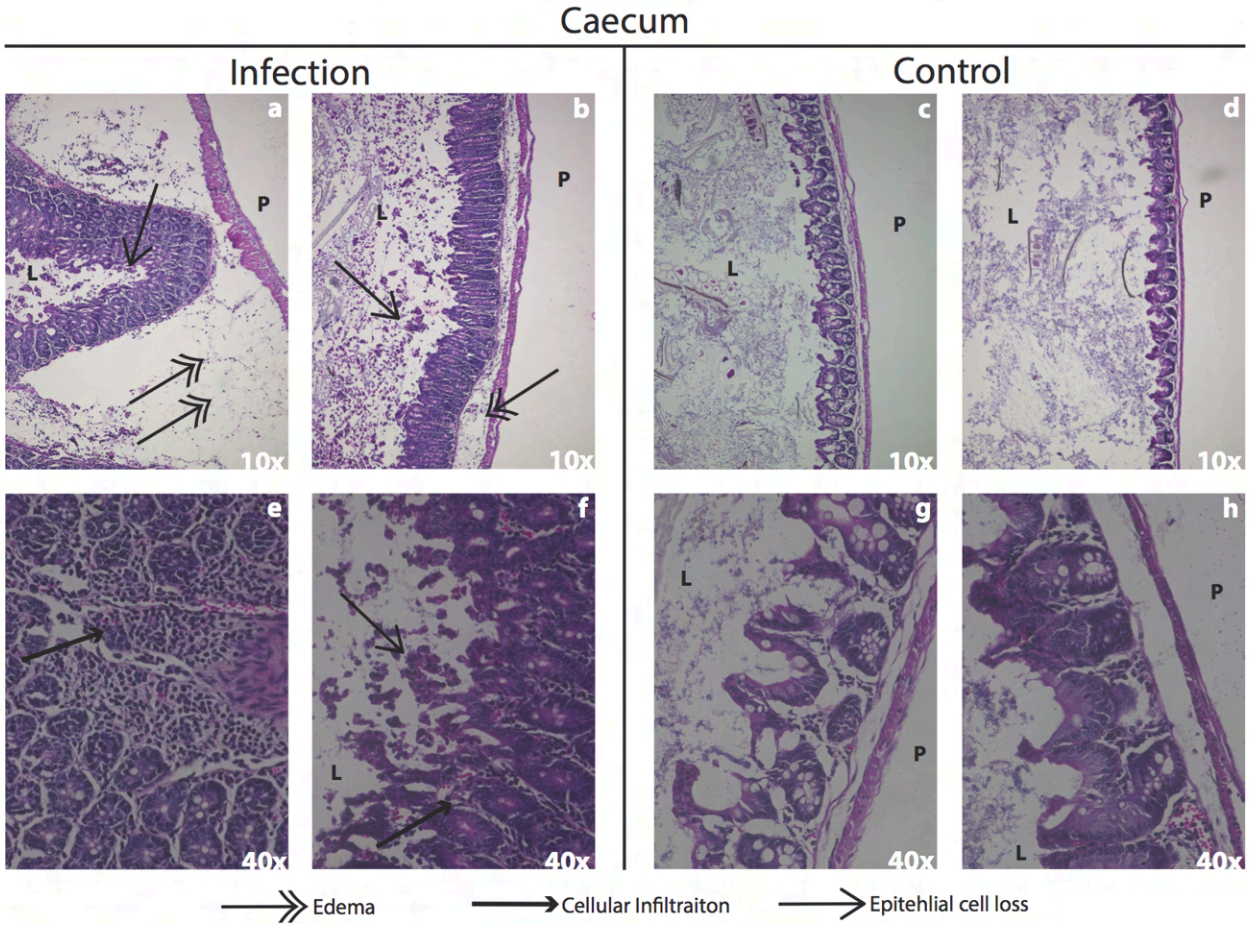

Figure 3.15: Histological signs of inflammation in colon of mice 2 days after infection with *C. difficile* (R27). Groups of C57BL/6J mice (n=5) purchased from Charles River Laboratories were treated as described in Fig. 4.13. From day -6 to -3 antibiotics were administered in drinking water and 200 µg of clindamycin injected intraperitoneally on day -1. On day 0 mice were infected with an inoculum of 10^6 CFU *C. difficile* R27 in 200 µl PBS (infection) and with 200 µl PBS only (control). Mice were sacrificed on day 2 post infection for histological analyses. Colon and caecum were removed, tissue with intestinal content was fixed overnight in PBS/ 4% PFA at 4°C, tissue was embedded in paraffin, cut into 4 µm thick slices, and stained using Hematoxylin-Eosin. Microscopical observation and documentation was carried out with 3D Laser Microscope VK 9700, Keyence equipped with a Colour CCD Image Sensor. (Histological processing was conducted by the Mauspathology Core Facility of the UKE). L = lumen of the intestine with content. P = peritoneal cavity.

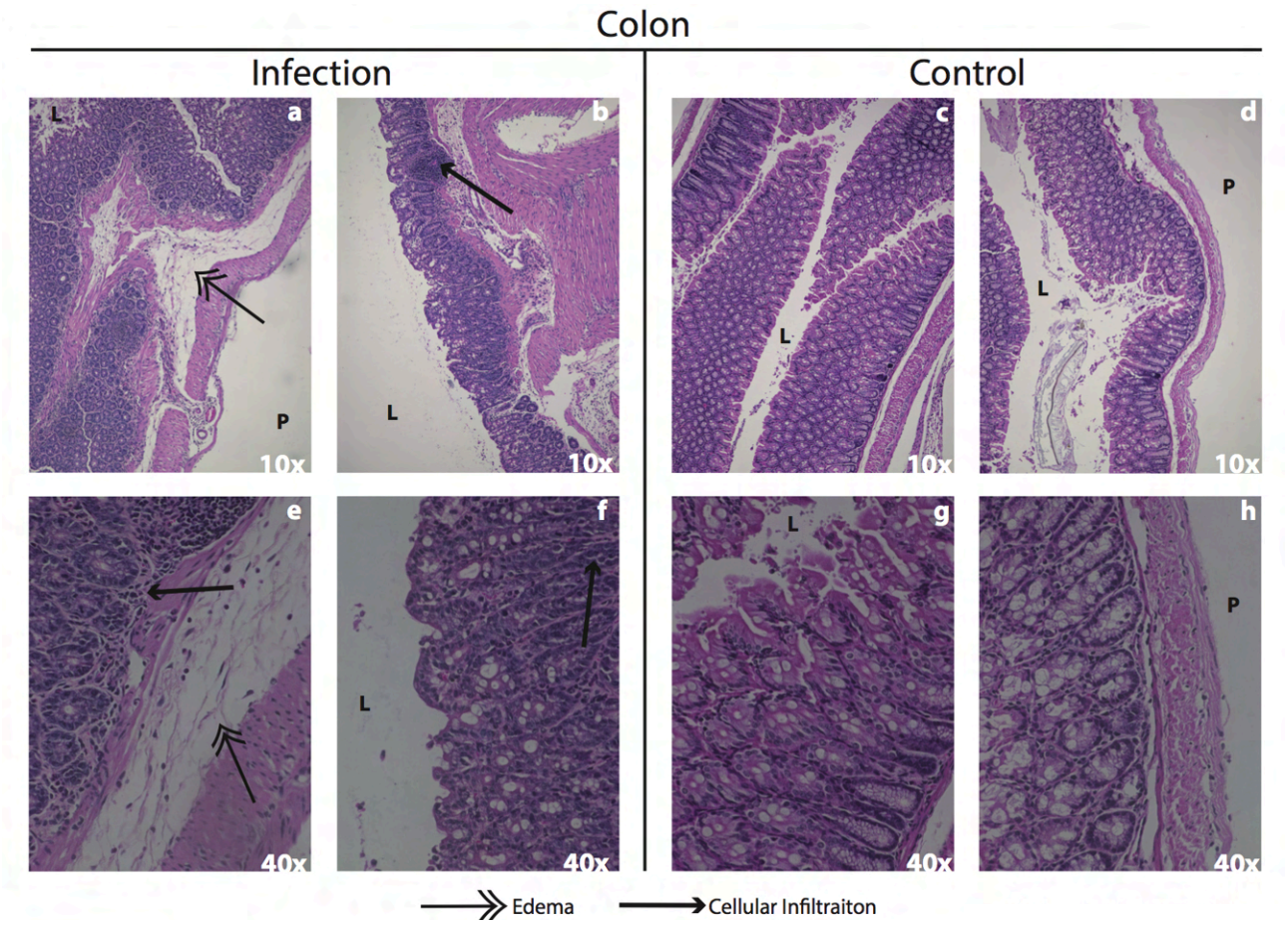

Figure 3.16: Further inflammation and cellular damage is observed in caecum of mice 2 days after infection by *C.difficile* (R27). The experiment and histological analysation were conducted as described in Fig. 4.14. L = lumen of the intestine with content. P = peritoneal cavity.

arrowheads), cellular infiltration of lymphocytes in the mucosa (small arrowheads) and epithelial cell loss of the mucosa (normal arrows). Signs of inflammation were more pronounced in the caecum than in the colon of mice. Epithelial cell loss of the mucosa was observed in the caecum of infected but not of uninfected mice (Fig. 3.15 and Fig 3.16).

4. Discussion

4.1 Llama derived single domain antibodies directed against CDTb

A common method to select recombinant single domain antibodies from immunized llamas is by panning of VHH-displaying phage libraries on the immobilised antigen (Holliger et al. 2005). For this purpose, the VHH-repertoire is amplified by PCR from cDNA of blood lymphocytes and cloned into a phage vector (Hoogenboom 2005). The VHH library generated for this work yielded after two to four rounds of panning numerous CDTb-specific VHHs (Supp. Fig. 7.1). Variety of sequences within a VHH family most likely originate from somatic hypermutation, a cellular mechanism of the immune system. Affinity maturation of immunoglobulins is accomplished by mutations in the hypervariable domains of the B-cell receptor locus, which correspond to the complement determining regions (Murphy et al. 2012). According to the amino acid sequence of the CDR3 region, if similar, VHHs were grouped into families. Some of these VHHs differ only by as little as one amino acid. It is likely that these VHHs originate from a common B-cell clone. The sequence is changed by somatic hypermutation, which in- or decreases its affinity towards the antigen.

High specificity and affinity for various antigens have been reported for many VHHs (Muyldermans 2013). VHHs possess a unique convex paratope, which is especially notable for the much longer CDR3 region compared to conventional variable regions of antibodies. This CDR3 region can form long finger like protrusions and interact with parts of the antigen normally not accessible, i.e. the active site of an enzyme (Desmyter et al. 1996, De Genst et al. 2006). In general, the immune system of lamas seems to possess the ability to generate VHHs capable of blocking the enzymatic activity of their target (Wesolowski et al. 2009). These characteristics may apply also to VHHs analyzed in this work.

VHHs selected on CDTb were produced in *E. coli* and tested for their binding specificity. The prokaryotic expression system in *E. coli* has the advantage of simple and cheap fermentation conditions (Arbabi-Ghahroudi et al. 2005). The protein production varied considerably even among the same VHH family members (Fig. 3.1). At the expected molecular weight, double bands can be observed. The upper band was recovered using metal affinity chromatography (NINTA) (not shown). Hence it is likely that some of the VHHs lose their c-terminal tags due to proteolytic

cleavage. For L-15.3 and L-15.1c a high level of production correlates with a clear ELISA signal. However a signal similar can be observed for L-15.1f and L-15.1g which differ considerably in their amount of protein. The L-3 family members showed a weak signal. This finding continued in later experiments for the L-3 family where VHHs were used from more consistent eukaryotic cell productions (Fig 3.3). *E. coli* also produces LPS (endotoxin) that might interfere in eukaryotic cytotoxicity assays. Considering LPS and the inconsistent production, VHH expression was moved to an eukaryotic expression system.

Seven VHH coding inserts were subcloned into the eukaryotic vector pCSE2.5, yielding three formats differing by their C-terminus (Fig. 3.2) tailored for different needs: VHH monomers with a 6xHIS and c-Myc *tag* were used to analyse the binding affinities (Fig. 3.3 B), VHHs linked to the CH2 and CH3 domain of a mouse-Fc IgG2c for mapping the differential epitopes (Fig. 3.4 A) and VHHs linked to avi *tag* can be used to create multivalent VHH formats. All three formats were produced at high and consistent yields of about 50-100 µg/ml in transiently transfected HEK293-6E cells cultured for 6 days in serum free medium (Fig. 3.3 A), comparable to rates reported by others for scFv-Fc antibodies (Jager et al. 2013). These production rates are higher than those for conventional monoclonal antibodies expressed in hybridoma cell lines (2-20 µg/ml).
Monovalent VHHs were analysed for their binding affinities to CDTb by serial dilution and ELISA, yielding high affinities in the lower nanomolar range (0.5 to > 50 nm)(Fig. 3.3 B and Table II, K_d). Using bivalent VHH antibody constructs in competitive binding ELISAs, three non-overlapping epitopes could be identified (Fig. 3.4 A). While the L-3 and L-15.1 families evidently bind to the same or an overlapping epitope, VHHs L-15.3 and L-19 bind independently of other VHHs (see also Table II, Epitope).
Nanobody based diagnostic tests have been developed previously, e.g. for the detection of human prostate-specific antigen (hPSA) (Saerens et al. 2005) or for the Marburg Virus (Sherwood et al. 2007). In patients, *C. difficile* is commonly detected in the stool by two types of test: Toxin enzyme immunoassays (EIAs) and nucleic acid amplification tests (NAATs). In patients, *C. difficile* is commonly detected in the stool by two types of test: Toxin enzyme immunoassays (EIAs) and nucleic acid amplification tests (NAATs). EIAs use monoclonal or polyclonal antibodies directed against Toxin A and/or B to identify infection by pathogenic *C. difficile* (Burnham et al. 2013). Because of potential false negative test results, most US hospitals use the more sensitive NAATs (Burnham et al. 2016). CDT has been detected from stool using crossreactive monoclonal antibodies against the related *Clostridium perfringens* Ib iota toxin (Carman et al. 2011). This

research based EIA showed a high specificity (no CDT negative cases were detected as positive), but lacked sensitivity as 32% of CDT positive strains were not identified. VHHs recognizing different epitopes of CDTb could be used to develop novel diagnostic assays. This could help to detect toxigenic *C. difficile* strains actively producing the binary toxin and to clarify its role in severe cases of CDI. Especially as only the presence of binary toxin genes has been correlated to infections, further characterisation of CDT positive cases is needed (Gerding et al. 2014).

Using HT-29 cells, which express LSR, the receptor for CDT, VHHs were tested for their potential to inhibit the cytotoxic effects of CDT. At high concentrations (8 fold excess) all members of the L-15.1 family tested were able to inhibit CDTa + CDTb mediated cytotoxicity (Fig. 3.6, 3.7). In contrast, neither L-19 and L-15.3 showed any protective effects even though both VHHs bind CDTb sufficiently (see ELISA Fig. 3.3, 3.4). Interestingly treatment with L-15.1g partially inhibited disruption of the cytoskeleton even at equimolar concentrations with CDT (Fig. 3.8, 3.9). This observation is in accord with the higher apparent affinity of L-15.1g (Fig. 3.3), compared to L-15.1b and L-15.1c, from which L-15.1g differs by one amino acid in the CDR3 region (Supp. Fig. 7.1). The competitive binding ELISA revealed an overlapping epitope for the L-15.1 and L-3 VHH families (Fig. 3.4). However, none of the L-3 VHH family members tested inhibited the cytotoxic effect of CDT. This might be due to the lower affinity of the L-3 VHH family (Fig. 3.1, 3.3). Another feasible explanation might be that L-15.1 and L-3 members bind to overlapping but distinct epitopes that sterically hinder each other from binding to CDTb, but only the L-15.1 VHHs hinder formation and/or entry of the binary toxin. The results of the cellular cytotoxicity assays are

anti-CDTb

VHH Family	CDR3	K_d	Epitope	IC_{50} Cytotoxicity
L-3	**RGY**	**> 50 nM**	**1**	**> 1 μM**
L-15.1	**KVGANILTRSIGYKY**	**0.5-2 nM**	**1**	**4 nM**
L-15.3	**TNKVYTDGRLEEYDY**	**9 nM**	**2**	**> 1 μM**
L-19	**DGRSNLRANYDSADYGMAY**	**15 nM**	**3**	**> 1 μM**

Tabel II: An outline of the characteristics found for the single domain antibodies directed against CDTb. The table shows a summary of the different characteristics found for the VHHs direct against CDTb. The K_d value represents the dissociation constant determined for the VHHs. Epitopes were given arbitrarily, if VHHs block one another in ELISA. IC_{50} cytotoxicity describes the concentration of VHHs needed to inhibit 50% of the cell rounding of HEK-29 cells incubated with CDT toxin. The CDR3 sequence of the VHH families is given and the position of the variant amino acid is highlighted in grey.

underlined by the results of a radioactive ADP-ribosylation assay, in which VHHs l-15.1b and L-15.1g both inhibited CDT-mediated ADP-ribosylation of actin in CDT-treated HT-29 cells (Fig. 3.10).

4.2 The binary toxin CDT

CDT belongs to a group of binary ADP-ribosylating toxins that consists of two different components (see Fig. 1.1). CDTa is responsible for the enzymatic activity, CDTb for the translocation of CDTa inside of the cell (Gerding et al. 2014). When the enzymatic component arrives in the cytosol, it ADP-ribosylates G-actin at arginine-177 using cellular NAD+ as substrate (Gulke et al. 2001). This inhibits the polymerisation of F-actin and causes rounding and cell death due to break-down of the cellular cytoskeleton (Aktories et al. 1989). In addition, microtubule-based protrusions are induced on the surface of epithelial cells by CDT, which appears to increase the adherence of bacteria (Schwan et al. 2009). Physiologically, polymerisation of microtubules is stopped by the cortical actin layer beneath the cell membrane. It is not yet understood how this capture function is altered by CDT (Aktories et al. 2017). Without the transport component CDTb, CDTa cannot enter the cytosol and inflict damage upon the cellulars cytoskeleton (Barth et al. 2004).

CDTb is composed of 876 amino acids with a molecular mass of 98.8 kDa (Perelle et al. 1997). The sequence shares similarities to other bacterial toxins, whereby 36% identity is found with the protective antigen (PA) of *B. anthracis* toxin (Young et al. 2007). The binding domain of CDT has not yet been crystalized. However based upon the structure of PA, the structure of CDTb and its different domains can be inferred (Gerding et al. 2014). CDTb can be modeled onto the 3D structure of PA (pdb code 1ACC) using SwissModel (Fig 4.1). SwissModel is a bioinformatics web-server used for homology modeling, a technique to generate a rough three-dimensional structure model of a protein that is related in sequence to a protein of known structure.

CDTb is expressed with a signal sequence of 42 amino acids. The activation domain, domain I is formed by the first 296 residues, which is cleaved by serine-type proteases, releasing a 20kD peptide from mature, activated 75 kDa CDTb (Perelle et al. 1997). PA is proteolytically activated at a surface loop of Domain I at the sequence RKKR (residues 164-167). This sequence is not found within CDTb. However cleavage is most likely to occur at the corresponding site between Lys209 and Leu210 (Gerding et al. 2014) (see also the sequence alignment of CDTb and PA in

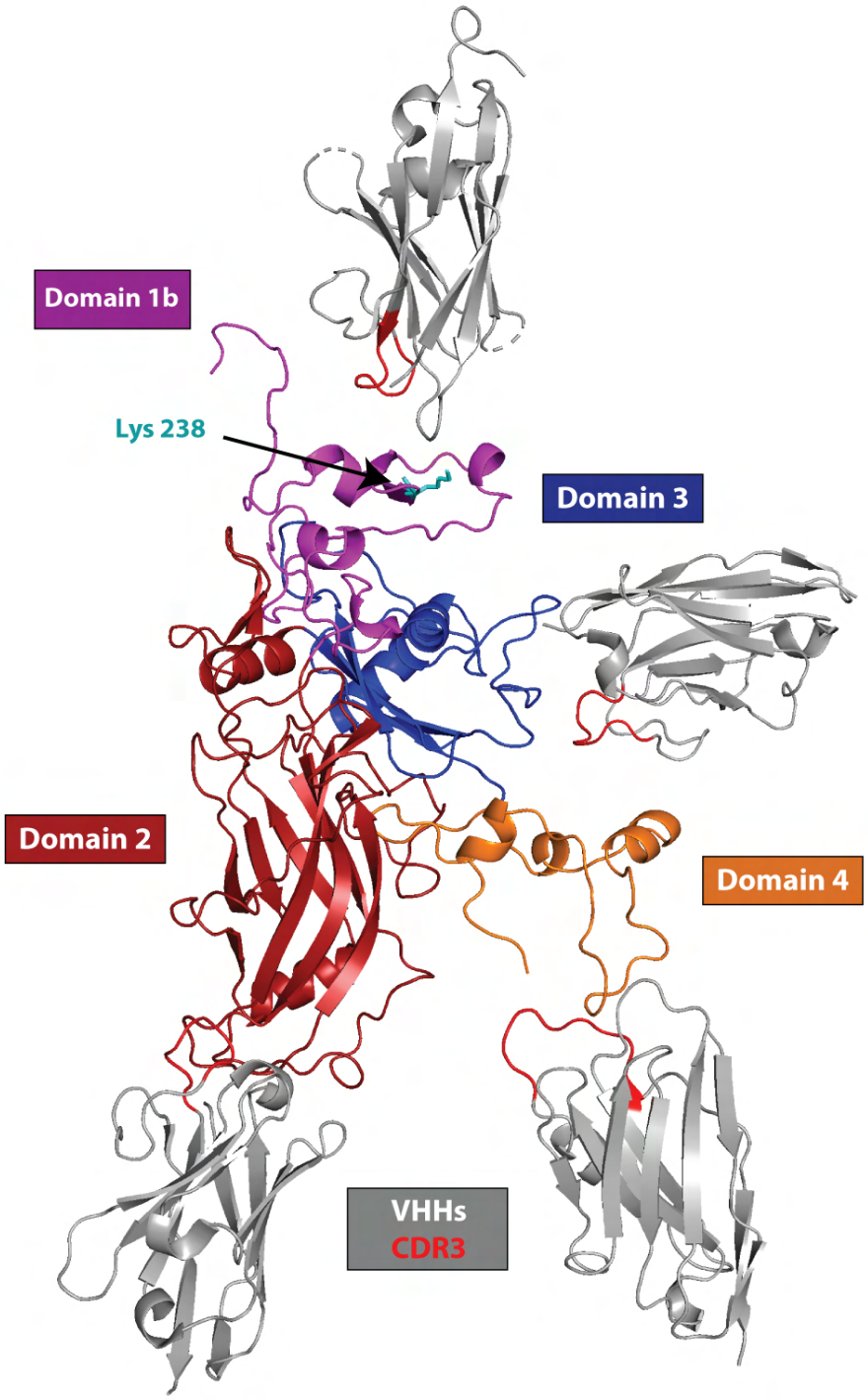

Figure 4.1: Llama derived single domain antibodies could potentially bind at four different domains of CDTb. The 3D structure of the protective antigen (PA) of *B. anthracis* toxin has been crytalized and much about its structure-function relation is known. As it shares about 36% sequence similarity to CDTb the different domains for CDTb can be hypothesised. CDTb was modeled onto the 3D structure of PA (pdb code 1ACC) using SwissModel. The VHHs selected could be interacting with Domain II- VI, which were used for immunization of the llama. Furthermore assembling of the catalytic domain CDTa to CDTb could be hindered, possibly by binding around Lysin 238 (cyan). Four CDTb non-specific VHHs were used to illustrate antigen- antibody interaction (PyMol was used to generate 3D models using the pdb files 1ACC, 1MEL, 5U64 and 5U65.). The CDR3 region of the four VHHs is coloured in red.

Supplementary Fig. 7.2). Domain III (residues 514- 617) is involved in oligomerization of CDTb into a heptamer in solution or on the cells surface (Barth et al. 2004). Domain III of PA adopts a ferridoxin-like fold. A similar structure can be observed in the CDTb model. The C-terminal Domain IV (residues 617- 876) mediates binding to the host cell receptor. This domain is only partially represented in the model of CDTb until residue 675, however similar to PA there is only marginal contact with the rest of the protein. Domain II (residues 297-513) is involved in membrane insertion and pore formation. Here the structure of a β-barrel core with extensive side loops with a modified greek key motif above can be observed. The 2β2–2β3 loop of the CDTb model shows approximately the same length as in domain II of PA. The 2β2–2β3 loop forms the the transmembrane portion of the β-barrel during pore formation (Benson et al. 1998, Qa'dan et al. 2005).

The crystallographic structure of the heptameric prepore of PA has been identified and studied (Young et al. 2007). The structural SwissModel of CDTb can be assembled into a heptamer by aligning it onto the individual PA molecules of the heptameric prepore using PyMol (Fig. 4.2). A hollow ring structure can be observed, with the individual CDTb molecules packed like pie wedges. Domain III and IV can be found on the outside, domain I and II on the inside of the ring structure. Compared to the multimer structure of PA several structural details can be found. On the top of the heptamer Lysin 238 can be observed, which corresponds to Lysin 197 of PA. It has been shown that the Lysins 197 of two adjacent PA molecules interact and cause binding of the enzymatic component of anthrax toxin (Melnyk et al. 2006). The PA heptamer can bind under saturating conditions only three molecules of the A subunit of the toxin (Pimental et al. 2004). For CDT the ratio still has to be shown. Notably, the two different ligands for PA, LF (90 kDa) and EF (89 kDa) are considerably larger then CDTa (48 kDa). Another significant structural detail of PA lies within the pore, residue Phe427. Studies have demonstrated that allocation of the enzymatic subunit to the inside of the host cell is not simply achieved by a passive process, but rather by active catalisation orchestrated by Phe427 (Krantz et al. 2005). It is not understood how precisely Phe427 provokes translocation. However Phe427 is likely to “clamp” the flexible N-terminus of the A subunit, creating within the channel an environment that mimics the hydrophobic core of the unfolded molten globular substrate, hence reducing some of the energy barrier to facilitate entrance into the cells cytosol. A corresponding residue can be found in the structure of CDTb, phenylalanin 455. The reposition of phenylalanine during prepore-to-pore conversion is presumably caused by two adjacent amino acids forming hydrogen bonds, glutamin 454 and glutamin 425 (see also

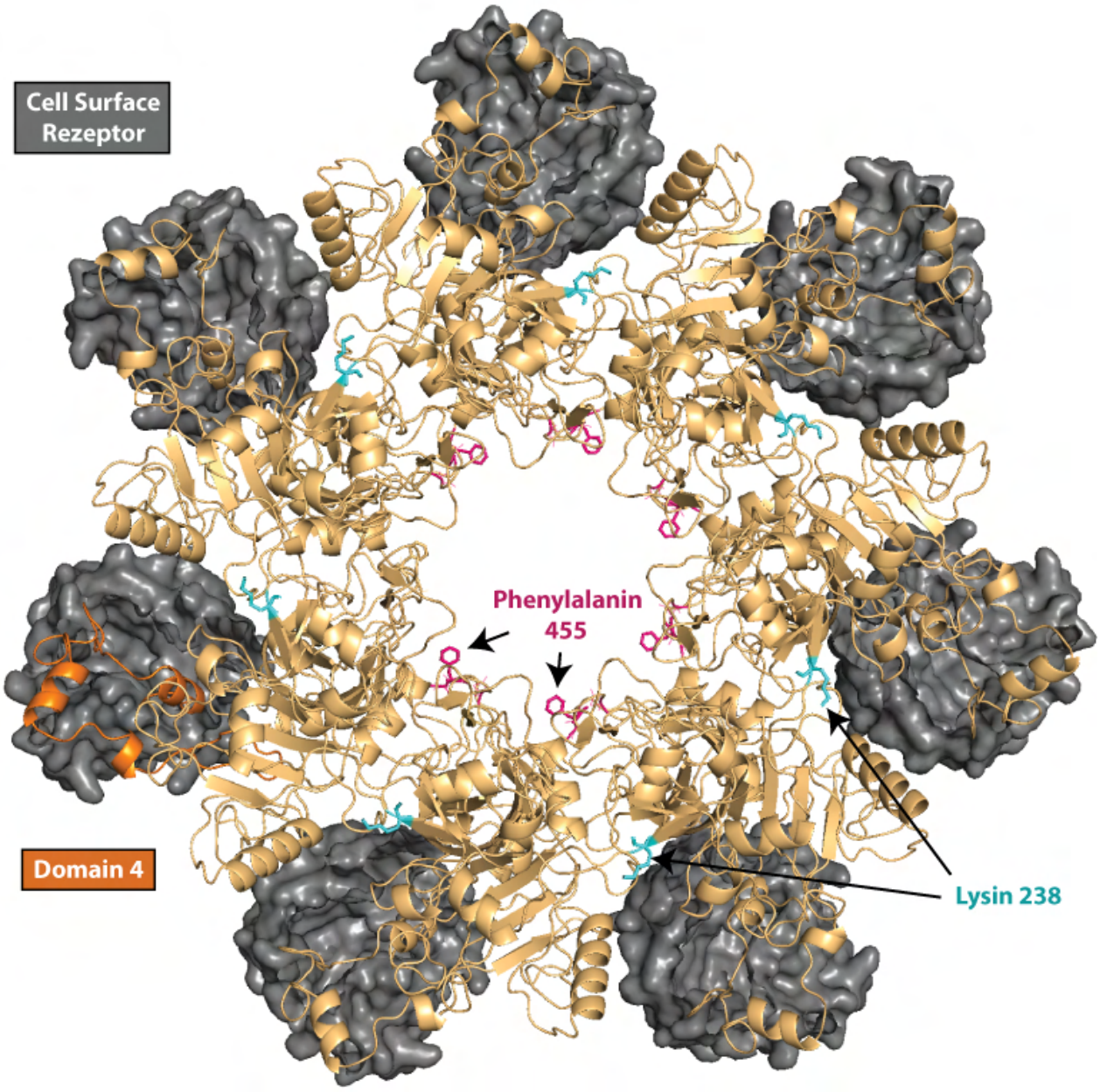

Figure 4.2: CDTb assembles into multimer upon binding host cells receptor. Besides the structure of a monomeric protective antigen (PA) of *B. anthracis* toxin, the pentameric multimer formed upon binding the cellular receptor has been studied and crystallised. The 3D structure of CDTb generated using SwissModel was assembled into the multimer by alignment with PA pentamer with its receptor (pdb code 3hvd) using PyMol. The CDTb pentamer can be seen from a top-down view with its four domains. The cell surface receptor of PA (ANTXR2 I domain) at the bottom of each domain IV was kept to illustrate potential binding of a CDTb multimer. Domain IV, responsible four binding the cell receptor is shown (orange). Residues Phenylalanin 455 (pink) and Lysin 238 (cyan) are also shown.

Supplementary Fig. 7.2). In PA and other binary toxins of *Bacillus* species the reposition is most likely orchestrated by a salt bridge between Asp426 and Lys397 (Melnyk et al. 2006).

The host cell receptor of CDT has been identified as the lipolysis-stimulated lipoprotein receptor (LSR), which is involved in lipoprotein clearance (Papatheodorou et al. 2011). After binding to LSR, CDT induces the accumulation of lipid rafts at the cell membrane, oligomerization occurs as well as binding of the enzymatic component (Papatheodorou et al. 2013). Subsequently the receptor-toxin complex is internalised by endocytosis. The structural model of CDTb raises the question of where the selected VHHs could bind and how the VHH L-15.1 family might inhibit cytotoxicity. Binding to the first 200 amino acids of the activation domain I is excluded, as CDTb

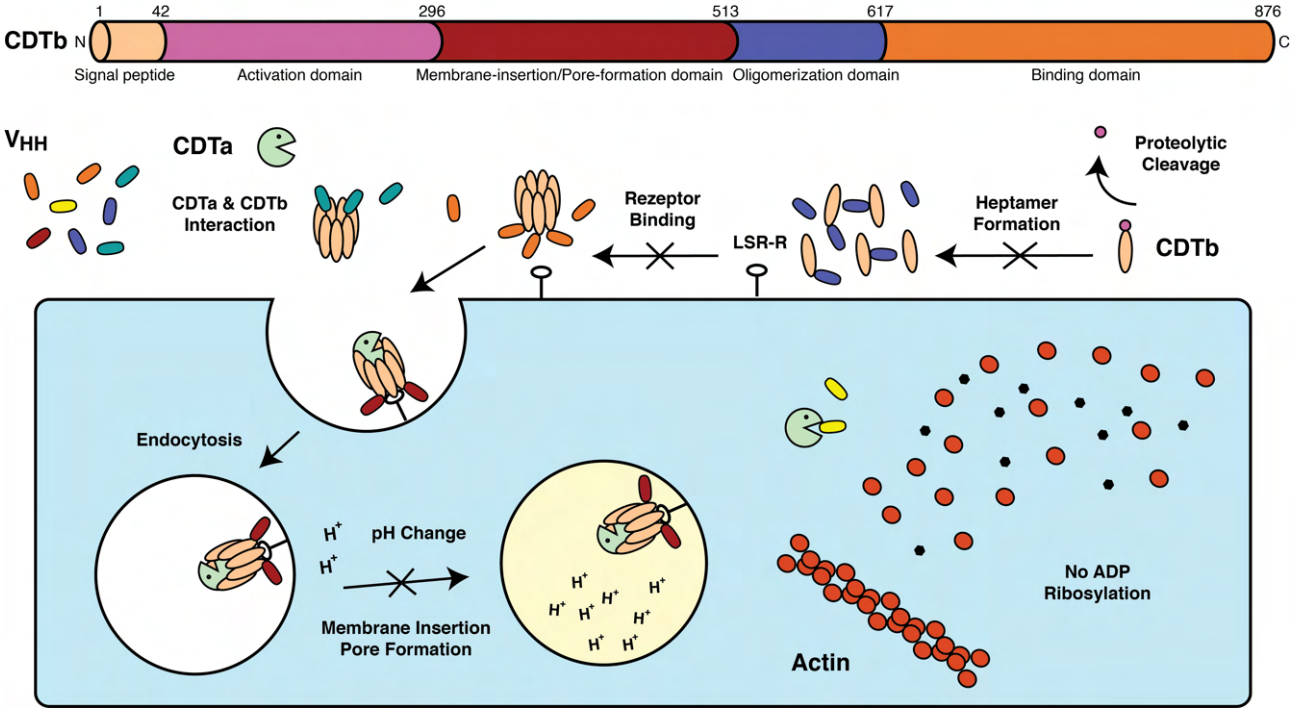

Figure 4.3: Inhibition of CDT could be achieved by VHHs binding at different sites of CDTb. The experiments conducted (Fig 4.6- 4.10) indicate that the L-15.1 family effectively neutralise the cytotoxicity CDT and prevent its enzymatic activity. The binding domain of CDT has not yet been crystalized, but shows great sequence similarities with the protective antigen (PA) of *B. anthracis* toxin. On the basis the structure of PA four different domains and their function can be hypothesised **(CDTb)**, which could be targeted by the VHHs selected **(VHH)**. It is unlikely that the VHHs interfere with the first domain **(purple/ Activation domain)**, as CDTb was activated by trypsin before the llama was immunised. Domain III **(blue/Oligomerization domain)** is responsible for the oligomerization of CDTb into heptamers and could be a potential epitope of the VHHs. LSR is the cell surface receptor of CDTb. The interaction could be inhibited by a VHH binding to domain VI **(orange/Binding domain)**. Independently of a certain domain a VHH could hinder the interaction between CDTa and CDTb **(green)**. Finally after the toxin-receptor complex is internalised, the membrane insertion and pore formation could be blocked, if a single domain antibody binds domain II ranging from amino acid 258 until 480 **(red/Memrane-insertion/Pore-foramtion domain)**. In addition an inhibition could be observed throughout the experiments for L+8, the CDTa specific VHH **(shown in yellow)**.

was activated by proteolytic cleavage before immunisation of the llamas. Therefore the selected VHHs could interact only with domains II-VI (Fig. 4.1). The L-15.1 VHH family could potentially block oligomerization (mediated by domain III), binding of LSR (mediated by domain IV) (Barth et al. 2004, Hussack et al. 2011) or steric blockade of the pore formed by domain II (Fig. 4.3). It is also conceivable that VHH L-15 inhibits binding of CDTa to CDTb. This could be achieved for example by binding near Lysin 238 of the nicked remaining residues of domain I. All possibilities could occur at the high affinities and for the inhibition at equimolar concentration observed. In any case, the nanobodies of the L-15 family represent a promising, potential therapeutical tool.

4.3 Murine *C. difficile* infection

C. difficile is one of the leading pathogen of nosocomial infections especially in developed countries. In 2011 *C. difficile* accounted for up to half a million infections and about 29.000 deaths in the US alone (Lessa et al. 2015). Particular circumstances and characteristics of the bacteria, patients and the health care system provide a window of opportunity for the infection to flourish. The persistence and spread of *C. difficile* in hospitals is facilitated by its ability to form spores, which are resistant to ethanol-based disinfection regimes (Lawley et al. 2010). Most cases of CDI are linked to a disruption of the commensal microbiota by an antibiotic regime, in particular with cephalosporins and clindamycin (Slimings et al. 2014). The commensal microbiota compete with *C. difficile* by producing bacteriocins (Rea et al. 2011). Indirectly the production of secondary bile acids and the fever consumption of sialic acid and succinate by the commensal microbiota seem to play a role in the protection against *C. difficile* (Ferreyra et al. 2014, Theriot et al. 2016). Lately the commensal bacteria *Clostridium scindens*, capable of producing secondary bile acids, has been identified as being highly associated with CDI resistance (Buffie et al. 2015). Once the infection by *C. difficile* has been established, virulence is associated with its toxins (Kelly et al. 2008). The rho-glycosylating Toxin A and B can induce diarrhoea and colitis (Aktories et al. 2017). The toxigenic ADP-ribosyltransferase CDT is additionally produced by 5-30% of all *C. difficile* strains. Its role during infection is still controversial and under investigation (Gerding et al. 2014). Hypervirulent *C. difficile* strains like ribotype 027 (NAP1) or 078 (NAP7,8) are able to produce CDT, but also possess a stop codon in the *tcdC* gene responsible for the regulation of Toxin A and B production (McDonald et al. 2005, Goorhuis et al. 2008). The inactive *tcdC* protein can lead to 16-(Tox A) and 23-fold (Tox B) higher toxin production (Warny et al. 2005). The presence of the binary toxin gene has been linked to recurrence of infection, whereby in the same study the lack of *tcdC* and ribotype

027 was not (Stewart et al. 2013). Among patients infected with CDT gene positive strains, more frequently increased white blood cell count, mucoid stool and even higher case-fatality rates could be observed (Bacci et al. 2011, Kim et al. 2013). In animal experiments, the effect of CDT has been assessed using *C.difficile* isolates that lack the expression of Toxin A and B. Four *C. difficile* isolates expressing CDT only could colonise clindamycin-treated hamsters, but did not cause diarrhoea or death (Geric et al. 2006). However the supernatant of these four strains showed an entertoxic effect using a rabbit ileal loop assay. A later study investigated CDI in hamster using *C. difficile* mutants derived from ribotype 027 with different combination of inactivated toxin genes (Kuehne et al. 2014). ere, significantly more hamsters died upon infection with mutants carrying active Toxin A as well as CDT genes. Fatality was even observed among strains with only CDT not being inactivated, though symptoms of CDI seen were not typical. It was speculated that CDT contributes to infection, but might not be sufficient to cause disease by itself. Recently it was reported that *C. difficile* suppresses eosinophils in the blood and colon of mice, hereby enhancing virulence (Cowardin et al. 2016). In this study using two ribotype 027 strains, CDT was found to elevate severity of infection and mortality (60% vs 100% survival) compared to strains with inactive CDT.

C. difficile was first described in 1935 from the fecal flora of healthy newborn infants (Hall et al. 1935). As the germ was difficult to isolate and grew slow in culture it was given the descriptive name *difficile* (Kelly et al. 1998). Challenges to work with *C. difficile* include strict anaerobic conditions for growth, specific culture media and the generation of spore stocks. In this work stable and high titer stocks were achieved following an established protocol for the laboratory maintenance of *C. difficile* (Sorg et al. 2009). Hamsters have been traditionally used to study CDI in animals, as they are highly susceptible to infection (Lusk et al. 1978). However, only a limited amount of animal specific reagents, genetically modified animals and knowledge about the genetic background is available for hamsters. A murine infection model would be more suitable for conventional laboratory settings. In addition, the fulminant course of disease is believed to not resemble the infection in humans. In 2008 an infection model in mice was described which closely represent the human disease (Chen et al. 2008). This model has been widely used by others and is the template for the animals experiments conducted in this work. Methods included a three day treatment of five antibiotics in the drinking water and clindamycin injected intraperitoneally to disrupt the commensal microbiota, followed by a *C. difficile* spore challenge by gavage (Fig. 3.11). Stable colonisation of the colon of mice from different animal facilities could be achieved using two

C. difficile strains. This was dependent upon the antibiotics given prior to infection, as otherwise *C. difficile* could not be recovered (Fig. 3.11 B).

In this work mortality in mice could not be observed, which has been described by others using the same methodology (Chen et al. 2008, Jarchum et al. 2011, Cowardin et al. 2016). Also the increase of antibiotics did not cause mortality or elevated the titer found in the colon of mice (Fig. 3.12 B). However signs of the disease were apparent as diarrhoea and soiling of cages (Fig. 3.12 C). This became especially apparent on the nesting paper provided (Fig. 3.13 A). Throughout the experiment altered nesting behaviour and soiling continued for at least five days after infection (Fig. 3.13 B). CDI in mice is also accompanied by weight loss and histopathology of the intestine. In one experiment, mice maintained their body weight throughout CDI (Fig 3.12 A), whereas in a subsequent experiment weight loss was observed in infected mice compared to a control group that received no clostridia (Fig. 3.14). On day three after infection, the weight was at its lowest and mice recovered from this point onwards, which is the typical pattern observed in murine CDI. Compared to previous infections mice were transferred daily into new cages with fresh floor covering, nesting paper and food, emphasising the role of the nesting environment of mice to achieve a successful infection. Histopathological changes were found in five mice which were sacrificed two days after infection (Fig 3.15, Fig 3.16). The intestinal damage seen can be compared to results found by others (Buffie et al. 2012). In future a pathological score should be established and histological examination carried out blindly by a pathologist. The commensal microbiota, an important for protection from CDI, is affected by maternal transmission, littermates and food provided (Ley et al. 2005, Turnbaugh et al. 2009, Ubeda et al. 2012). Therefore mice in this work might have been less amenable for infection, because of external circumstances affecting the flora of the intestine. This is underlined by an observation from the original mouse mode, where CDI did not induce any symptoms in the CD-1 mouse strain from Charles River Laboratories (Chen et al. 2008). Notwithstanding the difficulties, the murine infection model for *C. difficile* established here can be used in the future to study the role of CDT in CDI.

4.4 Therapeutic strategies targeting *C. difficile* infection

Since the 1970s the standard therapy for acute and recurrent *C. difficile* infection has been metronidazole and oral vancomycin, while vancomycin shows greater efficacy for severe cases (Leffler et al. 2015). Novel antibiotics include fidaxomicin, which reduces the risk of recurrence from 25 to 15% compared to vancomycin (Louie et al. 2011). However the rate of recurrence could

not be resolved for patients infected with ribotype 027 strains, pointing out the need of alternative therapeutical approaches especially for hypervirulent strains. As the burden of *C. difficile* is on the rise numerous approaches for novel treatments have been made. The infection rate of *C. difficile* can be reduced by 77% simply by prohibiting the routine use of ciprofloxacin and ceftriaxone accompanied by educational campaigning (Dancer et al. 2013). Probiotics have been used to prevent an infection, but with rather mixed results (Leffler et al. 2015). Another interesting prevention strategy is to co-administer agents that inactivate antibiotics in the large intestine used for systemic treatment, hence protecting the commensal microbiota (Miossec et al. 2014). At least two vaccines are undergoing clinical trials, which are mainly composed of Toxin A and B components (ClinicalTrials.gov numbers, NCT01887912 and NCT02117570). The recurrence of *C. difficile* can be reduced by administering the non-toxigenic *C. difficile* strain M3 after an antibiotic treatment (Gerding et al. 2015).

The capability to neutralise cytotoxicity at equimolar concentration render VHHs of the L-15 family potentially therapeutical tools. Therapeutic antibodies have been mainly targeted for the two major toxins, Toxin A and B. Actoxumab and bezlotoxumab, two fully human monoclonal antibodies, are leading the way in clinical development. Besides these antibodies, no others have been tested in clinical trials (Morrison 2015). Targeted against Toxin A and B, respectively, both bind the receptor-binding domain (RBD) of their target and potentially neutralise it in vitro (Babcock et al. 2006, Davies et al. 2013). Recently bezlotoxumab completed phase III trials, reducing recurrence for 12 weeks compared to placebo in conjunction with standard-of-care antibiotic therapy (Morrison 2015). Additional Toxin A/B antibodies will follow, as others have reported improved preclinical efficacy in reducing CDI recurrence and severity of diarrhoea (Davies et al. 2013, Anosova et al. 2015). Single domain antibodies have also been isolated against Toxin A/B (Hussack et al. 2012, Yang et al. 2014). The CDT specific nanbodies described here could potentially be used therapeutically, especially for the hyper virulent strains of *C. difficile*. No adverse side effects could be seen for the systemic application of llama derived nanobodies during clinical trials (Van Bockstaele et al. 2009). However due to their small size being below the renal filtration molecular mass cut-off, the serum half life is of VHHs is low (Kontermann 2011). This limitation can be overcome by genetically fusing nanobodies to the hinge, CH2, CH3 domains of a conventional IgG antibody (as conducted in this work Fig. 3.2, Fig. 3.3 A) or to a second albumin specific nanobody (Tijink et al. 2008).

The mucosal barrier in the gut raises concerns, whether systemic administered antibodies can sufficiently reach the site of infection. It has been shown that this, indeed, is possible through the compromised (leaky) gut wall barrier in infected animals (Zhang et al. 2015). Alternatively, the limitation could be overcome simply by oral administration. Advantages for a needle-free approach include higher patient compliance, less immunogenic reactions, lower costs due to less stringent manufacturing requirements, lower dosage because of higher specificity and potency and fever side effects as systemic effects are less likely (Reilly et al. 1997, Jones et al. 2016). The harsh conditions found in the gastrointestinal tract (acidic gastric fluid, digestive enzymes such as pepsin, trypsin and chymotrypsin) require further preparations to prevent protein degradation. A second disulfide bond can be introduced into the hydrophobic core of VHHs between FR2 and FR3, which results in higher protease resistance and thermal stability (Hussack et al. 2011). Other strategies might include decoy proteins, enzyme inhibition and encapsulation techniques (Reilly et al. 1997, Jones et al. 2016). Another exciting method to get nanobodies right to the site of infection, is to express them on the cell surface or as secretory proteins by *Lactobacillus* (Martin et al. 2011).

Besides toxin-neutralising antibodies, a highly successful approach has been fecal microbiota transplantation (FMT). FMT involves the transplantation of processed stool of a healthy donor to a patient's colon by enema, colonoscopy or through a nasogastric tube. Although FMT has only been used since a few years for recurrent CDIs, remarkable high success rates of more then 90% have been reported (Brandt et al. 2012). Because of its efficacy there is a growing interest to use FMT for acute cases of CDI (Zainah et al. 2015). Nanobodies could be added as a supplement to provide immediate relief, as the severity of infection correlates in particular with toxins being produced. Regardless of a rectal or oral administration, toxin neutralisation of VHHs could be enhanced through different formats. Thanks to the modular nature of nanobodies, reformatting can be done for specific and individual needs. A tetravalent construct consisting of four VHHs specific for Toxin A or B showed enhanced neutralisation potency *in vitro* and *in vivo* (Yang et al. 2014). Hussack *et al*. could demonstrate for Toxin A that a combination of different VHHs improved neutralisation capacity. VHHs in this work were produced with different *tags* (Fig. 3.2). VHHs in this work were produced with different *tags* (Fig. 3.2). The avi *tag* allows tetramerization by binding to streptavidin and the VHH-mFc fusion proteins could be multimerized via Protein G onto beads. Creating a multivalent structure could aid toxin absorption and rectal elimination, especially using VHHs directed against different epitopes.

5. Abstract

The bacterium *Clostridium difficile* is a primary cause of hospital acquired and antibiotic associated diarrhoea. Aged and multi morbid patients often show severe and even fatal courses of disease. The large clostridial toxins Toxin A and Toxin B have been identified as the two major virulence factors, that disrupt the cellular cytoskeleton by glucosylating small Rho proteins. A third toxin, *C. difficile* transferase (CDT), is found in hyper virulent strains, like ribotype 027. The heptameric CDTb subunit mediates binding to the host cell receptor, while the enzymatic CDTa subunit ADP-ribosylates actin at Arg177, causing disruption of the cellular cytoskeleton, increased bacterial adherence by microtubule-based cell protrusions, and depletion of protective eosinophils. Antibodies directed against Toxin A and B have been developed for diagnostic and therapeutic applications. Our lab has selected CDTb-specific single domain antibodies (VHHs or nanobodies) from immunized llamas. The unique structure of llama heavy chain antibodies (hcAbs) provides antigen binding via a single variable immunoglobulin domain.The goal of this thesis was to produce and characterize CDTb-specific VHHs and to establish a mouse infection model with CDT-expressing *C. difficile*. To this end, VHHs were produced in pro- and eukaryotic expression systems and analyzed in terms of their specificity and affinity of CDTb and their ability to inhibit the cytotoxicity of the binary CDT. V_HHs L-19, L-15.3 and all members of the V_HH family L-15.1 demonstrated specific binding to CDTb with affinities in the lower nanomolar range. VHH L-15.1g was able to inhibit CDT-mediated ADP-ribosylation of actin and disruption of the cellular cytoskeleton even at equimolar concentrations. These CDT-specific V_HHs could help to elucidate the pathogenic role of CDT and hold promise as new diagnostic and or therapeutic tools. Furthermore, colonisation of mice with CDT-expressing *C. difficile* stocks was achieved by prior treatment with antibiotics in the drinking water and clindamycin injection before oral challenge with *C. difficile* spores. Signs of the disease were observed by weight loss, soiled bedding, and histopathology. This model can be used in future to study *C. difficile* infection and to evaluate the potential diagnostic and therapeutic utility of the identified V_HHs.

6. Zusammenfassung

Das Bakterium *Clostridium difficile* ist eine Hauptursache von Krankenhaus- und Antibiotika-assoziierten Durchfall. Bei älteren und multimorbiden Patienten werden schwere und sogar tödliche Krankheitsverläufe beobachtet. Die beiden *large clostridial toxins* (LCTs) Toxin A und Toxin B wurden als wichtige Virulenzfaktoren identifiziert, die durch Glucosylierung kleiner Rho-GTPasen zu einem Zusammenbruch des zelluläre Zytoskelettes führen. Ein drittes binäres Toxin, die *C. difficile*-Transferase (CDT), wird in hypervirulenten Stämmen wie dem Ribotyp 027 gefunden. Die heptamere CDTb Untereinheit vermittelt die Bindung des Toxins an den Rezeptor der Wirtszelle und die Translokation der enzymatischen CDTa Untereinheit in das Zytosol. Die durch CDTa katalysierte ADP-Ribosylierung von Actin an Arg177 bewirkt ebenfalls eine Disintegration des zellulären Zytoskeletts. Außerdem erhöht es die bakterielle Adhäsion durch Mikrotubuli-basierte Zellprotrusionen und verhindert die Rekrutierung von schützenden eosinophilen Granulozyten. Antikörper gegen Toxin A und B haben bereits Einzug in die Diagnostik und Therapie erhalten. Unsere Arbeitsgruppe hat CDT-spezifische Einzeldomänen-Antikörper (V_HHs oder Nanobodies) aus immunisierten Lamas gewonnen. Die einzigartige Struktur von Lama Schwereketten-Antikörpern (hcAbs) ermöglicht die Antigenbindung über eine einzelne variable Immunglobulin Domäne (VHH). Ziele der vorliegenden Arbeit waren die Produktion und Charakterisierung CDTb-spezifischer Nanobodies sowie die Etablierung eines Maus-Modells für Infektionen mit CDT-exprimierenden *C. difficile*. Hierzu wurden V_HHs in prokaryotischen und eukaryotischen Zellen exprimiert, und hinsichtlich ihrer Spezifität und Affinität für CDTb, sowie einer möglichen Hemmung der Zytotoxizität von CDT analysiert. Die Ergebnisse bestätigen, dasss die V_HHs L-19, L-15.3 und die V_HHs der Familie L-15.1 CDTb spezifisch binden, mit K_D-Affinitäten im niederen und mittleren nanomolaren Bereich. Die VHH L-15.1g hemmt sogar noch im äquimolaren Bereich die durch Behandlung von Zellen mit CDT verursachte ADP-Ribosylierung von Aktin und Disintegration des Zytoskeletts. Zudem wurde in der vorliegenden Arbeit eine Kolonisation von *C. difficile* im Dickdarm von Mäusen durch eine vorangehende Verabreichung von Antibiotika im Trinkwasser und einer Clindamycin Injektion erreicht. Anzeichen der Erkrankung wurden durch Gewichtsverlust, Histopathologie und erhöhte Verschmutzung des Nestplatzes beobachtet. Das in dieser Arbeit etablierte Maus-Modell kann in Zukunft zur Klärung der Rolle von CDT für die Pathogenität von *C. difficile* Infektion verwendet werden, die in dieser Arbeit charakterisierten CDTb-spezifischen VHHs könnten in der Diagnostik und/oder Therapie von *C. difficile* Infektionen Verwendung finden.

7. Supplementary

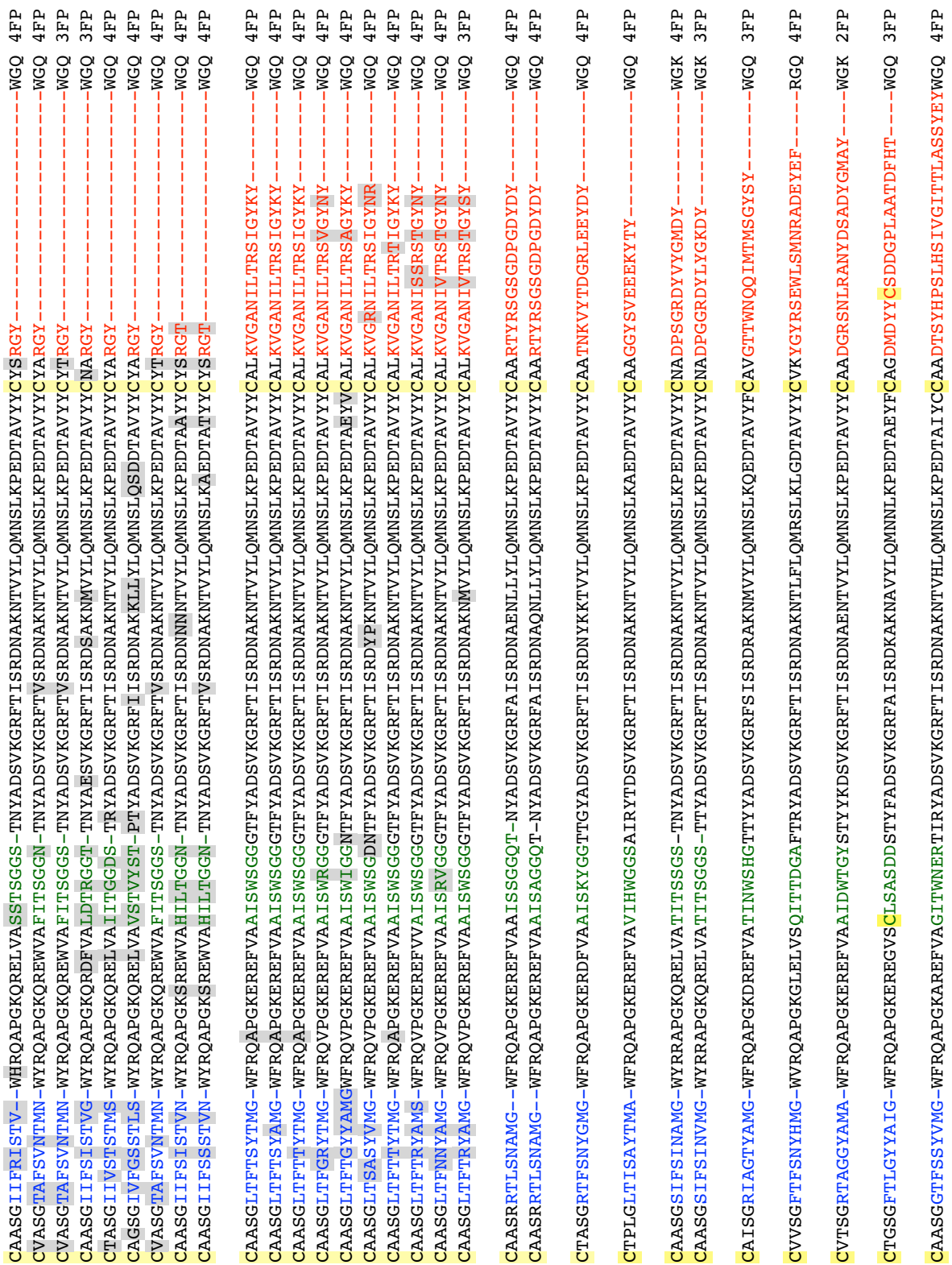

Supplementary Fig.7.1: Sequence alignment of selected CDTb specific VHHs. VHHs are grouped into families according to their CDR3 (red). CDR1 (blue), CDR2 (green) and disulfide bond (yellow) are shown.

```
CDTb  SNKKKEIVNEDILPNNGLMGYYFTDEHFKDLKLMAPIKDGNLKFEEKKVDKLLDKDKSDVKSIRWTGR 105
PA    VKQENRLLNESESSSQGLLGYYFSDLNFQAPMVVTSSTTGDLSIPSSELENIPSEN-QYFQSAIWSGF  97
       ::::.::**.  ..:**:****:* :*:   :::. . *:*.: ..:::::: .:: . .:*  *:*
CDTb  IIPSKDGEYTLSTDRDD-VLMQVNTESTI---SNTLKVNMKKGKEYKVRIELQDKNLGSIDNLSSPNL 169
PA    IKVKKSDEYTFATSADNHVTMWVDDQEVINKASNSNKIRLEKGRLYQIKIQYQRENPT--EKGLDFKL 162
      *  .*..***::*. *: * * *: :..*   **: *:.::**: *:::*: * :*    ::  . :*
CDTb  YWEL-DGMKKIIPEENLFLRDYSNIEKDDPFIPNNNFFDPKLMSDWEDEDLDTDNDNIPDSYERNGYT 236
PA    YWTDSQNKKEVISSDNLQLPELKQKSSNS---------RKKRSTSAGPTVPDRDNDGIPDSLEVEGYT 222
      **   :. *::*..:** * : .: ..:.          *  :.      * ***.**** * :***
CDTb  I----KDLIAVKWEDSFA-EQGYKKYVSNYLESNTAGDPYTDYEKASGSFDKAIKTEARDPLVAAYPI 299
PA    VDVKNKRTFLSPWISNIHEKKGLTKYKSSPEKWSTASDPYSDFEKVTGRIDKNVSPEARHPLVAAYPI 290
      :    *  :   * ..:  ::* .** *.  : .**.***:*:**.:* :** :..***.********
CDTb  VGVGMEKLIISTNEHASTD----QGKTVSRATTNSKTESNTA------------GVSVNVGYQNGFT 350
PA    VHVDMENIILSKNEDQSTQNTDSQTRTISKNTSTSRTHTSEVHGNAEVHASFFDIGGSVSAGFSNSNS 258
      * *.**::*:*.**. **:    * :*:*: *:.*:*.:. .            * **..*:.*. :
CDTb  ANVTTNYSHTTDNSTAVQDSNGESWNTGLSINKGESAYINANVRYYNTGTAPMYKVTPTTNLVLD-GD 417
PA    STVAIDHSLSL--------AGERTWAETMGLNTADTARLNANIRYVNTGTAPIYNVLPTTSLVLGKNQ 418
      :.*: ::* :         :. .:*   :.:*..::* :***:** ******:*:* ***.***. .:
CDTb  TLSTIKAQENQIGNNLSPGDTYPKKGLSPLALNTMDQFSSRLIPINYDQLKKLDAGKQIKLETTQVSG 485
PA    TLATIKAKENQLSQILAPNNYYPSKNLAPIALNAQDDFSSTPITMNYNQFLELEKTKQLRLDTDQVYG 486
      **:****:***:.: *:*.: **.*.*:*:***: *:***  *.:**:*: :*:  **::*:* ** *
CDTb  NFGTKNS-SGQI-VTEGNSWSDYISQIDSISASIILDTENE-SYERRVTAKNLQDPEDK-TPELTIGE 549
PA    NIATYNFENGRVRVDTGSNWSEVLPQIQETTARIIFNGKDLNLVERRIAAVNPSDPLETTKPDMTLKE 554
      *:.* *  .*:: *  *..**: :.**:. :* **:: ::    ***::* * .** :. .*::*: *
CDTb  AIEKAFGATKKDGLLYFNDIPIDESCVELIFDDNTANKIKDSLKTLSDKKIYN----VKLERGMNILI 613
PA    ALKIAFGFNEPNGNLQYQGKDITE--FDFNFDQQTSQNIKNQLAELNATNIYTVLDKIKLNAKMNILI 618
      *:: *** .: :* * ::.  * *  .:: **::*:::**:.*  *. .:**.    :**:  *****
CDTb  KTPTYFTNFDDYNNYP--STWSNVNTTNQDGLQGSANKLNGETKIKIPMSELKPYKRYVFSGYSKDPL 679
PA    RDKRFHY---DRNNIAVGADESVVKEAHREVINSSTEGL---------LLNIDKDIRKILSGYI---- 672
      :   :.    * ** .  :  * *: :::: ::.*:: *         : ::.   * ::***
CDTb  TSNSIIVKIKAKEEKTDYLVPEQGYTKFSYEFETTEKDSSNIEITLIGSGTTYLDNLSITELNSTPEI 707
PA    ------VEIEDTEGL--------------KEVINDRYDMLNIS-SLRQDGKTFIDF------------ 707
            *:*: .*                *. . . *  **. :*  .*.*::*
```

Supplementary Fig.7.2: Sequence alignment of PA and CDTb according to CDTb SwissModel. The four different domains for PA are underlined: Domain I (magenta), domain II (red), domain III (blue) and domain IV (orange). Further details are highlighted. The proteolytic cleavage site within domain I (yellow), Lysin 197 (cyan), phenylalanine 427, Asparagin 426 and Lysin 397 (magenta). Structural details have been described by Young et al. 2007.

8. Bibliography

Aktories, K., C. Schwan and T. Jank (2017). "Clostridium difficile Toxin Biology." Annu Rev Microbiol.

Aktories, K. and A. Wegner (1989). "ADP-ribosylation of actin by clostridial toxins." J Cell Biol **109**(4 Pt 1): 1385-1387.

Anosova, N. G., L. E. Cole, L. Li, J. Zhang, A. M. Brown, S. Mundle, J. Zhang, S. Ray, F. Ma, P. Garrone, N. Bertraminelli, H. Kleanthous and S. F. Anderson (2015). "A Combination of Three Fully Human Toxin A- and Toxin B-Specific Monoclonal Antibodies Protects against Challenge with Highly Virulent Epidemic Strains of Clostridium difficile in the Hamster Model." Clin Vaccine Immunol **22**(7): 711-725.

Arbabi-Ghahroudi, M., J. Tanha and R. MacKenzie (2005). "Prokaryotic expression of antibodies." Cancer Metastasis Rev **24**(4): 501-519.

Babcock, G. J., T. J. Broering, H. J. Hernandez, R. B. Mandell, K. Donahue, N. Boatright, A. M. Stack, I. Lowy, R. Graziano, D. Molrine, D. M. Ambrosino and W. D. Thomas, Jr. (2006). "Human monoclonal antibodies directed against toxins A and B prevent Clostridium difficile-induced mortality in hamsters." Infect Immun **74**(11): 6339-6347.

Bacci, S., K. Molbak, M. K. Kjeldsen and K. E. Olsen (2011). "Binary toxin and death after Clostridium difficile infection." Emerg Infect Dis **17**(6): 976-982.

Barth, H., K. Aktories, M. R. Popoff and B. G. Stiles (2004). "Binary bacterial toxins: biochemistry, biology, and applications of common Clostridium and Bacillus proteins." Microbiol Mol Biol Rev **68**(3): 373-402, table of contents.

Benson, E. L., P. D. Huynh, A. Finkelstein and R. J. Collier (1998). "Identification of residues lining the anthrax protective antigen channel." Biochemistry **37**(11): 3941-3948.

Bingley, P. J. and G. M. Harding (1987). "Clostridium difficile colitis following treatment with metronidazole and vancomycin." Postgrad Med J **63**(745): 993-994.

Blanc, M. R., A. Anouassi, M. Ahmed Abed, G. Tsikis, S. Canepa, V. Labas, M. Belghazi and G. Bruneau (2009). "A one-step exclusion-binding procedure for the purification of functional heavy-chain and mammalian-type gamma-globulins from camelid sera." Biotechnol Appl Biochem **54**(4): 207-212.

Brandt, L. J., O. C. Aroniadis, M. Mellow, A. Kanatzar, C. Kelly, T. Park, N. Stollman, F. Rohlke and C. Surawicz (2012). "Long-term follow-up of colonoscopic fecal microbiota transplant for recurrent Clostridium difficile infection." Am J Gastroenterol **107**(7): 1079-1087.

Buffie, C. G., V. Bucci, R. R. Stein, P. T. McKenney, L. Ling, A. Gobourne, D. No, H. Liu, M. Kinnebrew, A. Viale, E. Littmann, M. R. van den Brink, R. R. Jenq, Y. Taur, C. Sander, J. R. Cross, N. C. Toussaint, J. B. Xavier and E. G. Pamer (2015). "Precision microbiome reconstitution restores bile acid mediated resistance to Clostridium difficile." Nature **517**(7533): 205-208.

Buffie, C. G., I. Jarchum, M. Equinda, L. Lipuma, A. Gobourne, A. Viale, C. Ubeda, J. Xavier and E. G. Pamer (2012). "Profound alterations of intestinal microbiota following a single dose of clindamycin results in sustained susceptibility to Clostridium difficile-induced colitis." Infect Immun **80**(1): 62-73.

Burnham, C. A. and K. C. Carroll (2013). "Diagnosis of Clostridium difficile infection: an ongoing conundrum for clinicians and for clinical laboratories." Clin Microbiol Rev **26**(3): 604-630.

Burnham, C. A., E. R. Dubberke, L. K. Kociolek, C. R. Polage and T. V. Riley (2016). "Clostridium difficile-Diagnostic and Clinical Challenges." Clin Chem **62**(2): 310-314.

Carman, R. J., A. L. Stevens, M. W. Lyerly, M. F. Hiltonsmith, B. G. Stiles and T. D. Wilkins (2011). "Clostridium difficile binary toxin (CDT) and diarrhea." Anaerobe **17**(4): 161-165.

Chen, X., K. Katchar, J. D. Goldsmith, N. Nanthakumar, A. Cheknis, D. N. Gerding and C. P. Kelly (2008). "A mouse model of Clostridium difficile-associated disease." Gastroenterology **135**(6): 1984-1992.

Cowardin, C. A., E. L. Buonomo, M. M. Saleh, M. G. Wilson, S. L. Burgess, S. A. Kuehne, C. Schwan, A. M. Eichhoff, F. Koch-Nolte, D. Lyras, K. Aktories, N. P. Minton and W. A. Petri, Jr. (2016). "The binary toxin CDT enhances Clostridium difficile virulence by suppressing protective colonic eosinophilia." Nat Microbiol **1**(8): 16108.

D'Agostino, R. B., Sr., S. H. Collins, K. M. Pencina, Y. Kean and S. Gorbach (2014). "Risk estimation for recurrent Clostridium difficile infection based on clinical factors." Clin Infect Dis **58**(10): 1386-1393.

Dancer, S. J., P. Kirkpatrick, D. S. Corcoran, F. Christison, D. Farmer and C. Robertson (2013). "Approaching zero: temporal effects of a restrictive antibiotic policy on hospital-acquired Clostridium difficile, extended-spectrum beta-lactamase-producing coliforms and meticillin-resistant Staphylococcus aureus." Int J Antimicrob Agents **41**(2): 137-142.

Davies, N. L., J. E. Compson, B. Mackenzie, V. L. O'Dowd, A. K. Oxbrow, J. T. Heads, A. Turner, K. Sarkar, S. L. Dugdale, M. Jairaj, L. Christodoulou, D. E. Knight, A. S. Cross, K. J. Herve, K. L. Tyson, H. Hailu, C. B. Doyle, M. Ellis, M. Kriek, M. Cox, M. J. Page, A. R. Moore, D. J. Lightwood and D. P. Humphreys (2013). "A mixture of functionally oligoclonal humanized monoclonal antibodies that neutralize Clostridium difficile TcdA and TcdB with high levels of in vitro potency shows in vivo protection in a hamster infection model." Clin Vaccine Immunol **20**(3): 377-390.

De Genst, E., K. Silence, K. Decanniere, K. Conrath, R. Loris, J. Kinne, S. Muyldermans and L. Wyns (2006). "Molecular basis for the preferential cleft recognition by dromedary heavy-chain antibodies." Proc Natl Acad Sci U S A **103**(12): 4586-4591.

Desmyter, A., T. R. Transue, M. A. Ghahroudi, M. H. Thi, F. Poortmans, R. Hamers, S. Muyldermans and L. Wyns (1996). "Crystal structure of a camel single-domain VH antibody fragment in complex with lysozyme." Nat Struct Biol **3**(9): 803-811.

Fekety, R., J. Silva, R. Toshniwal, M. Allo, J. Armstrong, R. Browne, J. Ebright and G. Rifkin (1979). "Antibiotic-associated colitis: effects of antibiotics on Clostridium difficile and the disease in hamsters." Rev Infect Dis **1**(2): 386-397.

Ferreyra, J. A., K. J. Wu, A. J. Hryckowian, D. M. Bouley, B. C. Weimer and J. L. Sonnenburg (2014). "Gut microbiota-produced succinate promotes C. difficile infection after antibiotic treatment or motility disturbance." Cell Host Microbe **16**(6): 770-777.

Gerding, D. N., S. Johnson, M. Rupnik and K. Aktories (2014). "Clostridium difficile binary toxin CDT: mechanism, epidemiology, and potential clinical importance." Gut Microbes **5**(1): 15-27.

Gerding, D. N., T. Meyer, C. Lee, S. H. Cohen, U. K. Murthy, A. Poirier, T. C. Van Schooneveld, D. S. Pardi, A. Ramos, M. A. Barron, H. Chen and S. Villano (2015). "Administration of spores of nontoxigenic Clostridium difficile strain M3 for prevention of recurrent C. difficile infection: a randomized clinical trial." JAMA **313**(17): 1719-1727.

Geric, B., R. J. Carman, M. Rupnik, C. W. Genheimer, S. P. Sambol, D. M. Lyerly, D. N. Gerding and S. Johnson (2006). "Binary toxin-producing, large clostridial toxin-negative Clostridium difficile strains are enterotoxic but do not cause disease in hamsters." J Infect Dis **193**(8): 1143-1150.

Goorhuis, A., D. Bakker, J. Corver, S. B. Debast, C. Harmanus, D. W. Notermans, A. A. Bergwerff, F. W. Dekker and E. J. Kuijper (2008). "Emergence of Clostridium difficile infection due to a new hypervirulent strain, polymerase chain reaction ribotype 078." Clin Infect Dis **47**(9): 1162-1170.

Gulke, I., G. Pfeifer, J. Liese, M. Fritz, F. Hofmann, K. Aktories and H. Barth (2001). "Characterization of the enzymatic component of the ADP-ribosyltransferase toxin CDTa from Clostridium difficile." Infect Immun **69**(10): 6004-6011.

Hall, I. and E. O'Toole (1935). "Intestinal flora in newborn infants with description of a new pathogenic anaerobe." Am. J. Dis. Child **49**: 390–402.

Hensgens, M. P., E. C. Keessen, M. M. Squire, T. V. Riley, M. G. Koene, E. de Boer, L. J. Lipman, E. J. Kuijper, M. European Society of Clinical and d. Infectious Diseases Study Group for Clostridium (2012). "Clostridium difficile infection in the community: a zoonotic disease?" Clin Microbiol Infect **18**(7): 635-645.

Holliger, P. and P. J. Hudson (2005). "Engineered antibody fragments and the rise of single domains." Nat Biotechnol **23**(9): 1126-1136.

Hoogenboom, H. R. (2005). "Selecting and screening recombinant antibody libraries." Nat Biotechnol **23**(9): 1105-1116.

Hussack, G., M. Arbabi-Ghahroudi, H. van Faassen, J. G. Songer, K. K. Ng, R. MacKenzie and J. Tanha (2011). "Neutralization of Clostridium difficile toxin A with single-domain antibodies targeting the cell receptor binding domain." J Biol Chem **286**(11): 8961-8976.

Hussack, G., T. Hirama, W. Ding, R. Mackenzie and J. Tanha (2011). "Engineered single-domain antibodies with high protease resistance and thermal stability." PLoS One **6**(11): e28218.

Hussack, G., C. R. Mackenzie and J. Tanha (2012). "Characterization of single-domain antibodies with an engineered disulfide bond." Methods Mol Biol **911**: 417-429.

Jager, V., K. Bussow, A. Wagner, S. Weber, M. Hust, A. Frenzel and T. Schirrmann (2013). "High level transient production of recombinant antibodies and antibody fusion proteins in HEK293 cells." BMC Biotechnol **13**: 52.

Jank, T. and K. Aktories (2008). "Structure and mode of action of clostridial glucosylating toxins: the ABCD model." Trends Microbiol **16**(5): 222-229.

Jarchum, I., M. Liu, L. Lipuma and E. G. Pamer (2011). "Toll-like receptor 5 stimulation protects mice from acute Clostridium difficile colitis." Infect Immun **79**(4): 1498-1503.

Jones, A. M., E. J. Kuijper and M. H. Wilcox (2013). "Clostridium difficile: a European perspective." J Infect **66**(2): 115-128.

Jones, R. G. and A. Martino (2016). "Targeted localized use of therapeutic antibodies: a review of non-systemic, topical and oral applications." Crit Rev Biotechnol **36**(3): 506-520.

Kelly, C. P. and J. T. LaMont (1998). "Clostridium difficile infection." Annu Rev Med **49**: 375-390.

Kelly, C. P. and J. T. LaMont (2008). "Clostridium difficile--more difficult than ever." N Engl J Med **359**(18): 1932-1940.

Khanna, S., D. S. Pardi, S. L. Aronson, P. P. Kammer, R. Orenstein, J. L. St Sauver, W. S. Harmsen and A. R. Zinsmeister (2012). "The epidemiology of community-acquired Clostridium difficile infection: a population-based study." Am J Gastroenterol **107**(1): 89-95.

Kim, J., M. R. Seo, J. O. Kang, T. Y. Choi and H. Pai (2013). "Clinical and Microbiologic Characteristics of Clostridium difficile Infection Caused by Binary Toxin Producing Strain in Korea." Infect Chemother **45**(2): 175-183.

Knoop, F. C. (1979). "Clindamycin-associated enterocolitis in guinea pigs: evidence for a bacterial toxin." Infect Immun **23**(1): 31-33.

Kontermann, R. E. (2011). "Strategies for extended serum half-life of protein therapeutics." Curr Opin Biotechnol **22**(6): 868-876.

Krantz, B. A., R. A. Melnyk, S. Zhang, S. J. Juris, D. B. Lacy, Z. Wu, A. Finkelstein and R. J. Collier (2005). "A phenylalanine clamp catalyzes protein translocation through the anthrax toxin pore." Science **309**(5735): 777-781.

Kuehne, S. A., S. T. Cartman, J. T. Heap, M. L. Kelly, A. Cockayne and N. P. Minton (2010). "The role of toxin A and toxin B in Clostridium difficile infection." Nature **467**(7316): 711-713.

Kuehne, S. A., M. M. Collery, M. L. Kelly, S. T. Cartman, A. Cockayne and N. P. Minton (2014). "Importance of toxin A, toxin B, and CDT in virulence of an epidemic Clostridium difficile strain." J Infect Dis **209**(1): 83-86.

Lawley, T. D., S. Clare, L. J. Deakin, D. Goulding, J. L. Yen, C. Raisen, C. Brandt, J. Lovell, F. Cooke, T. G. Clark and G. Dougan (2010). "Use of purified Clostridium difficile spores to facilitate evaluation of health care disinfection regimens." Appl Environ Microbiol **76**(20): 6895-6900.

Leffler, D. A. and J. T. Lamont (2015). "Clostridium difficile infection." N Engl J Med **372**(16): 1539-1548.

Leffler, D. A. and J. T. Lamont (2015). "Clostridium difficile Infection." N Engl J Med **373**(3): 287-288.

Lessa, F. C., Y. Mu, W. M. Bamberg, Z. G. Beldavs, G. K. Dumyati, J. R. Dunn, M. M. Farley, S. M. Holzbauer, J. I. Meek, E. C. Phipps, L. E. Wilson, L. G. Winston, J. A. Cohen, B. M. Limbago, S. K.

Fridkin, D. N. Gerding and L. C. McDonald (2015). "Burden of Clostridium difficile infection in the United States." N Engl J Med **372**(9): 825-834.

Ley, R. E., F. Backhed, P. Turnbaugh, C. A. Lozupone, R. D. Knight and J. I. Gordon (2005). "Obesity alters gut microbial ecology." Proc Natl Acad Sci U S A **102**(31): 11070-11075.

Lofgren, E. T., S. R. Cole, D. J. Weber, D. J. Anderson and R. W. Moehring (2014). "Hospital-acquired Clostridium difficile infections: estimating all-cause mortality and length of stay." Epidemiology **25**(4): 570-575.

Loo, V. G., L. Poirier, M. A. Miller, M. Oughton, M. D. Libman, S. Michaud, A. M. Bourgault, T. Nguyen, C. Frenette, M. Kelly, A. Vibien, P. Brassard, S. Fenn, K. Dewar, T. J. Hudson, R. Horn, P. Rene, Y. Monczak and A. Dascal (2005). "A predominantly clonal multi-institutional outbreak of Clostridium difficile-associated diarrhea with high morbidity and mortality." N Engl J Med **353**(23): 2442-2449.

Louie, T. J., M. A. Miller, K. M. Mullane, K. Weiss, A. Lentnek, Y. Golan, S. Gorbach, P. Sears, Y. K. Shue and O. P. T. C. S. Group (2011). "Fidaxomicin versus vancomycin for Clostridium difficile infection." N Engl J Med **364**(5): 422-431.

Lusk, R. H., R. Fekety, J. Silva, R. A. Browne, D. H. Ringler and G. D. Abrams (1978). "Clindamycin-induced enterocolitis in hamsters." J Infect Dis **137**(4): 464-475.

Lyras, D., J. R. O'Connor, P. M. Howarth, S. P. Sambol, G. P. Carter, T. Phumoonna, R. Poon, V. Adams, G. Vedantam, S. Johnson, D. N. Gerding and J. I. Rood (2009). "Toxin B is essential for virulence of Clostridium difficile." Nature **458**(7242): 1176-1179.

Martin, M. C., N. Pant, V. Ladero, G. Gunaydin, K. K. Andersen, B. Alvarez, N. Martinez, M. A. Alvarez, L. Hammarstrom and H. Marcotte (2011). "Integrative expression system for delivery of antibody fragments by lactobacilli." Appl Environ Microbiol **77**(6): 2174-2179.

McDonald, L. C., G. E. Killgore, A. Thompson, R. C. Owens, Jr., S. V. Kazakova, S. P. Sambol, S. Johnson and D. N. Gerding (2005). "An epidemic, toxin gene-variant strain of Clostridium difficile." N Engl J Med **353**(23): 2433-2441.

Melnyk, R. A. and R. J. Collier (2006). "A loop network within the anthrax toxin pore positions the phenylalanine clamp in an active conformation." Proc Natl Acad Sci U S A **103**(26): 9802-9807.

Melnyk, R. A., K. M. Hewitt, D. B. Lacy, H. C. Lin, C. R. Gessner, S. Li, V. L. Woods, Jr. and R. J. Collier (2006). "Structural determinants for the binding of anthrax lethal factor to oligomeric protective antigen." J Biol Chem **281**(3): 1630-1635.

Miossec, C., S. Sayah-Jeanne and V. Augustin (2014). "DAV131, an oral adsorbent-based product, exerts a dose- dependent protection of hamsters against moxifloxacin-induced Clostridium difficile lethal infection." ECCMID, Barcelona, Spain.

Morrison, C. (2015). "Antibacterial antibodies gain traction." Nat Rev Drug Discov **14**(11): 737-738.

Murphy, K. P., C. A. Janeway, P. Travers, M. Walport, A. Mowat and C. T. Weaver (2012). Janeway's Immunobiology. London, Garland Science.

Muyldermans, S. (2001). "Single domain camel antibodies: current status." J Biotechnol **74**(4): 277-302.

Muyldermans, S. (2013). "Nanobodies: natural single-domain antibodies." Annu Rev Biochem **82**: 775-797.

Papatheodorou, P. and K. Aktories (2016). "Receptor-Binding and Uptake of Binary Actin-ADP-Ribosylating Toxins." Curr Top Microbiol Immunol.

Papatheodorou, P., J. E. Carette, G. W. Bell, C. Schwan, G. Guttenberg, T. R. Brummelkamp and K. Aktories (2011). "Lipolysis-stimulated lipoprotein receptor (LSR) is the host receptor for the binary toxin Clostridium difficile transferase (CDT)." Proc Natl Acad Sci U S A **108**(39): 16422-16427.

Papatheodorou, P., D. Hornuss, T. Nolke, S. Hemmasi, J. Castonguay, M. Picchianti and K. Aktories (2013). "Clostridium difficile binary toxin CDT induces clustering of the lipolysis-stimulated lipoprotein receptor into lipid rafts." MBio **4**(3): e00244-00213.

Perelle, S., M. Gibert, P. Bourlioux, G. Corthier and M. R. Popoff (1997). "Production of a complete binary toxin (actin-specific ADP-ribosyltransferase) by Clostridium difficile CD196." Infect Immun **65**(4): 1402-1407.

Pimental, R. A., K. A. Christensen, B. A. Krantz and R. J. Collier (2004). "Anthrax toxin complexes: heptameric protective antigen can bind lethal factor and edema factor simultaneously." Biochem Biophys Res Commun **322**(1): 258-262.

Qa'dan, M., K. A. Christensen, L. Zhang, T. M. Roberts and R. J. Collier (2005). "Membrane insertion by anthrax protective antigen in cultured cells." Mol Cell Biol **25**(13): 5492-5498.

Rea, M. C., A. Dobson, O. O'Sullivan, F. Crispie, F. Fouhy, P. D. Cotter, F. Shanahan, B. Kiely, C. Hill and R. P. Ross (2011). "Effect of broad- and narrow-spectrum antimicrobials on Clostridium difficile and microbial diversity in a model of the distal colon." Proc Natl Acad Sci U S A **108 Suppl 1**: 4639-4644.

Reilly, R. M., R. Domingo and J. Sandhu (1997). "Oral delivery of antibodies. Future pharmacokinetic trends." Clin Pharmacokinet **32**(4): 313-323.

Reveles, K. R., G. C. Lee, N. K. Boyd and C. R. Frei (2014). "The rise in Clostridium difficile infection incidence among hospitalized adults in the United States: 2001-2010." Am J Infect Control **42**(10): 1028-1032.

Saerens, D., F. Frederix, G. Reekmans, K. Conrath, K. Jans, L. Brys, L. Huang, E. Bosmans, G. Maes, G. Borghs and S. Muyldermans (2005). "Engineering camel single-domain antibodies and immobilization chemistry for human prostate-specific antigen sensing." Anal Chem **77**(23): 7547-7555.

Sayedy, L., D. Kothari and R. J. Richards (2010). "Toxic megacolon associated Clostridium difficile colitis." World J Gastrointest Endosc **2**(8): 293-297.

Schirrmann, T. and K. Büssow (2010). "Transient production of scFv-Fc fusion proteins in mammalian cells." Antibody engineering: 387-398.

Schwan, C., A. S. Kruppke, T. Nolke, L. Schumacher, F. Koch-Nolte, M. Kudryashev, H. Stahlberg and K. Aktories (2014). "Clostridium difficile toxin CDT hijacks microtubule organization and reroutes vesicle traffic to increase pathogen adherence." Proc Natl Acad Sci U S A **111**(6): 2313-2318.

Schwan, C., B. Stecher, T. Tzivelekidis, M. van Ham, M. Rohde, W. D. Hardt, J. Wehland and K. Aktories (2009). "Clostridium difficile toxin CDT induces formation of microtubule-based protrusions and increases adherence of bacteria." PLoS Pathog **5**(10): e1000626.

Sherwood, L. J., L. E. Osborn, R. Carrion, Jr., J. L. Patterson and A. Hayhurst (2007). "Rapid assembly of sensitive antigen-capture assays for Marburg virus, using in vitro selection of llama single-domain antibodies, at biosafety level 4." J Infect Dis **196 Suppl 2**: S213-219.

Slimings, C. and T. V. Riley (2014). "Antibiotics and hospital-acquired Clostridium difficile infection: update of systematic review and meta-analysis." J Antimicrob Chemother **69**(4): 881-891.

Sorg, J. A. and S. S. Dineen (2009). "Laboratory maintenance of Clostridium difficile." Curr Protoc Microbiol **Chapter 9**: Unit9A 1.

Stanley, H. F., M. Kadwell and J. C. Wheeler (1994). "Molecular evolution of the family Camelidae: a mitochondrial DNA study." Proc Biol Sci **256**(1345): 1-6.

Stewart, D. B., A. Berg and J. Hegarty (2013). "Predicting recurrence of C. difficile colitis using bacterial virulence factors: binary toxin is the key." J Gastrointest Surg **17**(1): 118-124; discussion p 124-115.

Theriot, C. M., A. A. Bowman and V. B. Young (2016). "Antibiotic-Induced Alterations of the Gut Microbiota Alter Secondary Bile Acid Production and Allow for Clostridium difficile Spore Germination and Outgrowth in the Large Intestine." mSphere **1**(1).

Tijink, B. M., T. Laeremans, M. Budde, M. Stigter-van Walsum, T. Dreier, H. J. de Haard, C. R. Leemans and G. A. van Dongen (2008). "Improved tumor targeting of anti-epidermal growth factor receptor Nanobodies through albumin binding: taking advantage of modular Nanobody technology." Mol Cancer Ther **7**(8): 2288-2297.

Turnbaugh, P. J., V. K. Ridaura, J. J. Faith, F. E. Rey, R. Knight and J. I. Gordon (2009). "The effect of diet on the human gut microbiome: a metagenomic analysis in humanized gnotobiotic mice." Sci Transl Med **1**(6): 6ra14.

Ubeda, C., L. Lipuma, A. Gobourne, A. Viale, I. Leiner, M. Equinda, R. Khanin and E. G. Pamer (2012). "Familial transmission rather than defective innate immunity shapes the distinct intestinal microbiota of TLR-deficient mice." J Exp Med **209**(8): 1445-1456.

Unger, M., A. M. Eichhoff, L. Schumacher, M. Strysio, S. Menzel, C. Schwan, V. Alzogaray, V. Zylberman, M. Seman, J. Brandner, H. Rohde, K. Zhu, F. Haag, H. W. Mittrucker, F. Goldbaum, K. Aktories and F. Koch-Nolte (2015). "Selection of nanobodies that block the enzymatic and cytotoxic activities of the binary Clostridium difficile toxin CDT." Sci Rep **5**: 7850.

Van Bockstaele, F., J. B. Holz and H. Revets (2009). "The development of nanobodies for therapeutic applications." Curr Opin Investig Drugs **10**(11): 1212-1224.

Warny, M., J. Pepin, A. Fang, G. Killgore, A. Thompson, J. Brazier, E. Frost and L. C. McDonald (2005). "Toxin production by an emerging strain of Clostridium difficile associated with outbreaks of severe disease in North America and Europe." Lancet **366**(9491): 1079-1084.

Wegner, A. and K. Aktories (1988). "ADP-ribosylated actin caps the barbed ends of actin filaments." J Biol Chem **263**(27): 13739-13742.

Wesolowski, J., V. Alzogaray, J. Reyelt, M. Unger, K. Juarez, M. Urrutia, A. Cauerhff, W. Danquah, B. Rissiek, F. Scheuplein, N. Schwarz, S. Adriouch, O. Boyer, M. Seman, A. Licea, D. V. Serreze, F. A. Goldbaum, F. Haag and F. Koch-Nolte (2009). "Single domain antibodies: promising experimental and therapeutic tools in infection and immunity." Med Microbiol Immunol **198**(3): 157-174.

Yang, Z., D. Schmidt, W. Liu, S. Li, L. Shi, J. Sheng, K. Chen, H. Yu, J. M. Tremblay, X. Chen, K. H. Piepenbrink, E. J. Sundberg, C. P. Kelly, G. Bai, C. B. Shoemaker and H. Feng (2014). "A novel multivalent, single-domain antibody targeting TcdA and TcdB prevents fulminant Clostridium difficile infection in mice." J Infect Dis **210**(6): 964-972.

Young, J. A. and R. J. Collier (2007). "Anthrax toxin: receptor binding, internalization, pore formation, and translocation." Annu Rev Biochem **76**: 243-265.

Zainah, H., M. Hassan, L. Shiekh-Sroujieh, S. Hassan, G. Alangaden and M. Ramesh (2015). "Intestinal microbiota transplantation, a simple and effective treatment for severe and refractory Clostridium difficile infection." Dig Dis Sci **60**(1): 181-185.

Zhang, J., R. MacKenzie and Y. Durocher (2009). "Production of chimeric heavy-chain antibodies." Methods Mol Biol **525**: 323-336, xv.

Zhang, Z., X. Chen, L. D. Hernandez, P. Lipari, A. Flattery, S. C. Chen, S. Kramer, J. D. Polishook, F. Racine, H. Cape, C. P. Kelly and A. G. Therien (2015). "Toxin-mediated paracellular transport of antitoxin antibodies facilitates protection against Clostridium difficile infection." Infect Immun **83**(1): 405-416.

Zimlichman, E., D. Henderson, O. Tamir, C. Franz, P. Song, C. K. Yamin, C. Keohane, C. R. Denham and D. W. Bates (2013). "Health care-associated infections: a meta-analysis of costs and financial impact on the US health care system." JAMA Intern Med **173**(22): 2039-2046.

10. Eidesstattliche Versicherung

Ich versichere ausdrücklich, dass ich die Arbeit selbständig und ohne fremde Hilfe verfasst, andere als die von mir angegebenen Quellen und Hilfsmittel nicht benutzt und die aus den benutzten Werken wörtlich oder inhaltlich entnommenen Stellen einzeln nach Ausgabe (Auflage und Jahr des Erscheinens), Band und Seite des benutzten Werkes kenntlich gemacht habe.

Ferner versichere ich, dass ich die Dissertation bisher nicht einem Fachvertreter an einer anderen Hochschule zur Überprüfung vorgelegt oder mich anderweitig um Zulassung zur Promotion beworben habe.

Ich erkläre mich einverstanden, dass meine Dissertation vom Dekanat der Medizinischen Fakultät mit einer gängigen Software zur Erkennung von Plagiaten überprüft werden kann.

Unterschrift: .....